AD-A240 311

PL-TR-91-2104

Particle Acceleration in Space and
Radiation Belt Depletion

C.R. Menyuk
D. Papadopoulos

Science Applications International Corporation
1710 Goodridge Drive
McLean, Virginia 22102

30 April 1991

SEP 12 1991

Final Report
March 1, 1987 - February 28, 1991

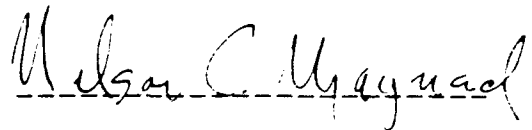APPROVED FOR PUBLIC RELEASE; DISTRIBUTION UNLIMITED.

91-10183

"This technical report has been reviewed and is approved for publication."
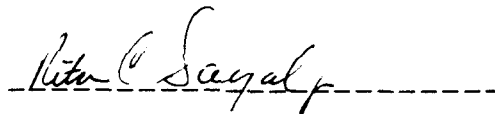

WILLIAM J. BURKE
Contract Manager

NELSON C. MAYNARD
Branch Chief

FOR THE COMMANDER

RITA C. SAGALYN
Division Director

REPORT DOCUMENTATION PAGE

1. AGENCY USE ONLY (Leave blank)	2. REPORT DATE	3. REPORT TYPE AND DATES COVERED	
	30 April 1991	Final	3/1/87 - 2/28/91

4. TITLE AND SUBTITLE
Particle Acceleration in Space and Radiation Belt Depletion

5. FUNDING NUMBERS
PE 62101F
PR 7601   TA 50   WU AD
Contract F19628-87-C-0085

6. AUTHOR(S)
C. R. Menyuk
D. Papadopoulos

7. PERFORMING ORGANIZATION NAME(S) AND ADDRESS(ES)
Science Applications International Corp
1710 Goodridge Drive
McLean, VA 22102

8. PERFORMING ORGANIZATION REPORT NUMBER

9. SPONSORING/MONITORING AGENCY NAME(S) AND ADDRESS(ES)
Phillips Laboratory
Hanscom AFB, MA 01731-5000

Contract Manager: William Burke/PHA

10. SPONSORING/MONITORING AGENCY REPORT NUMBER

PL-TR-91-2104

11. SUPPLEMENTARY NOTES
This also constitutes the final report for ILIROA

12a. DISTRIBUTION/AVAILABILITY STATEMENT

APPROVED FOR PUBLIC RELEASE; DISTRIBUTION UNLIMITED

12b. DISTRIBUTION CODE

13. ABSTRACT (Maximum 200 words)

Particle acceleration and the accompanying radiation belt depletion are studied theoretically. The effect of stochastic particle acceleration on a distribution of electrons is studied using a finite element method, combined with resonance overlap techniques. In particular cases, these are also studied using particle simulations and good agreement is found. We next focus on particle acceleration in the Alfvèn wave maser. It is shown that the maser is naturally well-confined but will not lead to significant acceleration. It is shown, however, that the kinetic Alfvèn wave will lead to significant acceleration, although it has to be ducted to remain confined. An experimental approach to stimulate these waves artificially by heating electrons is then proposed.

14. SUBJECT TERMS
electron acceleration, kinetic Alfvèn waves, stochasticity

15. NUMBER OF PAGES
134

16. PRICE CODE

17. SECURITY CLASSIFICATION OF REPORT	18. SECURITY CLASSIFICATION OF THIS PAGE	19. SECURITY CLASSIFICATION OF ABSTRACT	20. LIMITATION OF ABSTRACT
Unclassified	Unclassified	Unclassified	SAR

Table of Contents

iii

I. INTRODUCTION

During the contract period the work focused on two activities: studies of high energy electron acceleration and studies of the Alfvèn maser. The work on acceleration focused on determining the intensity and scale lengths required to accelerate electrons to energies of 5 MeV or more. It was found in earlier work, that a very high intensity of 20 W/cm^2 is required for this purpose in the nighttime ionosphere, while the optimum frequency is roughly twice the electron gyrofrequency. During the present contract period, a diffusion code which solves the Fokker-Planck equation along the Hamiltonian surfaces to determine the evolution of the distribution function was completed. Intensities roughly a factor of four over threshold are required to yield good agreement between the particle and diffusion codes. The diffusion code runs far more rapidly than the particle code and allows us to make broad studies of parameter space. The work led to two manuscripts submitted for publication to *Physical Review Letters* and *Journal of Geophysical Research*. These are included in Appendix A.

The work on the Alfvèn maser started by determining the mode structure of low-order shear Alfvèn modes in the magnetosphere, including their transverse structure, and ensuring that their coupling to the compressive modes is weak. With the study of the mode structure completed, resonant acceleration mechanisms to determine if the Alfvèn wave alone is sufficient to precipitate high energy ions were investigated. The results indicate that localized, low-order MHD shear Alfvèn waves are not sufficient to precipitate a large number of particles. It was, however, found that parallel electric fields caused by plasma kinetic effects in conjunction with values of $k_\perp \rho_i \approx 0.1$ can induce significant high energy particle precipitation for electric fields above a threshold value which was derived. Such waves can propagate inside natural or induced magnetospheric ducts. We note that the physical mechanism of resonant excitation described here is quite different physically from previous schemes discussed by Trakhtengerts and co-workers.

II. IONOSPHERIC DIFFUSION

A. Test-Particle Results

The diffusion code which we have written is based on the concepts of stochasticity and resonance overlap.[1] These concepts have played an increasingly important role in plasma physics during the last decade. Our basic particle Hamiltonian may be written[2]

$$H = \left[(c\mathbf{P} - q\mathbf{A})^2 + m^2 c^4 \right]^{1/2} + q\Phi = mc^2 \gamma + q\Phi, \tag{2.1}$$

where

$$\mathbf{A} = A_1 \frac{k_\parallel}{k} \sin\psi \hat{\mathbf{e}}_\mathbf{x} + A_2 \cos\psi \hat{\mathbf{e}}_\mathbf{y} - A_1 \frac{k_\perp}{k} \sin\psi \hat{\mathbf{e}}_\mathbf{z} + x B_0 \hat{\mathbf{e}}_\mathbf{y},$$
$$\Phi = \Phi_0 \sin\psi, \tag{2.2}$$
$$\psi = k_\perp x + k_\parallel z - \omega t,$$

and q is the particle's charge. This Hamiltonian represents single particle in an applied electromagnetic wave propagating obliquely with respect to a magnetic field. We now use a series of canonical transformations to reduce the Hamiltonian to the form[2]

$$H \simeq H_0 + H_1, \tag{2.3}$$

The zero-order Hamiltonian is given by

$$\begin{aligned} H_0 &= mc^2 \left(1 + \frac{p_\perp^2}{m^2 c^2} + \frac{p_\parallel^2}{m^2 c^2} \right)^{1/2} - \frac{\omega}{k_\parallel} p_\parallel \\ &= mc^2 \gamma_0 - \frac{\omega}{k_\parallel} p_\parallel, \end{aligned} \tag{2.4}$$

where $p_\perp$ and $p_\parallel$ are momentume perpendicular and parallel to the magnetic field, and the first-order Hamiltonian is given by

$$H_1 = \sum_{l=-\infty}^{\infty} Z_l \sin(k_\parallel z + l\theta), \tag{2.5}$$

where θ is the gyroangle and

$$\begin{aligned} Z_l = \frac{mc^2}{\gamma_0} \Bigg\{ &\epsilon_1 \left[\frac{q}{|q|} \frac{p_\parallel}{mc} \sin\alpha - \frac{q}{|q|} \frac{\Omega l}{k_\perp c} \cos\alpha \right] J_l(k_\perp \rho) \\ &+ \epsilon_2 \frac{p_\perp}{mc} J_l'(k_\perp \rho) + \epsilon_3 \frac{q}{|q|} \gamma_0 J_l(k_\perp \rho) \Bigg\}, \end{aligned} \tag{2.6}$$

2

with

$$\epsilon_1 = \frac{|q|A_1}{mc^2}, \qquad \epsilon_2 = \frac{|q|A_2}{mc^2}, \qquad \epsilon_3 = \frac{|q|A_3}{mc^2}. \tag{2.7}$$

Here, α is the angle of wave propagation with respect to the magnetic field and Ω is the magnitude of the nonrelativisitic gyrofrequency.

Resonances occur when $\dot{k}_\perp + l\dot{\theta} = 0$ or

$$\omega - \frac{k_\parallel p_\parallel}{m\gamma_0} - \frac{l\Omega}{\gamma_0} = 0, \tag{2.8}$$

a result which is well-known from linear plasma theory. The resonance surfaces are elliptic when the H-surfaces are hyperbolic and vice-versa. If the wave amplitude is small, than an electron will be affected by at most one resonance. In this case, all but that single resonance's contribution to the Hamiltonian can be ignored, and the Hamiltonian becomes

$$H = H_0(p_\parallel, p_\perp) + Z_l \sin(k_\parallel z), \tag{2.9}$$

where z has been re-defined to absorb $l\theta$. In this re-defined coordinate system, the resonance occurs at a point $(p_{\parallel r}, p_{\perp r})$ where $\dot{z} = 0$. Writing

$$H_0(p_\parallel, p_\perp) \simeq H_0(p_{\parallel r}, p_{\perp r}) + \frac{1}{2} \left.\frac{\partial^2 H_0}{\partial p_\parallel^2}\right|_r (p_\parallel - p_{\parallel r})^2, \tag{2.10}$$

and letting

$$M^{-1} \equiv \left.\frac{\partial^2 H_0}{\partial p_\parallel^2}\right|_r, \tag{2.11}$$

we find that the Hamiltonian becomes

$$\frac{1}{2M}(p_\parallel - p_{\parallel r})^2 + Z_l \sin(k_\parallel z), \tag{2.12}$$

which is just the standard pendulum Hamiltonian.[1] The trapping width and the bounce frequency are given by

$$\Delta p_\parallel = 4|MZ_l|^{1/2} \tag{2.13}$$

and

$$\omega_b = k_\parallel |Z_l/M|^{1/2}, \tag{2.14}$$

respectively.

It is important to note that the term "trapped" has a very specific meaning: it refers to orbits close enough to resonance so that within the rest frame of the resonance (not

3

the wave) the electrons undergo libratory rather than rotatory motion. Electrons not close to a resonance still undergo acceleration but it is far weaker than the acceleration undergone by those which are trapped. Standard rf heating schemes make use of the resonant acceleration just described. Of course, acceleration is limited by the trapping width. While this limitation is of no importance in schemes to heat a bulk plasma to moderate energies, it is of great importance in schemes to heat electrons to ultrarelativistic energies. In this latter case, a stochastic mechanism is needed to break the constraint imposed by the finite trapping widths of the individual resonances. The separation on an H-surface between two adjacent resonances is given by

$$\delta p_\parallel = \frac{mc^2 \Omega k_\parallel}{\omega^2 - k_\parallel^2 c^2}.$$

(2.15)

The stochasticity threshold condition based on the overlap criterion now becomes[2]

$$4\frac{\gamma_0 \omega_b}{\Omega} \gtrsim 1.$$

(2.16)

Once this threshold has been exceeded, it is possible to accelerate electrons from resonance to resonance. We can determine in this way the intensity required to accelerate ionospheric electrons to 10 MeV or more. These calculations may be found in reference 2.

B. Diffusion Equation

One can obtain the basic diffusion equation using either a Fokker-Planck approach[3-5] or a quasilinear approach.[6-7] In either case, one obtains the equation

$$\frac{\partial f}{\partial t} = \frac{\partial}{\partial v}\left(D\frac{\partial f}{\partial v}\right).$$

(2.17)

The Hamiltonian is a function of $p_\parallel$ and $p_\perp$; thus, it is convenient to start with the relativistic diffusion equation in cylindrical coordinates

$$\frac{\partial f}{\partial t} = \frac{1}{p_\perp}\frac{\partial}{\partial p_\perp}\left[p_\perp\left(D_{\perp\parallel}\frac{\partial}{\partial p_\parallel} + D_{\perp\perp}\frac{\partial}{\partial p_\perp}\right)f\right] + \frac{\partial}{\partial p_\parallel}\left[\left(D_{\parallel\parallel}\frac{\partial}{\partial p_\parallel} + D_{\parallel\perp}\frac{\partial}{\partial p_\perp}\right)f\right],$$

(2.18)

where

$$D_{\parallel\parallel} = \int_0^\infty d\tau\, \langle \dot{p}_\parallel(t)\dot{p}_\parallel(t+\tau)\rangle,$$

$$D_{\perp\perp} = \int_0^\infty d\tau\, \langle \dot{p}_\perp(t)\dot{p}_\perp(t+\tau)\rangle,$$

(2.19)

$$D_{\parallel\perp} = D_{\perp\parallel} = \int_0^\infty d\tau\, \langle \dot{p}_\perp(t)\dot{p}_\parallel(t+\tau)\rangle,$$

4

The angular brackets indicate an average over the gyroangle. It is assumed that any initially inhomogeneity in the angular distribution is rapidly smoothed out. Integrating over unperturbed orbits—the standard approximation of quasilinear theory—we find

$$D_{\|\|} = \frac{\pi}{2} k_{\|}^2 \sum_{l=-\infty}^{\infty} Z_l^2 \delta\left(\omega - \frac{k_{\|}p_{\|}}{m\gamma} - \frac{l\Omega}{\gamma}\right),$$

$$D_{\perp\perp} = \frac{\pi}{2}(m\Omega)^2 \sum_{l=-\infty}^{\infty} \frac{l^2}{p_{\perp}} Z_l^2 \delta\left(\omega - \frac{k_{\|}p_{\|}}{m\gamma} - \frac{l\Omega}{\gamma}\right), \qquad (2.20)$$

$$D_{\|\perp} = D_{\perp\|} = \frac{\pi}{2} k_{\|} m\Omega \sum_{l=-\infty}^{\infty} \frac{l}{p_{\perp}} Z_l^2 \delta\left(\omega - \frac{k_{\|}p_{\|}}{m\gamma} - \frac{l\Omega}{\gamma}\right).$$

where Z_l are resonance coefficients from Eq. (2.6) and $\delta(x)$ indicates the usual Dirac δ-function.

These diffusion coefficients are not useful as they stand because they do not take into account the decorrelation due to stochasticity which results in their broadening.[8] Here, we will assume that the δ-functions are broadened by an amount which equals the trapping widths of the undisturbed resonances. This assumption works well in practice as will shortly be apparent from our results. Thus, we replace the δ-function by a function f(x), where

$$f(x) = \begin{cases} 1/4\omega_b, & \text{if } |x| \leq 2\omega_b \\ 0. & \text{if } |x| > 2\omega_b \end{cases} \qquad (2.21)$$

The quantity ω_b corresponds to the bounce frequency in the $l$the resonance.

Because the Hamiltonian H is a conserved quantity, the diffusion proceeds along a constant H-surface, and we can reduce the diffusion equation to one dimension. We replace the coordinates $(p_{\|}, p_{\perp})$ with (H, γ) and obtain the diffusion equation in the form

$$\frac{\partial f}{\partial t} = \frac{1}{\gamma}\frac{\partial}{\partial \gamma}\left(\gamma D_{\gamma\gamma}\frac{\partial f}{\partial \gamma}\right), \qquad (2.22)$$

where

$$D_{\gamma\gamma} = \frac{\pi}{8}\frac{\omega}{(1 - k_{\|}^2 c^2/\omega^2)} \sum_{l=-\infty}^{\infty} \left(\frac{Z_l}{mc^2}\right)^{3/2} \gamma^{1/2} f(\gamma). \qquad (2.23)$$

Note that while the problem has been reduced to one dimension, it is parametcrized by H, and Eq. (2.23) must be solved for the entire range of H-values important in any given problem.

We now must discretize Eqs. (2.22) and (2.23) so that they can be solved numerically. The way in which we have defined $D_{\gamma\gamma}$ implies that its derivative is everywhere zero except

5

on a countable set of points where it becomes infinite: hence, the discretization requires great care. We use a finite element discretization approach which effectively averages the derivatives. including the δ-functions, over a range in γ.[9,10] Multiplying Eq. (2.22) by $\gamma g(\gamma)$, where $g(\gamma)$ is a weight function to be made explicit shortly, and integrating over the domain $\Gamma = (\gamma_{min}, \gamma_{max})$, we find

$$\int_{\Gamma} \gamma g(\gamma) \frac{\partial f}{\partial t} \, d\gamma = - \int_{\Gamma} \gamma D_{\gamma\gamma} \frac{\partial g}{\partial \gamma} \frac{\partial f}{\partial \gamma} \, d\gamma, \tag{2.24}$$

where we have used integration by parts and particle conservation to eliminate the second derivative of f with respect to γ. Dividing the range Γ into N equal sized elements, we may write f as

$$f = \sum_{j=1}^{N} f_j(t) \psi_j(\gamma), \tag{2.25}$$

where the $\psi_j(\gamma)$ are the basis functions for the elements, defined so that

$$\psi_i = \begin{cases} (\gamma - \gamma_{i-1}/(\gamma_i - \gamma_{i-1}, & \gamma_{i-1} \leq \gamma \leq \gamma_i \\ (\gamma_{i+1} - \gamma)/(\gamma_{i+1} - \gamma_i), & \gamma_i \leq \gamma \leq \gamma_{i+1} \\ 0, & \text{otherwise} \end{cases} \tag{2.26}$$

Using the ψ_i as weighting functions and defining the matrices A and B, such that

$$\mathsf{A}_{ij} = \int_{\Gamma} \psi_i \psi_j \gamma \, d\gamma, \qquad \mathsf{B}_{ij} = - \int_{\Gamma} \frac{\partial \psi_i}{\partial \gamma} D_{\gamma\gamma} \gamma \frac{\partial \psi_j}{\partial \gamma} \, d\gamma, \tag{2.27}$$

we find

$$\mathsf{A} \cdot \frac{\partial \mathbf{f}}{\partial t} = \mathsf{B} \cdot \mathbf{f}, \tag{2.28}$$

where $\mathbf{f}$ indicates the vector consisting of the f_j. Since A and B are both tridiagonal, Eq. (2.27) is not difficult to solve.

We have tested the code by running it for cases where the diffusion coefficient has analytical solutions and found the agreement between numerical and analytical results to be excellent. We have also found the number of particles to be typically constant to better than one part in 10^{-5}.

C. Computational Results

In all our numerical calculations, we have taken the initial distribution to be a δ-function at $\gamma = 1$ and we have varied our parameters over a wide range of wave energies. The parameter values we have chosen are consistent with the daytime and nighttime

6

ionospheres.[11] In crucial instances, we have compared single particle calculations with the results from the diffusion code. In these calculations, we have used 256 particles. While this number of particles is not large enough to give us a good solution for the overall evolution of the distribution functions, it is sufficient to allow us to solve for crucial statistical parameters such as the average distance travelled by the electrons and the first two moments: $\langle \gamma - \gamma_0 \rangle$ and $\langle (\gamma - \gamma_0)^2 \rangle$, where γ_0, the initial γ-value, equals one. We carry out our studies for a length of time $\Omega t = 30,000$, which corresponds typically to travel distance of about 20 km for the electrons.[2]

First, we consider the diffusion due to a R-x mode with $\omega/\Omega = 1.97$, $\alpha = 80°$, and $\omega_p/\Omega = 0.3$. The value $\omega_p/\Omega = 0.3$ corresponds to the nighttime ionosphere at 130 km.[11] The threshold for the onset of stochasticity is $\epsilon_{thrs} \sim 0.2$.

We carry out our comparison for wave amplitudes ranging from 0.19 to 10.0. The variation of several quantities is shown in Fig. 1 for $\epsilon = 0.19$. The quantity $\langle (\gamma - \gamma_0)^2 \rangle$ is seen to increase in an approximately linear fashion as expected from the Fokker-Planck equation. For this set of parameters, $D_{\gamma\gamma}$ eventually becomes very small, and $\langle (\gamma - \gamma_0)^2 \rangle$ flattens out, but that does not occur until $\Omega t \gg 3000$. The quantity D/D_{QL}, which is the ratio of the orbit calculation of $\langle (\gamma - \gamma_0)^2 \rangle$ to that obtained from the diffusion code, deviates significantly from unity at earlier times but settles down close to its asymptotic value for $\Omega t \gtrsim 750$. The deviation from quasilinear behavior at early times is largely due to two effects, stickiness and excess coherence due to a small number of resonances.[2] The quantities $\langle z \rangle$ and $\langle z \rangle_{\gamma \geq 10}$ correspond to the average distance travelled for all the electrons and only those electrons with $\gamma = 10$. These two quantities become increasingly equal at large times as an increasing fraction of the electrons surpass the value $\gamma = 10$. We can estimate the value of v_z to be[2]

$$v_z = (\gamma - 1)k_\parallel c^2/\omega\gamma \simeq k_\parallel c^2/\omega \quad , \tag{2.29}$$

which holds for highly relativistic electrons. The solid line in Figs. 1d-e is given by Eq. 2.29, and the deviation indicates that not all the electrons have become relativistic.

The fraction of electrons have $\gamma > 10$ is plotted in Fig. 2. The curves obtained from the diffusion code (solid line) and the particle code (dotted line) agree quite well. Similar results are shown in Figs. 3-6 for wave amplitudes given by $\epsilon = 3.99$ and $\epsilon = 10.0$. The agreement only improves in these cases. In Fig. 7, we show D/D_{QL} in the range $\epsilon = 0.19$

7

to $\epsilon = 10.0$. The quasilinear theory embodied in our diffusion code evidently works well over this range.

We next consider the diffusion due to the L-o mode with $\omega/\Omega = 2.6$, $\alpha = 80°$, and $\omega_p/\Omega = 0.3$. The threshold for stochastic acceleration is given roughly by $\epsilon_{thrs} = 0.4$. Results for several different energies can be found in Figs. 8–10. In this case, a substantial fraction of the electrons are not stochastic even when the threshold is exceeded, and that has an important effect on D/D_{QL}, $\langle z \rangle$, and $\langle z \rangle_{\gamma \geq 10}$. Nonetheless, the fraction of electrons with $\gamma > 10$ agrees well with both methods.

The results of our study of electron acceleration generally confirm the results obtained using simpler methods in reference 2. In particular, large intensities of roughly 20 W/cm^2 are needed to reach the required stochasticity thresholds and acceleration distance on the order of 20 km are needed in order to accelerate a substantial fraction of electrons beyond 5 MeV. The power requirements appear to be well beyond what can be managed with present-day devices. Other mechanisms based on field inhomogeneities, pre-acceleration, and precipitation of already high energy particles remain to be more thoroughly explored.

III. ALFVÈN MASER

A. Overview

The Alfvèn maser (A-maser), as first described by Trakhtengerts and co-workers[12-13], is based on enhancing the reflectivity of the Alfvèn wave within a narrow tube ($\sim$ 10 km $\times$ 10 km) along the field lines in the magnetosphere. This change in reflectivity could be accomplished by rf heating of the ionosphere in the region near the poles where the magnetic field lines are tied down. Trakhtengerts and his colleagues focused primarily on methods for generating the ion cyclotron instability, as was appropriate for the problem of precipitating relatively low energy ions which he was considering. Our focus has been the precipitation of higher energy ions and the exploration of resonant methods which can accomplish this precipitation. Papadopoulos. et al.[14] have shown that the mechanisms discussed by Trakhtengerts and co-workers are insufficient for this purpose for several reasons. namely:

(i) No specific wave mode that interacts strongly with energetic protons ($\epsilon > 1$ MeV) was identified.

(ii) The models rely on quasilinear wavepacket theory. As a result their applicability is limited to proton energies below 1-2 MeV.

(iii) The transverse variation of the medium and finite ion gyroradius effects were ignored.

As a result. we concentrated on scenarios which excite the highly localized ($m \to \infty$) poloidal oscillations of the magnetospheric cavity at the appropriate L value by modulated RF heating of the F-region ionosphere. These modes are thought to be excited naturally by inverted ion distribution functions,[15,16] electron beams,[17] surface waves due to the Kelvin-Helmholtz instability,[18,19] and/or external impulses.[20,21] These are monochromatic field line oscillations and have often been observed in conjunction with energetic particle precipitation. We have named the process Field Resonance Induced Precipitation (FRIP). Notice that the physics of FRIP is completely different than the physics of the Trakhtengerts A-Maser. based on quasilinear diffusion. both in the mode excitation processes as well as the particle precipitation process. The differences will be emphasized later on. The two important issues related to the feasibility of FRIP are

(i) Identification and verification of the physics related to the induced energetic proton precipitation.

(ii) The requirements and location for exciting the appropriate field line resonances

These are discussed in the next section.

B. Radiation Belt Dynamics

Before entering the discussion of the physics issued related to the FRIP concept we briefly present the parameters that control the trapping and the precipitation of the energetic protons in the earth's radiation belts. Figure 11 shows the trajectory of a trapped particle in the earth's dipole field. Particles trapped in the earth's RB execute three types of motions. First, a gyration about the magnetic field with the local gyrofrequency Ω_c, second a longitudinal motion governed by the effective potential energy,

$$u_\parallel = \mu B(s) \tag{3.1}$$

where $\mathbf{B}$ is the magnetic field, s is the coordinate along a line of force and

$$\mu = \frac{v_\perp^2}{2B} = \frac{v^2 \sin^2 \alpha}{2B} \tag{3.2}$$

is the orbital magnetic moment; α is the angle between the velocity $\mathbf{v}$ and the field $\mathbf{B}$. This motion results in the particle bouncing between mirror points along the field line with a frequency ω_b. Third is a slow azimuthal drift. These motions are shown in Fig. 11. The value of the magnetic field B_E at the equator is given approximately by

$$B_E(L) = \frac{.3}{L^3} \text{ gauss}, \tag{3.3}$$

while the average value of the gyrofrequency in the dipole field is given by

$$\bar{\Omega}_c = \Omega_{cE} \frac{F(\alpha)}{G(\alpha)}, \tag{3.4}$$

10

where $\Omega_{cE} = 3 \times 10^3/L^3$ sec^{-1}, $G(\alpha) = 1.3 - .56 \sin \alpha$, and $F(\alpha) \simeq (-0.2 \sin^2 \alpha + 0.7 \sin \alpha + 2)/\sin^2 \alpha$. In the absence of interactions, the magnetic moment μ is an adiabatic invariant. The same holds true for the action

$$J = \oint \mathbf{v} \cdot d\mathbf{s} \quad,$$

which is associated with the bounce motion. There is also a third adiabatic invariant, the flux invariant Φ, associated with the drift motion.

C. Induced Precipitation

Energetic protons will be confined in the radiation belts as long as their adiabatic invariants are conserved. The rate at which protons enter the loss cone and precipitate depends mainly on the time scale on which the adiabatic invariant J changes. Two general types of processes exist. First, low frequency, random fluctuations will lead to a quasilinear, diffusive random walk in J. Second, coherent fields can lead to resonant excitation and stochasticity. It is this latter type of process which we are proposing to use, rather than the former type proposed by Trakhtergents and co-workers.[12,13]

The guiding center of a trapped particle oscillates between its mirror points with a frequency given approximately by

$$\omega_b = 2.2 \frac{\sqrt{T(\text{MeV})}}{L} \quad. \tag{3.5}$$

In general, the magnetic field does not vary quadratically with distance along the field line, leading to a significant anharmonicity in the bounce frequency. In other words, $\omega_b = \omega_b(\beta_E)$, where β_E is the particle's pitch angle at the equator, for particles with the same value of T. However, this anharmonicity does not significantly alter the results and does complicate the discussion. So, we ignore it here. Our equation of motion is given by

$$\ddot{s} + \omega_b^2 s = 0 \quad, \tag{3.6}$$

which comes from the Hamiltonian

$$H_o = \frac{p_s^2}{2m} + \frac{1}{2} m \omega_b^2 s^2 = 0 \quad. \tag{3.7}$$

11

Making the action-angle transformation,

$$p_s = (2Im\omega_b)^{1/2}\cos\theta \ , \quad s = (2I/m\omega_b)^{1/2}\sin\theta \ . \tag{3.8}$$

the Hamiltonian becomes

$$H_o = \omega_b I \ , \tag{3.9}$$

with equations of motion

$$\dot{I} = 0 \ , \quad \dot{\theta} = \omega_b \ . \tag{3.10}$$

The presence of electromagnetic forces with components parallel to **B**, will change the value of J. Forces parallel to **B** can be due to parallel electric fields $E_\parallel$ or due to compressional magnetic perturbations $b_\parallel$. The latter represent a form of Fermi acceleration. In the presence of such forces, the equation of motion becomes

$$\ddot{s} + \omega_b^2 s = \frac{eE_\parallel(s,t)}{m} - \mu\frac{\partial b_\parallel(s,t)}{\partial s} \ . \tag{3.11}$$

The strongest interaction will of course occur for forces oscillating near ω_b.

We now suppose that the fields are fluctuating with random time variations. Such fluctuations induce random variations in the oscillation amplitude, causing a random walk of a particle's J value and a redistribution of J described by a Fokker-Planck equation. Roberts and Schultz[22] showed that spatial variations allow the oscillator to interact with the fields at harmonics of the bounce frequency. However, the overall effectiveness of the bounce resonance processes is reduced for oscillation amplitudes large with respect to the scale of the spatial variations. For situations where $\mu = \text{const}$, the Fokker-Planck equation describing the evolution of the distribution function $f(\epsilon_\parallel, \epsilon_\perp)$ is

$$\frac{\partial f(\epsilon)}{\partial t} = \frac{\partial}{\partial \epsilon_\parallel} D \frac{\partial}{\partial \epsilon_\parallel} f \ , \tag{3.12a}$$

$$D = \omega_b^2 \sum_{n=1}^{\infty} n^2 \int_{-\infty}^{\infty} \frac{dk_\parallel}{2\pi} J_n^2(k_\parallel s_m) \frac{K_p(k_\parallel, n\omega_b)}{k_\parallel^2} \ , \tag{3.12b}$$

12

where s_m is the maximum value of s in the unperturbed oscillation, the J_n are Bessel functions, and K_p is the relevant power spectrum. These relations can be derived from Eq. (3.11) by using second order perturbation theory and defining D as

$$D = \frac{1}{2} \frac{< (\Delta \epsilon_\parallel)^2 >}{\tau} \tag{3.13}$$

Of greater interest to us is the case where we may assume $E_\parallel(s,t) = E_o \cos(ks - \omega t)$. In later sections, we will explicitly consider Alfvèn waves in which case

$$ks \rightarrow \int_o^s \frac{\omega}{v_A(s')} \, ds' \quad , \tag{3.14}$$

and E_o becomes a weakly varying function of s. The effect is to add harmonics of the fundamental wavenumber

$$E_o \cos(ks - \omega t) \rightarrow \sum_{n=0}^{\infty} E_n \cos\left[(2n + 1)ks - \omega t\right] \quad , \tag{3.15}$$

which has little impact on the final result. Our equation of motion now becomes

$$\ddot{s} + \omega_b^2 s = \frac{eE_o}{m} \cos(ks - \omega t) \quad , \tag{3.16}$$

Letting $\sigma = ks$ and $\tau = \omega_b t$, Eq. (3.16) becomes

$$\ddot{\sigma} + \sigma = \frac{eE_o k}{m\omega_b^2} \cos(\sigma - \Omega\tau) \quad , \tag{3.17}$$

where $\Omega = \omega/\omega_b$. This equation of motion can be derived from the Hamiltonian

$$H = \frac{p_\sigma^2}{2} + \frac{\sigma^2}{2} + \Omega R - \frac{eE_o k}{m\omega_b^2} \sin(\sigma - \phi) \quad , \tag{3.18}$$

where (R, ϕ) are a canonical pair of variables. Making the action-angle transformation

$$\sigma = (2I)^{1/2} \sin\theta \quad , \quad p_\sigma = (2I)^{1/2} \cos\theta \quad , \tag{3.19}$$

13

so that in physical units $I = (U - \mu B_E)k^2/m\omega_B^2$, where U is the kinetic energy and B_E is the magnetic field at the equation, our Hamiltonian now becomes

$$H = I + \Omega R - \epsilon \sin\left[(2I)^{1/2}\sin\theta - \phi\right] \quad , \qquad (3.20)$$

where $\epsilon = eE_o k/m\omega_c^2$ which is, to within a phase, the well-known Hamiltonian considered by Karney[23] in the context of rf heating. For a fixed value of ϵ and Ω, Karney showed that the orbits are stochastic in the range

$$\Omega - \epsilon^{1/2} < (2I)^{1/2} < (4\epsilon\Omega)^{2/3}(2/\pi)^{1/3} \quad , \qquad (3.21)$$

where the latter value holds exactly in the limit $(2I)^{1/2} \gg \Omega$ but yields a reasonable approximation even when $(2I)^{1/2} \sim \Omega$. An illustration of the stochastic region for a fixed value of Ω is shown in Fig. 12.

As an example, we find that if $\Omega = 10$, then the threshold for stochasticity is approximately at $\epsilon = 1$; however, larger values are required to obtain significant acceleration. In physical units, our conditions become

$$\frac{\omega}{\omega_B} - \left(\frac{eE_o}{m\omega_B v_{AE}}\frac{\omega}{\omega_B}\right)^{1/2} < \left(\frac{2T}{3mv_{AE}^2}\frac{\omega^2}{\omega_B^2}\right)^{1/2} < \left(\frac{2}{\pi}\right)^{1/3}\left(4\frac{eE_o}{m\omega_B v_{AE}}\frac{\omega^2}{\omega_B^2}\right)^{2/3} \quad , \quad (3.22)$$

where $v_{AE} = v_A$ at the equator. Writing

$$\frac{eE_o}{m\omega_B v_{AE}} = 0.01\frac{E_o(\text{mV/m})}{\sqrt{T(\text{Mev})}}L^{5/2} \quad ,$$

$$\frac{2T}{3mv_{AE}^2} = 3.3\left[T(\text{Mev})\right]L^3 \quad , \qquad (3.23)$$

we see that at $L = 4$, and setting as before $\Omega = 5$, a field of 7 mV/m is needed to achieve $\epsilon = 5$ for a 200 kev proton. At this value of E, protons are stochastic if $30 < I < 430$ and our 200 kev proton has $I = 42$. We see that if $\epsilon = 5$ and $\Omega = 10$ are maintained by ramping up the E-field and the frequency, a parallel energy gain of 10 is possible, leading to precipitation of most 200 kev protons. One can think of many other possible scenarios for precipitation. As will be discussed later, such fields can be excited due to finite ion

14

gyroradius effects when Alfvèn field aligned resonances are driven by periodic heating of the F-region.

D. Geomagnetic Field Tube Oscillations

A number of authors[24-26] have calculated the eigenfrequencies of magnetic field lines for various distributions of v_A along the magnetic field lines using the boundary condition $E(s = \pm l) = 0$. This boundary condition is correct only for sufficiently large ionospheric conductivities. The resonant frequencies are independent of the conductivity only when $v_A(s) = $ const and the conjugate ionospheres are symmetric. In this case, the fundamental resonance frequency $\omega_o(L)$ is given by

$$\omega_o \approx \frac{\pi v_A}{L r_o} \quad .$$

(3.24)

where r_o is the earth radius. A complete analysis using the inhomogeneous wave equation was performed by Arykov and Maltsev.[27] The wave equation for guided Alfvèn waves is given by

$$\frac{\partial^2}{\partial s^2} \frac{\mathbf{E}}{\sqrt{B_o}} = \frac{1}{v_A^2(s)} \frac{\partial^2}{\partial t^2} \left(\frac{\mathbf{E}}{\sqrt{B_o}} \right)$$

(3.25)

In Eq. (3.25), the field curvature and the transverse dependence of v_A are neglected. This is correct for relatively small transverse dimensions.[28] The resonator properties can be described by introducing the function A, defined as[27]

$$\frac{\Delta E}{E_o} = A \sqrt{\frac{B_o}{B_{oi}}} \frac{\Delta \Sigma}{2 \Sigma_{PN}} \quad ,$$

(3.26)

where $\Delta \Sigma$ is the change of the ambient electric field E_o in the ionosphere if the Pedersen conductivity varies from Σ_{PN} by $\Delta \Sigma$ in the northern hemisphere; B_{oi} is the magnetic field on the ionosphere. Note that if $A = 1$, then $\Delta \Sigma$ equals the polarization field in the modified area, on condition that there is vacuum above the ionosphere. Assuming that $\Delta \Sigma$ varies periodically with frequency ω, the equation describing the excitation factor A is

$$\frac{\partial^2}{\partial s^2} A + \frac{\omega^2}{vA^2} A = 0 \quad ,$$

(3.27)

15

with the boundary conditions

$$A + \frac{c^2}{4\pi i\omega\Sigma_{PS}}\frac{\partial A}{\partial s} = 0 \quad s = -l \quad, \tag{3.28a}$$

$$A + \frac{c^2}{4\pi i\omega\Sigma_{PN}}\frac{\partial A}{\partial s} = 0 \quad s = +l \quad. \tag{3.28b}$$

The function A depends only on the frequency and on the characteristics of the resonator only. Equation (3.28a) gives passive reflection of the guided waves from the southern conjugate, while (3.28b) describes reflection and generation. For the magnetosphere, an analogous excitation factor A_B defined by

$$\Delta\mathbf{B} = -A_B\frac{c}{v_A}\frac{1}{\sqrt{B_oB_{oi}}}\frac{\mathbf{B}_o\times\mathbf{E}_o\Delta\Sigma}{2\Sigma_{PN}} \quad, \tag{3.29}$$

can be introduced. Following Arykov and Maltsev,[27] we approximate $v_A(s)$ by

$$v_A(s) = v_{AE}\left(1 + \frac{s^2}{a^2}\right) \tag{3.30}$$

In this case Eq. 3.27 can be solved to give

$$A = \sqrt{\frac{s^2 + a^2}{l^2 + a^2}}\frac{1}{\eta_-^N}\frac{e^{iu_o - iu} + R_s e^{3iu_o + iu}}{1 - R_N R_s e^{4iu_o}} \quad, \tag{3.31}$$

where

$$R_{N,S} = -\frac{\eta_+^{N,S}}{\eta_-^{N,S}} \quad, \tag{3.32a}$$

$$\eta_\pm^{N,S} = \frac{c^2}{4\pi i\omega E_{PN,S}}\frac{l \pm ia\sqrt{1 + a^2\omega^2/v_{AE}^2}}{l^2 + a^2} \quad, \tag{3.32b}$$

$$u = \sqrt{1 + a^2\omega^2/v_{AE}^2}\arctan(s/a) \quad, \tag{3.32c}$$

$$u_o = u(s = l) \quad. \tag{3.32d}$$

16

In order to analyze the situation further we note that using WKB theory, we find

$$\omega_o = \frac{\pi}{\int_{-l}^{l} \frac{ds}{v_A(s)}} = \frac{\pi V_{AE}}{2a \arctan(l/a)} \quad , \tag{3.33}$$

where ω_o is the frequency of the fundamental mode. We now introduce the inhomogeneity parameter $\lambda = l/a$ and the ratio of the ionospheric conductivity to the wave conductivity at the equator, $\sigma = \Sigma_p/\Sigma_w$, where $\Sigma_w = c^2/4\pi v_{AE}$. If $\lambda = 0$, corresponding to a homogeneous magnetosphere, we find

$$A = \frac{1 - R_N}{2} \frac{\exp\left[-\frac{\pi}{2}i\frac{\omega}{\omega_o}\left(\frac{s}{l}-1\right)\right] + R_s \exp\left[\frac{\pi}{2}i\frac{\omega}{\omega_o}\left(\frac{s}{l}+3\right)\right]}{1 - R_N R_S \exp\left(2\pi i\frac{\omega}{\omega_o}\right)} \quad , \tag{3.34}$$

where

$$R_{N,S} = (1 - \sigma_{N,S})/(1 + \sigma_{N,S}) \quad . \tag{3.35}$$

Arykov and Maltsev[27] calculate the value of A in the conjugate ionospheres. Our interest here lies on the equatorial plane $s = 0$. The results are shown in Fig. 13, for symmetric and antisymmetric ionospheres. The most interesting result is the one shown in Fig. 14 which shows the amplitude-frequency characteristic for $A_B = i(v_A/\omega)(\partial A/\partial s)$. A strong resonance is not possible on the odd harmonics, but only on the even ones, i.e., $\omega = 2n\omega_o$.

Using the simple model, $v_A = v_{Ao}(r_o/r)^{3/2}$, where $v_{Ao} = 4.4 \times 10^8$ cm/sec is the Alfvèn speed near the Earth's surface and r_o is the Earth's radius, we find from integration of Eq. (3.33) that $\omega_o = 6.8 \times 10^{-2}$ sec^{-1} when $L = 4$. Hence, in the example of the previous section in which $\omega = 10\omega_B = 2.5$ sec^{-1} we find that $n \simeq 18$.

E. Stability of the Shear Alfvèn Wave

In this section, we will show that the transverse mode structure can be determined separately from the longitudinal structure and that the shear Alfvèn wave is stable. We have investigated both diffraction and mode-mode coupling and shown that they are completely negligible at the low parallel mode numbers of the shear Alfvèn wave. Indeed, the only limitation on the transverse size of the mode is that it must be large compared to an ion gyroradius for the basic dispersion relation to be valid.

17

Our starting point is the equations

$$\nabla \times \mathbf{B} = -\frac{i\omega}{c}\mathsf{K} \cdot \mathbf{E},$$

$$\nabla \times \mathbf{E} = \frac{-i\omega}{c}\mathbf{B},$$

(3.36)

where, assuming we have low frequency modes, but keeping higher-order cyclotron corrections, we have

$$\mathsf{K} = \begin{pmatrix} 1 + \frac{c^2}{v_A^2}\left(1 + \frac{\omega^2}{\Omega_i^2}\right) & i\frac{c^2}{v_A^2}\frac{\omega}{\Omega_i} & 0 \\ -i\frac{c^2}{v_A^2}\frac{\omega}{\Omega_i} & 1 + \frac{c^2}{v_A^2} & 0 \\ 0 & 0 & \frac{\omega_{pe}^2}{\omega^2} \end{pmatrix},$$

(3.37)

where, writing $\mathbf{E} = (E_1, E_2, E_3)^t$, E_1 and E_2 are transverse to the zero-order magnetic field and E_3 is directed along it. At low frequencies, E_3 is essentially zero for consistency. To drive an appropriate Fresnel criterion for Alfvèn waves in magnetospheric flux tubes, we first ignore geometric effects and obtain

$$\det \begin{vmatrix} 1 + \frac{c^2}{v_A^2}\left(1 + \frac{\omega^2}{\Omega_i^2}\right) - \frac{c^2 k_\parallel^2}{\omega^2} & i\frac{c^2}{v_A^2}\frac{\omega}{\Omega_i} \\ -i\frac{c^2}{v_A^2}\frac{\omega}{\Omega_i} & 1 + \frac{c^2}{v_A^2}\left(1 + \frac{\omega^2}{\Omega_i^2}\right) - \frac{c^2 k^2}{\omega^2} \end{vmatrix} = 0.$$

(3.38)

To lowest order in ω^2/Ω_i^2, we obtain the dispersion relation

$$v_A^2 = \frac{\omega^2}{k_\parallel^2} + \frac{\omega^2}{\Omega_i^2}\frac{\omega^2}{k_\perp^2}$$

(3.39)

when $k_\perp \gg k_\parallel$ as in the case in a confined mode. We then find that

$$\frac{d\omega}{dk_\perp} = \frac{\omega}{\Omega_i^2}v_A\frac{k_\parallel^3}{k_\perp^3}.$$

(3.40)

Thus, the more we *reduce* the transverse dimensions of the wave, the less it diffracts! We conclude that diffraction imposes no limit on the transverse width of the mode. The width need only be large enough to validate the dispersion relation, *i.e.*, it must be large compared to the ion gyroradius. This radius is roughly 10 m when $L = 4$. Hence, a transverse width of a kilometer or more should be sufficient to provide confinement.

18

To investigate the effect of mode coupling, we first note that

$$\frac{v_s^2}{v_A^2} = 4\pi N k T B_0^2 \simeq 10^{-4} \tag{3.41}$$

when $L = 4$. Hence, acoustic coupling is completely negligible. To consider coupling to the magnetosonic wave, we write Eq. (3.36) in dipole (Radoski) coordinates.[28] It becomes

$$\frac{1}{h_\nu h_\mu} \frac{\partial}{\partial \mu} h_\nu B_\nu = \frac{is}{h_\nu} \left(\frac{mc}{\omega h_\phi} E_\nu - \frac{sc}{\omega h_\nu} E_\phi \right) + \frac{i\omega}{c} \left(1 + \frac{c^2}{v_A^2} \right) E_\phi, \tag{3.42a}$$

$$+ \frac{\omega^2}{\Omega_i^2} \frac{c}{v_A^2} E_\nu,$$

$$\frac{1}{h_\phi h_\mu} \frac{\partial}{\partial \mu} h_\phi B_\phi = \frac{im}{h_\phi} \left(\frac{mc}{\omega h_\phi} E_\nu - \frac{sc}{\omega h_\nu} E_\phi \right) - \frac{i\omega}{c} \left(1 + \frac{c^2}{v_A^2} \right) E_\nu, \tag{3.42b}$$

$$+ \frac{\omega^2}{\Omega_i^2} \frac{c}{v_A^2} E_\phi,$$

$$\frac{1}{h_\nu h_\mu} \frac{\partial}{\partial \mu} h_\nu E_\nu = -\frac{i\omega}{c} B_\phi, \tag{3.42c}$$

$$\frac{1}{h_\phi h_\mu} \frac{\partial}{\partial \mu} h_\phi E_\phi = \frac{i\omega}{c} B_\nu, \tag{3.42d}$$

where for any quantity, we have let

$$X(\mu, \nu, \phi) = X(\mu) \exp(is\nu + im\phi). \tag{3.43}$$

Defining now,

$$R_1 = \frac{m}{h_\phi} E_\nu - \frac{s}{h_\nu} E_\phi,$$
$$R_2 = \frac{m}{h_\phi} E_\phi + \frac{s}{h_\nu} E_\nu, \tag{3.44}$$

so that R_1 corresponds to the magnetosonic wave and R_2 corresponds to the shear Alfvèn wave, we find that

$$\frac{1}{h_\mu} \frac{\partial}{\partial \mu} \frac{1}{h_\mu} \frac{\partial}{\partial \mu} h_\mu R_1 - \left(\frac{h_\phi}{h_\nu} \frac{\partial}{\partial \mu} \frac{h_\nu}{h_\phi} \right) \frac{1}{h_\mu^2} \frac{\partial}{\partial \mu} \frac{(m^2 h_\nu^2 - s^2 h_\phi^2)}{(m^2 h_\nu^2 + s^2 h_\phi^2)} h_\mu R_1$$

$$- \left(\frac{m^2}{h_\phi^2} + \frac{s^2}{h_\nu^2} \right) h_\mu R_1 + \frac{\omega^2}{v_A^2} h_\mu R_1 \tag{3.45}$$

$$= \left(\frac{h_\phi}{h_\nu} \frac{\partial}{\partial \mu} \frac{h_\nu}{h_\phi} \right) \frac{2}{h_\mu^2} \frac{\partial}{\partial \mu} \frac{m s h_\nu h_\phi}{(s^2 h_\phi^2 + m^2 h_\nu^2)} h_\mu R_2,$$

19

where we neglect the vacuum and cyclotron contributions to Eq. (3.42). If either m or s is equal to zero, the magnetosonic wave is not coupled to the shear Alfvèn wave. That is because curvature induces a field pointed in the radial direction to produce a component in the parallel direction while a field pointed in the azimuthal direction is not affected by curvature. Coupling cannot be induced in either case. Noting that at low parallel mode numbers all parallel derivatives $\partial / h_\mu \partial \mu$ scale as $1/r_0$, and assuming as well that $k_\perp r_0 \gg 1$. where

$$k_\perp^2 = \frac{m^2}{h_\phi^2} + \frac{s^2}{h_\nu^2}, \qquad (3.46)$$

we find that

$$R_1 \sim \frac{\lambda_\perp^2}{R_0^2} R_2, \qquad (3.47)$$

where $\lambda_\perp$ roughly equals the transverse width of the confined mode. Thus, the intensity of the magnetosonic wave is a completely negligible fraction of the shear Alfvèn wave and leads to negligible attenuation.

$$\frac{1}{h_\mu} \frac{\partial}{\partial \mu} I_A \sim -\frac{\lambda_\perp^4}{R_0^4} I_A. \qquad (3.48)$$

Thus, we may set $R_1 = 0$ and all dependence on m and s disappears in Eq. (3.42). We may in principle determine the entire mode structure by solving one pair of equations, for instance

$$\frac{1}{h_\nu h_\mu} \frac{\partial}{\partial \mu} h_\nu B_\nu = \frac{i \omega c}{v_A^2} E_\phi,$$
$$\frac{1}{h_\phi h_\mu} \frac{\partial}{\partial \mu} h_\phi B_\phi = \frac{i \omega}{c} B_\nu, \qquad (3.49)$$

and determining E_ν and B_ϕ through the relations

$$\frac{m}{h_\phi} E_\nu = \frac{s}{h_\nu} E_\phi,$$
$$\frac{m}{h_\phi} B_\phi = \frac{s}{h_\nu} B_\nu. \qquad (3.50)$$

20

These results imply that the longitudinal and transverse parts separate and that the transverse portion is substantially but not completely arbitrary. From Eq. (3.49), we may write a solution which satisfies a particular set of boundary conditions as

$$E_\phi = g_1^e(\mu) f_\alpha(\nu, \varphi),$$
$$B_\nu = g_1^b(\mu) f_\alpha(\nu, \varphi). \tag{3.51}$$

The two functions $g_1^e(\mu)$ and $g_1^b(\mu)$ are determined from Eq. (3.49), which is purely longitudinal. Note that the transverse shape factor for E_ϕ and B_ν is necessarily the same. Similarly, we may write

$$E_\nu = h_1^e(\mu) f_\beta(\nu, \varphi),$$
$$B_\phi = -h_1^b(\mu) f_\beta(\nu, \varphi). \tag{3.52}$$

Our task now is to determine what constraints Eq. (3.50) imposes on the relationship between f_α and f_β. Using Fourier transform methods, we can show that this equation implies

$$\frac{\partial}{\partial \phi} f_\beta(\nu, \phi) = \frac{\partial}{\partial \nu} f_\alpha(\nu, \phi), \tag{3.53}$$

and, what is more, Eq. (3.53) implies Eq. (3.50). Thus, we choose *either* f_α or f_β arbitrarily, but the other is then fixed to within a constant.

As an example, we may consider

$$f_\alpha(\nu, \phi) = f_0 \exp\left[-a(\nu - \nu_0)^2 - b(\phi - \phi_0)^2\right], \tag{3.54}$$

which corresponds to a localized Alfvèn mode. It follows that

$$f_\beta = \frac{b}{a} f_\alpha(\nu, \phi), \tag{3.55}$$

so that the relative strength of these two shape factors is determined by the falloff of the overall amplitude. Equation (3.55) can be viewed as a result of quasi-neutrality. In this example, the wave is linearly polarized, but other polarizations result when we allow a and b to be complex. In particular, if we set

21

$$a = \frac{1-i}{\sqrt{2}} A, \qquad b = \frac{1+i}{\sqrt{2}} A, \tag{3.56}$$

we find that the resulting wave is circularly polarized. As a final point, we note that a circularly symmetric shape cannot in general be maintained along an entire Alfvèn tube. To obtain a circularly symmetric shape at a single point, we demand that

$$f_\alpha \propto f_\beta \propto F\left\{ \left[a(\nu - \nu_0)^2 + b(\phi - \phi_0)^2 \right]^{1/2} \right\}, \tag{3.57}$$

where $a = h_{\nu_0}^2$ and $b = h_{\phi_0}^2$ at that point. As h_ν and h_ϕ change along the field line, the shape will become assymmetric.

We may thus determine the resonant frequencies by solving the one-dimensional longitudinal equations. In the WKB approximation, we obtain the frequencies derived in the previous section.

F. Kinetic Alfvèn Wave and Proton Precipitation

The analysis presented in the previous two sections was based on MHD equations, In the presence of transverse gradients, the Alfvèn mode has a singularity.[18,19] For time varying waves this effect is manifested in an increase in the transverse wave vector of the wave described by [29]

$$\frac{\partial \mathbf{k}}{\partial t} = -\frac{\partial \omega}{\partial \mathbf{x}}, \qquad \frac{\partial \mathbf{x}}{\partial t} = \frac{\partial \omega}{\partial \mathbf{k}}. \tag{3.58}$$

Under magnetospheric conditions this increase in the wave-number occurs over a very fast scale,[30] so that the transverse wave-vector $k_\perp$ becomes larger than $k_\parallel$. In order to account for the transverse structure, non-ideal MHD effects must be incorporated. These are the electron inertia (c/ω_e) and the ion gyroradius R_i. Incorporating these effects, the dispersion relation becomes[31]

$$\omega = k_\parallel v_A (1 + k_\perp^2 A^2) . \tag{3.59}$$

The value of A depends on the ion temperature. For cold ions, $\beta < m_e/m_i$, and we find c/ω_e, while in the opposite limit we find $A \simeq \sqrt{3}R_i/2$. In the latter case, a kinetic analysis yields[31]

22

$$\omega^2 = k_z^2 v_A^2 \frac{\lambda_i}{1 - I_o(\lambda_i)\exp(-\lambda_i)} + \lambda_s \quad , \tag{3.60}$$

where $\lambda_i = k_\perp^2 R_i^2$, $\lambda_s^2 = \lambda_i T_i/T_e$, and I_o is the modified Bessel function of the first kind. This wave is known as the kinetic Alfvèn wave (KAW). The presence of a weak transverse dispersion produces a small group velocity across $\mathbf{B}$, given by

$$\frac{\partial \omega}{\partial k_\perp} = \omega k_\perp A^2 \quad . \tag{3.61}$$

For $k_\perp \leq (\omega/\Omega_i)^{1/2} k_\parallel$, the presence of weak dispersion can trap the KAW near the minimum of the transverse profile of v_a and produce an Alfvèn waveguide for the KAW similar to the one discussed in the previous sections for the shear Alfvèn wave. Such a waveguide can be produced by the plasmapause as well as by magnetospheric ducts. Notice that Pc1 pulsations have been interpreted as eigenmodes of such waveguides.[32,33]

The presence of guided KAW modes allowed us to identify a new process that can break the second adiabatic invariance of multi-Mev protons. The process relies on the fact that the KAW has an electric field component E_z parallel to the magnetic field. It is given by[34]

$$E_\parallel = \left| \frac{\omega \delta B_\perp}{k_\perp \times \hat{e}_z} \right| \frac{\left[1 - I_o(k_\perp^2 R_i^2)e^{-k_\perp^2 R_i^2}\right](T_e/T_i)}{1 + \left[1 - I_o(k_\perp^2 R_i^2)e^{-k_\perp^2 R_i^2}\right](T_e/T_i)} \quad . \tag{3.62}$$

For $(k_\perp R_i)^2 \ll 1$, $T_e < T_i$, we find

$$E_\parallel = \frac{k}{k_\perp} \cdots (k_\perp^2 R_i^2) \quad . \tag{3.63}$$

Assuming, $k_\perp R_i = 0.1$ which is a reasonable value for the Pc1 pulsations, we find that $E_\perp \sim 10$ mV/cm in the example of section 3B. This field strength can be obtained from ground-based transmitters.

IV. EXPERIMENTAL REQUIREMENTS

A. Concept Summary

The FRIP concept (Fig. 15) relies on injection of large amplitude ULF waves, generated by modulated heating of the ionosphere, into the geomagnetic force tube bounded by the modified ionospheric area. If the modulation frequency equals one of the field tube resonances or its harmonic, the plasma filled force tube behaves as a high Q cavity. As a result the excitation level of its resonant modes (i.e., shear Alfvèn waves) increases substantially. The guided Alfvèn waves are incompressive and their electric field is transverse to the ambient magnetic field. However, magnetic field and plasma inhomogeneities, finite ion Larmor radius effects and dynamics couple the shear Alfvèn wave, to a kinetic Alfvèn wave (KAW). The kinetic Alfvèn wave is also a confined mode in the presence of plasma ducts.

The KAW has an electric field component parallel to the magnetic field. When the value of the parallel electric field in the equatorial region exceeds values of mV/m protons with Mev energy become strochastic (i.e., their second adiabatic invariant is broken) and can thus precipitate.

The requirements for breakdown of the second adiabatic invariant and induced proton precipitation can be approximated by

$$\omega_b = 2n\omega_o \tag{1}$$

$$E_o > \frac{m}{e}\omega_b^2 L R_E \tag{2}$$

where E_o is the parallel electric field of the KAW, ω_b is the bounce frequency of the precipitated protons, ω_o is the fundamental frequency of Alfvènic oscillations of the field line with fixed ends, n the harmonic number, R_E the earth radius and L the magnetic shell number. If we assume a simple model of the equatorial values in the radiation belts

$$B = .3\frac{1}{L^3}G \tag{3}$$

$$n_e = 5 \times 10^4 \frac{1}{L^4} \#/cm^3 \tag{4}$$

24

and take

$$\omega_b \approx \frac{2.2}{L} \sqrt{\frac{T}{MeV}} \qquad (5)$$

We can express (1) and (2) in a quantitative fashion. The value of n required for precipitating protons of energy T(MeV) at a value L is given by

$$n = \frac{L}{5.5} \sqrt{\frac{T}{\text{MeV}}} \qquad (6)$$

and the associated value of E_o is given by

$$E_o > \frac{14}{L} \left(\frac{T}{\text{MeV}}\right) \text{mV/m} \qquad (7)$$

Figure 16 gives the value of $f_o = \omega_o/2\pi$ as a function of L for the model given by (3) and (4).

For example, in order to precipitate 1 Mev protons at L = 6 we should drive the shell at its fundamental frequency f_o = .03 Hz, with sufficient strength that the value of E_o at the equator exceeds 2 mV/m. To precipitate 4 Mev protons we should drive the field at its second harmonic, i.e., .06 Hz, and the required value of E_o would be 8 mV/m, etc. The practical implementation of the system depends on the efficiency with which ground based HF power can be converted into KAW power in the magnetospheric cavity. This is examined next.

B. System Requirements

In terms of implementing FRIP, the major issue concerns the efficiency with which modulated HF power injected in the ionosphere is transformed into power in the KAW in the equatorial region. We present below estimates based on modifying the ionospheric conductivity of the lower ionosphere (D-E region) (Figure 15).

For a dipole magnetic field the value of ΔE of the electric field in the equatorial plane is given by

$$\Delta E \simeq A \ \frac{1}{\cos^3 \varphi} \ \frac{1}{L^{3/2}} \ \frac{\Delta \Sigma}{\Sigma_p} \ E_o$$

25

where E_o is the ionospheric field, φ the latitude and A is the amplitude frequency characteristic of oscillating tube of force with allowance for the resonance properties. (A $\approx$ 1-10). The value of the height integrated Pedersen conductivity Σ_p varies from .1 mho for night time conditions to 1-10 mho during daytime conditions. The value of E_o is of the order of 25 mV/m in the high latitude ionosphere and reaches values of 100-150 mV/m during substorms. It is obvious that night time conditions are favored. Values of $\Delta E_\perp \approx 10$ mV/m compatible with threshold require values of $\Delta \Sigma \approx .1$ mho. This implies an energy deposition into electrons of 10^{15} eV/m^2 per ULF period. For an area of 25 km^2, the required energy deposition to electrons will be of the order 1-2 kJ. Since the frequency is of the order of a second, the required power absorption by electrons will be of the order of 1-2 kW. Given the inefficiency of long time electron heating in the D-E region it will require an HF facility with 1-2 MW ground power operating in the 4-7 MHz region.

C. Key Research Issues

1. What is the value of the electric field generated in the region for frequencies in the range .01-10 Hz as a function of the HF power density and frequency and ambient conditions?

2. What is the Q value (i.e., value of A) for the magnetospheric shell cavity modes and their harmonics?

3. What is the conversion efficiency from the shear to the kinetic Alfvèn wave in the equatorial plane?

4. Are there any feedback effects due to the enhanced precipitation?

A combination of satellite and/or rocket experiments in conjunction with the operation of a strong high frequency (i.e., 5-12 MHz) heater can provide quantitative answers to these questions. Preliminary experiments can be performed using the Tromso Max Planck facility. However the planned HAARP facility could be a good instrument to investigate the FRIP concept.

REFERENCES

1. A. J. Lichtenberg and M. A. Lieberman, *Regular and Stochastic Motion*, (Springer-Verlag, New York, 1983).

2. C.R. Menyuk, A.T. Drobot, K. Papadopoulos, and H. Karimadabi, *Phys. Rev. Lett.*, **58**, 2071 (1987); and *Phys. Fluids*, **31**, 3768 (1988).

3. S. Chandrasekhar, *Rev. Mod. Phys.*, **15**, 1 (1943).

4. Y.A. Romanov and G.F. Filipov, *Sov. Phys.*, JETP **13**, 87 1961).

5. P.A. Sturrock, *Phys. Rev.*, **141**, 186 (1966).

6. A.A. Vedenov, E.P. Velikhov, and R.Z. Sagdeev, *Nucl. Fusion*, **1**, 82 (1961); *Nucl. Fusion Suppl.* **2**, 465 (1962).

7. W.E. Drummond and D. Pines, *Nucl. Fusion Suppl.*, **3**, 1049 (1962).

8. T.H. Dupree, *Phys. Fluids* **9**, 1773 (1966).

9. L. Muschietti, K. Appert, and J. Vaclavik, *Phys. Fluids* **24**, 151 (1981).

10. G. Dhatti and G. Touzot, *The Finite Element Displayed* (John Wiley, New York, 1984).

11. Y.L. Alpert and D.S. Fligel, *Propagation of ELF and VLF Waves Near the Earth* (Consultants Bureau, New York, 1970), p. 7.

12. V.Y. Trakhtegerts and Z. Vselennaya, *Active Experiments in Space*, **ESA SP-195**, p. 61, 1983.

13. P.A. Bespalov and V.Y. Trakhtengerts, *Reviews of Plasma Physics*, Vol. 10, p. 155, M.A. Leontovich, Ed., Consultants Bureau, N.Y.-London (1986).

14. K. Papadopoulos, R. Smith, and A. Drobot, SAIC Report to AFGL 1988.

15. W.J. Hughers, R.L. McPherron, and J.N. Barfield, *J. Geoph. Res.*, **83**, 1109 (1978).

16. V.I. Karpman, B.I. Meerson, A.B. Mikhailovsky, and O.P. Pokhotelov, *Planet. Space Sciences.* **25**, 573 (1977).

17. A. Hasegawa, *Geophys. Res. Lett.*, **6**, 644 (1979).

18. L. Chen and A. Hasegawa, *J. Geophys. Res.*, **79**, 1024 (1974).

19. D.J. Southwood, *Planet. Space Sci.*, **22**, 483 (1974).

20. L.J. Lauzenotti, H. Fukushini, A. Hasegawa, and L. Chen, *Phys. Rev. Lett.*, **31**, 324 (1974).

21. L. Chen and A. Hasegawa, *J. Geophys. Res.*, **79**, 1024 (1974).

22. C.S. Roberts and M. Shulz, *J. Geophys. Res.*, **73**, 7361 (1968).

23. C.F.F. Karney, *Phys. Fluids* **21**, 1584 (1978).

24. A.V. Gul'yel'mi and A.R. Polyakov, *Geomagnetism and Aeronomy*, **23**, 281 (1983).

25. H.S. Singer, *J. Geophys. Res.*, **86**, 4589 (1981).

26. W.D. Cummings, R.J. O'Sullivan, and P.J. Coleman, Jr., *J. Geophys. Res.*, **74**, 778 (1969).

27. A.A. Arykov and Yu P. Mal'tsev, *Planet. Space Sci.*, **4**, 463 (1979).

28. H.R. Radoski, *J. Geophys. Res.*, **72**, 18 (1967).

29. A.V. Timofeev, *Reviews of Plasmas Physics*, Vol. 9, Consultants Bureau, N.Y. (1986).

30. A.S. Leonovich and V.A. Mazur, *Sov. J. Pl. Physics*, **13**, 461, (1986).

31. A. Hasegawa and C. Uberoi, *The Alfvèn Wave*, (Tech. Inf. Center, USDOE, 1982).

32. I.S. Dimitriemco and V.A. Mazur, *Planet Space Sci.*, **33**, 471 (1985).

33. A.S. Leonovich, *Geomagnetism and Aeronomy*, **24**, 75 (1984).

34. A. Hasegawa and L. Chen, *Phys. Fluids*, **19**, 1924 (1976).

FIGURE CAPTIONS

1. Time evolution of various quantities for $\omega/\Omega = 1.97$, $\omega_p/\Omega = 0.3$, $\alpha = 80°$, and $\epsilon = 0.19$. The wave is an R-x mode. The unmarked lines in d and c are obtained assuming $v_z = n_{\parallel}c$.

2. Time evolution of $F(\delta > 10)$. Time evolution of various quantities for $\omega/\Omega = 1.97$, $\omega_p/\Omega = 0.3$, $\alpha = 80°$, and $\epsilon = 0.19$. The unmarked curve is from the diffusion code and the marked curve is from the particle code.

3. Time evolution of various quantities for $\omega/\Omega = 1.97$, $\omega_p/\Omega = 0.3$, $\alpha = 80°$, and $\epsilon = 3.9$. The wave is an R-x mode. The unmarked lines in d and c are obtained assuming $v_z = n_{\parallel}c$.

4. Time evolution of $F(\delta > 10)$. Time evolution of various quantities for $\omega/\Omega = 1.97$, $\omega_p/\Omega = 0.3$, $\alpha = 80°$, and $\epsilon = 3.9$. The unmarked curve is from the diffusion code and the marked curve is from the particle code.

5. Time evolution of various quantities for $\omega/\Omega = 1.97$, $\omega_p/\Omega = 0.3$, $\alpha = 80°$, and $\epsilon = 10.0$. The wave is an R-x mode. The unmarked lines in d and c are obtained assuming $v_z = n_{\parallel}c$.

6. Time evolution of $F(\delta > 10)$. Time evolution of various quantities for $\omega/\Omega = 1.97$, $\omega_p/\Omega = 0.3$, $\alpha = 80°$, and $\epsilon = 10.0$. The unmarked curve is from the diffusion code and the marked curve is from the particle code.

7. D/D_{QL} as a function of wave amplitude. The scale of the x-axis is linear but the scale from 0.19 to 0.99 is different than that fron 0.99 to 10.

8. Time evolution of various quantities for $\omega/\Omega = 2.6$, $\omega_p/\Omega = 0.3$, $\alpha = 80°$, and $\epsilon = 0.427$. The wave is an L-o mode. Some particles are accelerated in the negative z-direction and the approximation $v_z = n_{\parallel}c$, given by the unmarked line, is no longer adequate.

9. Time evolution of various quantities for $\omega/\Omega = 2.6$, $\omega_p/\Omega = 0.3$, $\alpha = 80°$, and $\epsilon = 3.9$. The wave is an L-o mode. Some particles are accelerated in the negative z-direction and the approximation $v_z = n_{\parallel}c$, given by the unmarked line, is no longer adequate.

10. Time evolution of various quantities for $\omega/\Omega = 2.6$, $\omega_p/\Omega = 0.3$, $\alpha = 80°$, and $\epsilon = 10.0$. The wave is an L-o mode. Some particles are accelerated in the negative z-direction and the approximation $v_z = n_{\parallel}c$, given by the unmarked line, is no longer adequate.
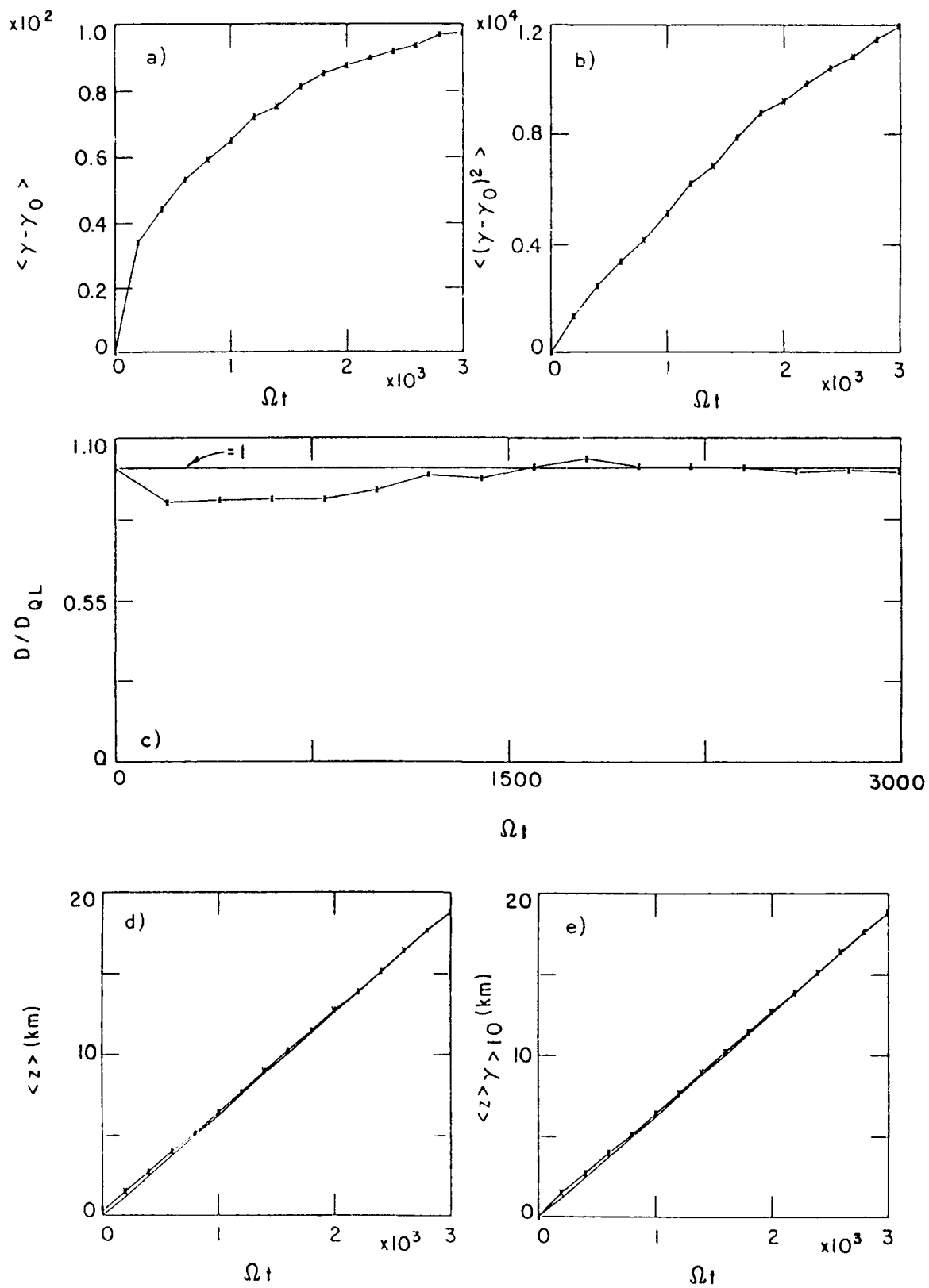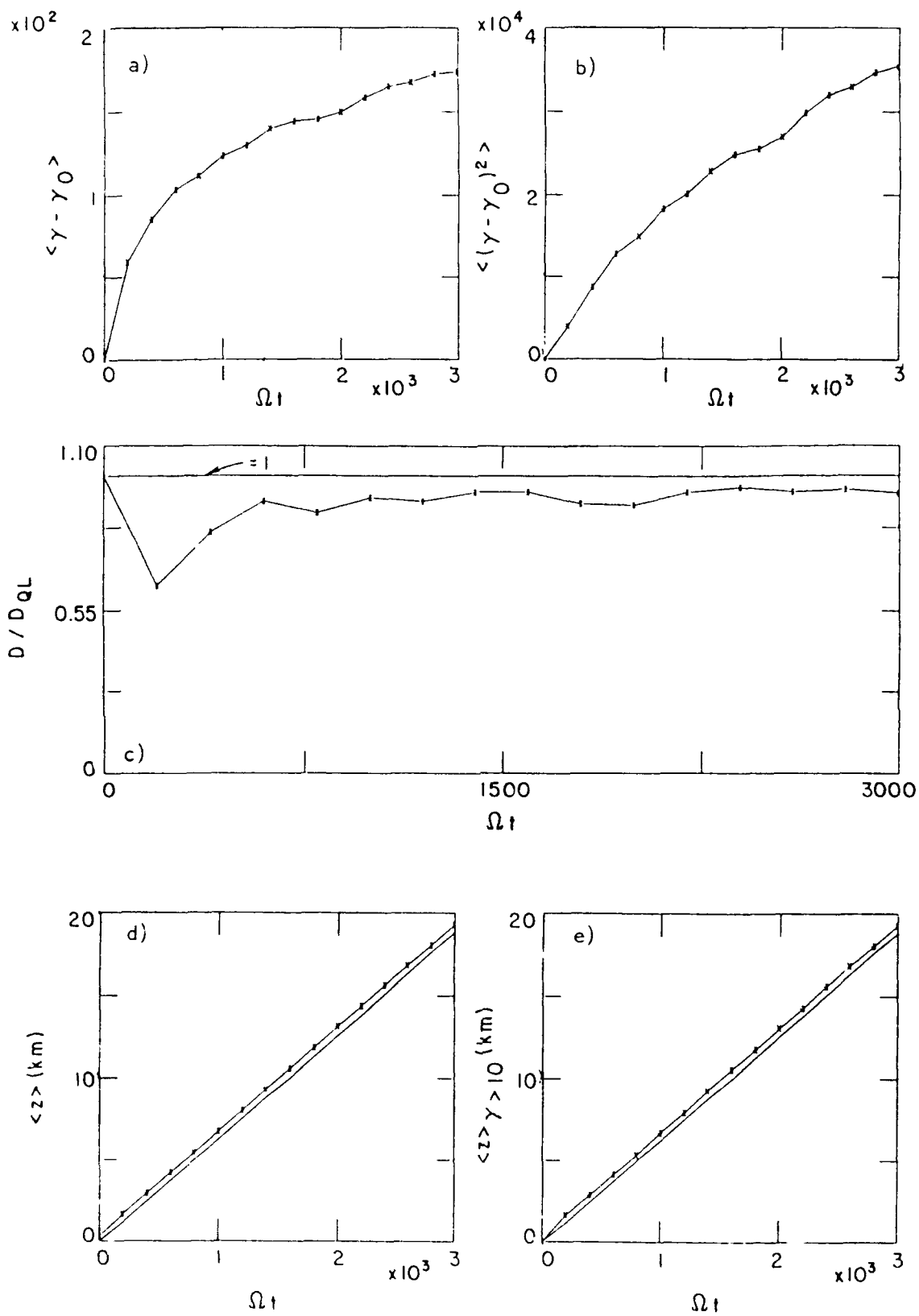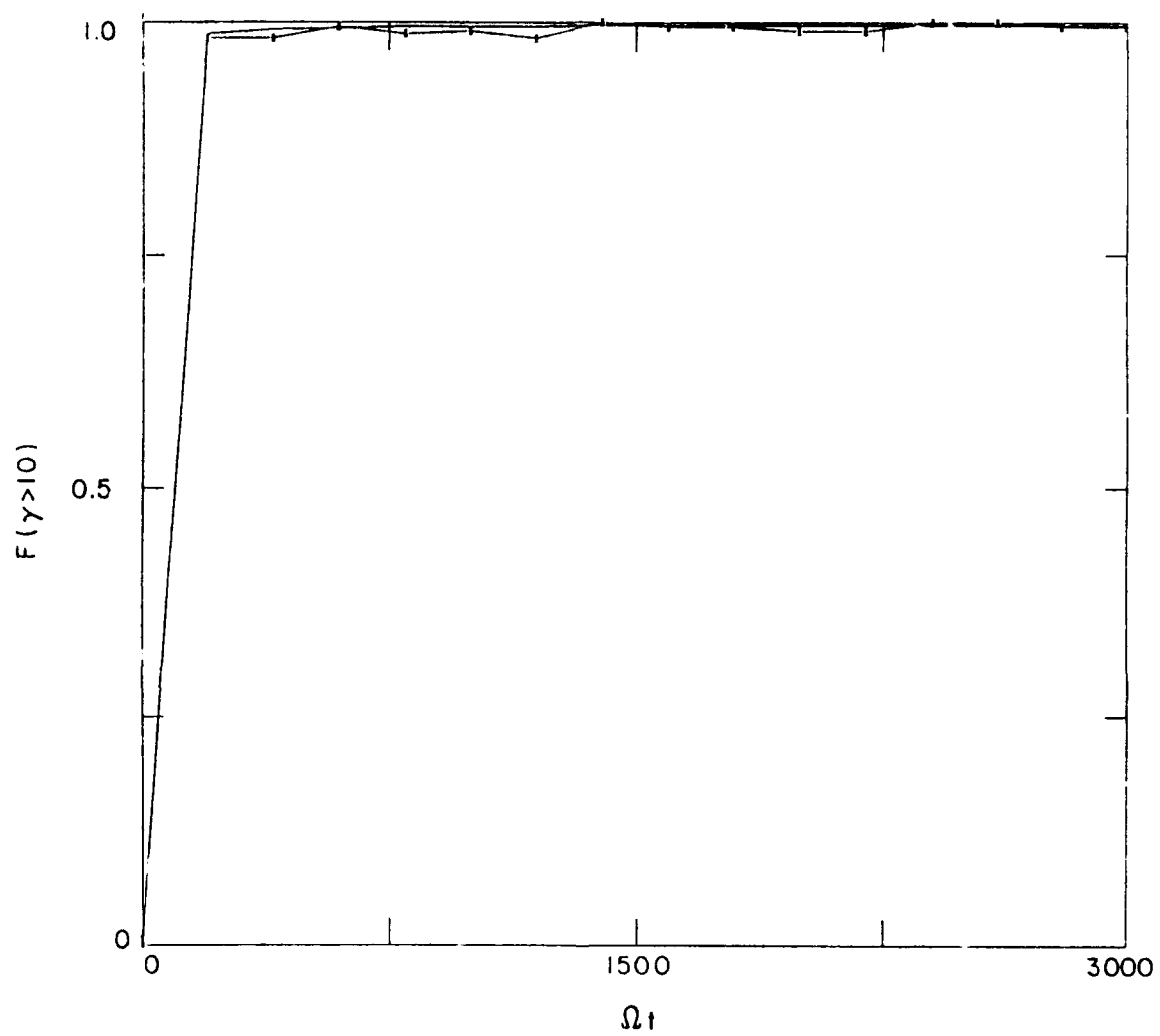
Figure 1

Figure 2

Figure 3
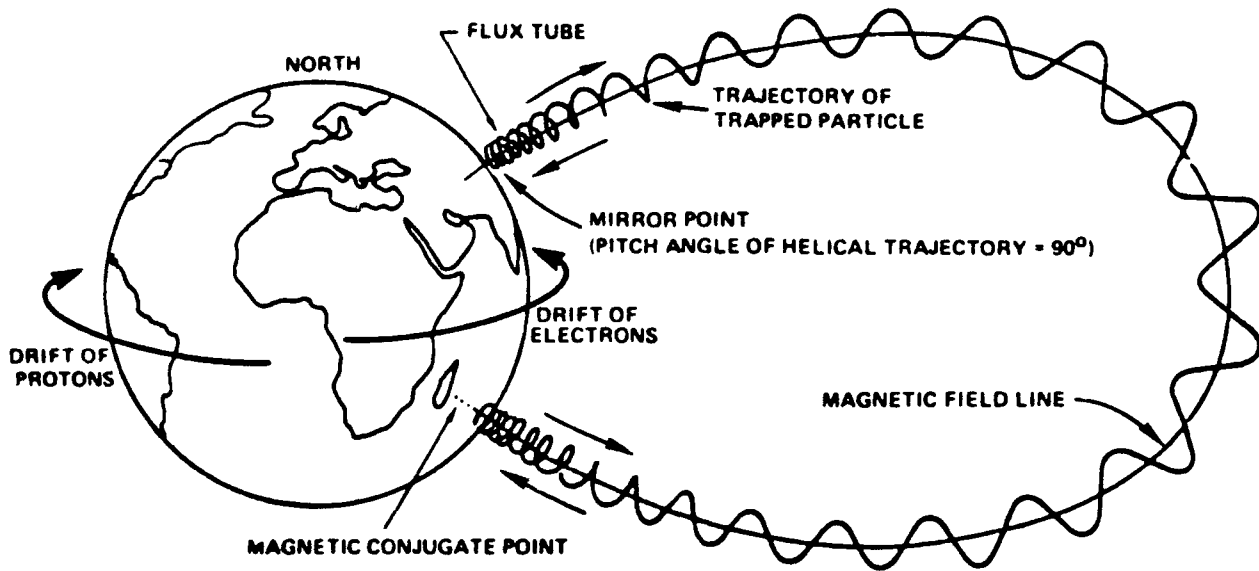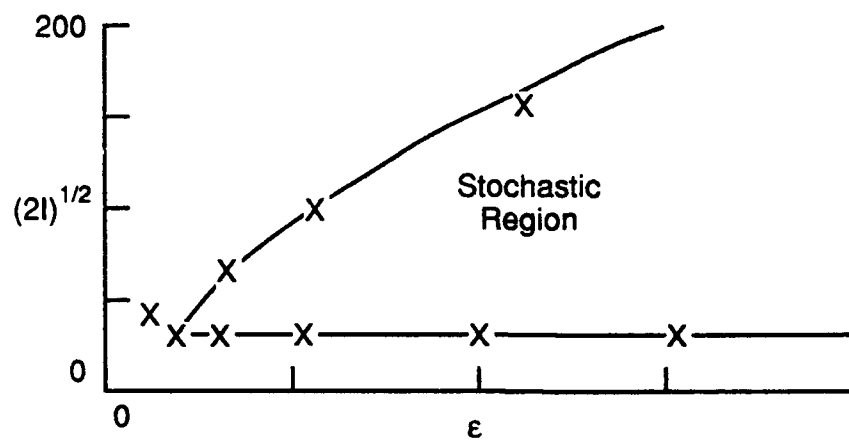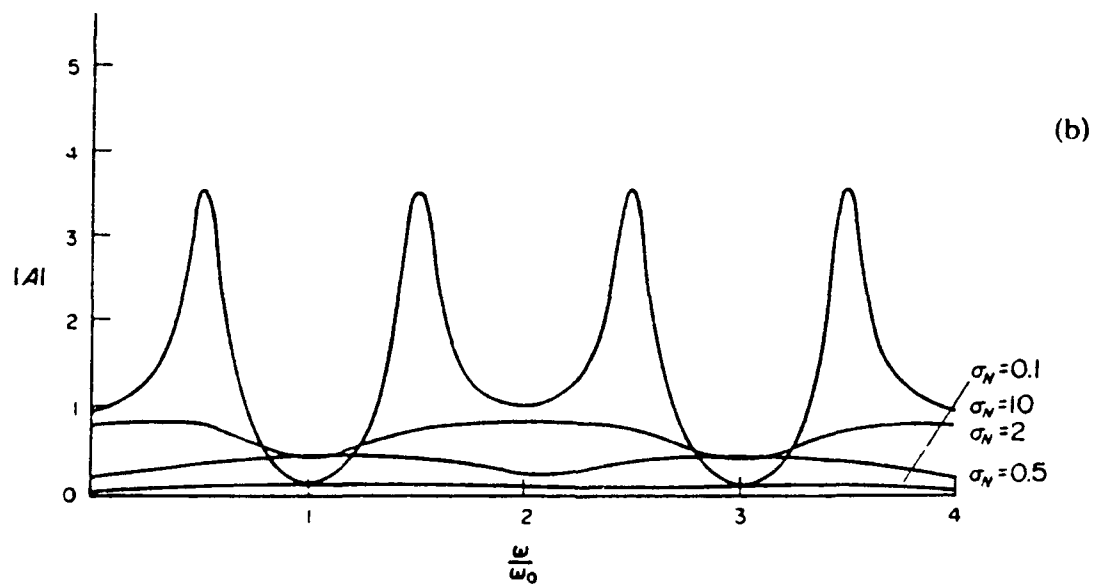
33

Figure 4

34

Figure 5

Figure 6

36

Figure 7

Figure 8

Figure 9

39

Figure 10

40

FLUX TUBE

NORTH

TRAJECTORY OF
TRAPPED PARTICLE

MIRROR POINT
(PITCH ANGLE OF HELICAL TRAJECTORY = 90°)

DRIFT OF
ELECTRONS

DRIFT OF
PROTONS

MAGNETIC FIELD LINE

MAGNETIC CONJUGATE POINT
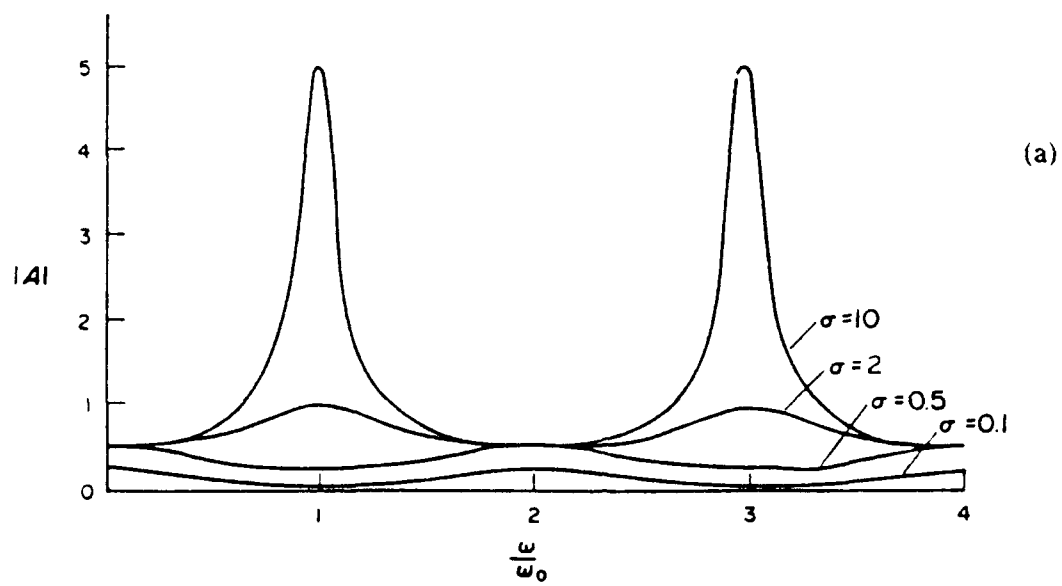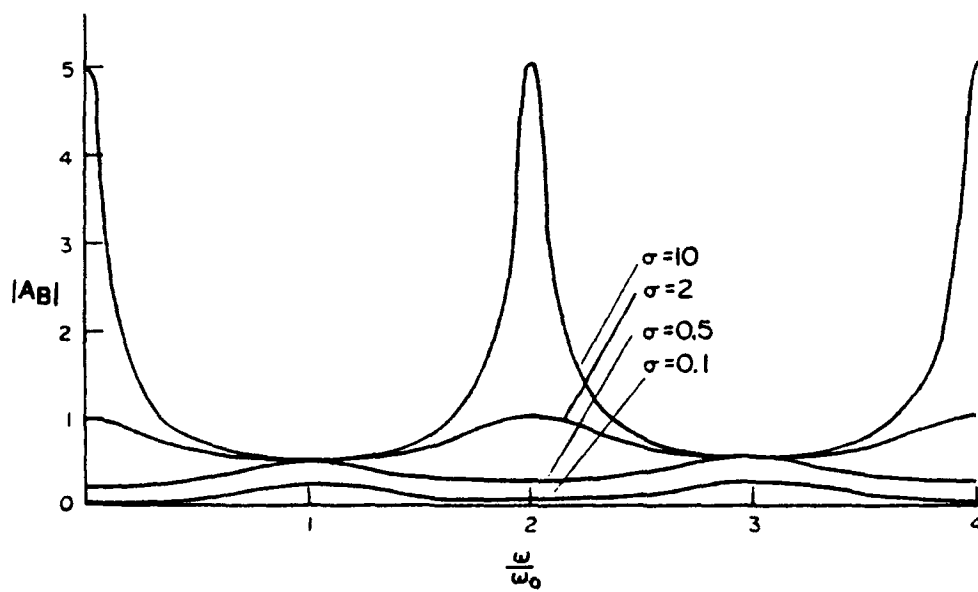
Figure 11

41

Figure 12

Figure 13

43

Figure 14

44

Figure 15

Figure 16

Appendix A

Nature of the Diffusion above the Chaotic Threshold

H. Karimabadi, C. R. Menyuk[a]

Deaprtment of Electrical and Computer Engineering
University of California, San Diego, California 92093

Abstract

The diffusion coefficient for particles in a magnetized plasma and in the presence of a coherent wave was calculated numerically. The results were compared with the solution of a diffusion equation based on the quasilinear theory. The ratio of the numerical to the quasilinear diffusion coefficient D/D_{QL} was found to be between 0.9 and 1.4 for wave amplitudes sufficiently above the stochasticity threshold. No coherent oscillation of D/D_{QL} as a function of wave amplitude was observed. The above results held up in all of our parameter study.

(a) Department of Electrical Engineering, University of Maryland, Baltimore, Maryland 21228.

The quasilinear theory[1] and its domain of validity has remained an area of active research due to its relevance to so many different areas of physics. Recent advances in nonlinear dynamics have revealed that even systems of low dimensionality can exhibit complex behavior. Thus, more recent tests of the quasilinear theory have been for systems of low dimensionalities. Using the standard map to model a chaotic system, several authors[2] found that the true diffusion oscillates about the quasilinear value as a function of the nonlinearity parameter with the discrepancy between the two reaching as high as 2.5. The key question is how much of the discrepancy is due to the nature of the approximations made and how much is due to the limitations of quasilinear theory. In this letter, we consider the validity of the quasilinear theory in a physical system. We investigate the problem of particle diffusion in a magnetized plasma and in the presence of a coherent wave. We derive a diffusion equation and model the diffusion coefficient based on the resonance broadening theory[3]. We have developed an algorithm that allows a rapid and accurate solution of the diffusion equation. Thus we have been able to carry out a detailed study of the particle diffusion and its comparison withe quasilinear theory.

In a magnetized plasma, there are many resonances given by $\omega - k_\parallel v_\parallel = \ell\Omega/\gamma$. When the wave amplitude is small, the resonances are separated and the particle motion is integrable. As the wave amplitude becomes larger than a certain threshold, the adjacent resonances overlap and particle motion becomes chaotic[4] and can in turn be desribed by a diffusion equation. We start our analysis with the usual diffusion equation in 2-D that is averaged over the gyroangle. The solution of the 2-D diffusion equation is in general difficult and computationally expensive. It has, however, been shown[5] that the particles follow the constant Hamiltonian surface in phase space. Thus by transforming to a coordinate system that has the Hamiltonian as one of the axes, we can further reduce the diffusion equation to 1-D. The decorr   ion due to stochasticity is incorporated into the diffusion coeeficient by means of the resonance oroadening theory. The usual delta function associated with each resonance in the diffusion coefficient is now replaced by a box having a width of $2\omega_b$ and a height proportional to $1/\omega_b$, where ω_b is the bounce frequency. The resulting diffusion equation is:

$$\frac{\partial f}{\partial t} = \frac{1}{\gamma}\frac{\partial}{\partial \gamma}\left(\gamma D_{\gamma\gamma}\frac{\partial f}{\partial \gamma}\right), \tag{1a}$$

where

$$D_{\gamma\gamma} = \frac{\pi}{8} \frac{\omega}{(1 - N_{\parallel}^2)^{1/2}} \sum_{\ell=-\infty}^{\infty} (\frac{Z_\ell}{mc^2})^{3/2} \gamma^{1/2}. \tag{1b}$$

In the regions where resonances overlap, the height of the boxes add.. The resulting diffusion coefficient is quite bumpy as shown in Figure 1 and we use the finite element technique to solve the diffusion equation.

We have tested the code by running it for cases where the diffusion equation has analytic solutions and found the agreement between the results of simulation and analysis to be excellent. The number of particles are typically constant to better than one part in 10^{-5}.

In order to test the quasilinear theory, we have solved the diffusion equation for many different parameters and compared the results with exact orbit calculations. We take the initial particle distribution function to be a delta function centered at $\gamma = 1$. In the exact orbit calculations, we follow the orbits of 256 particles, all with initial $\gamma = 1$ and phases distributed uniformly between 0 and 2π, up to $\Omega t = 3000$. The reason for the choice of the integration time is made clear below. The resulting distribution function is very bumpy due to the small number of particles used. To obtain smooth distributions, millions of particles would need to be used - an approach which is both both impractical and unnecessary. Instead, we compare the moments of the two distribution functions. The small number of particles which we use is sufficient in this case to yield an accurate result. In what follows, we use the quantities $< \gamma - \gamma_0 > \equiv < \Delta\gamma >$ and $< (\gamma - \gamma_0)^2 > \equiv < (\Delta\gamma)^2 >$ to make the comparison, where γ_0 is the initial γ of the particles and the brackets indicate an average over the initial conditions:

$$< (\gamma - \gamma_0)^2 > = \frac{\int_1^\infty (\gamma - \gamma_0)^2 f(\gamma, t) d\gamma}{\int_1^\infty f(\gamma, t) d\gamma}. \tag{2S}$$

Note that $D_{\gamma\gamma} \propto < (\Delta\gamma)^2 >$.

We present the results for two sets of parameters: First, we consider the diffusion due to a R-x mode with $\omega/\Omega = 1.97$, $\alpha = 80°$, and $\omega_p/\Omega = 0.3$. The values of stochasticity threshold ϵ_{thrs} calculated from analysis and simulations are 0.19 and 0.143, respectively. We carry out our comparison for wave amplitudes ranging from 0.19 to 10. The variation of several quantities as functions of time are shown in Fig.2 for $\epsilon = 0.19$. The quantity $< (\Delta\gamma)^2 >$ is seen to follow a linear increase in time in accord with the underlying assumptions built into the Fokker-Planck equation. The particles have not had enough time to sample all the available resonances and as a result the

quantity $< (\Delta\gamma)^2 >$ increases with time. Once the particles reach the energies beyond which $D_{\gamma\gamma}$ becomes very small, the $< (\Delta\gamma)^2 >$ flattens out as a function of time and diffusion stops. For the parameters of Fig.2, the flattening out does not happen until $\Omega t \gg 3000$.

The quantity D/D_{QL} which is the ratio of the exact orbit calculation of $< (\Delta\gamma)^2 >$ to that obtained from the diffusion code, deviates significantly from unity at early times (Fig.10c) but settles down close to its asymptotic value for $\Omega t \gtrsim 750$. This is expected since the diffusion formalism is strictly valid for times long compared with correlation time scales. Similar results were also seen at higher amplitudes.

The deviation of particle motion from the predicted quasilinear diffusion at early times can occur due to at least two effects: First, there can exist small but finite islands of stability within an otherwise stochastic phase space. A particle coming close to such an island can get temporarily trapped. Such stickiness in phase space can obviously have an effect on the diffusion of the particles. As it turns out, however, this effect is not that important in general and does not play a significant role for $\Omega t \gtrsim 750$. As we mentioned earlier, the trapping width increases as a function of harmonic number and in the transition to global chaos, the border of chaos lies at the lowest energies. Since we start the particles at $\gamma = 1$, and the stickiness is most important at the border of chaos which is also at $\gamma \sim 1$, the particles often experience some initial stickiness; however, once the particles reach the higher energies, they diffuse freely. Thus, there exists a finite time before all the particles can diffuse freely. The second source of deviation from the predicted quasilinear behavior is that the particles may initially sample a few resonances in which case the motion is closer to a coherent acceleration than diffusion. The first effect results in a retardation in the diffusion and the second effect leads to diffusion larger than D_{QL}. The balance between these two effects determines D/D_{QL} at early times. For $\Omega t \gtrsim 750$, the above two effects become much less important.

We have plotted $< \gamma > / < \gamma_s >$ and D/D_{QL} at $\Omega t = 3000$, for a range of wave amplitudes as shown in Fig.3. The quasilinear theory appears to be quite adequate in describing the particle motion over this rather large range in wave amplitude. For $\epsilon \gg 10$, the particle motion approaches the integrable regime of unmagnetized plasma in which case the diffusion equation would no longer be valid. The deviation of D/D_{QL} from unity as a function of wave amplitude has a sporadic behavior and does not seem to follow a nice oscillating pattern. In short, we have found no evidence

for oscillations of D/D_{QL} as a function of wave amplitude, in contrast to earlier studies based on the standard mapping[2]. Furthermore, the fluctuation amplitude of D/D_{QL} is much smaller than that seen in previous numerical work. The presence of resonances of different sizes clearly leads to averaging beyond that which is found in the standard map and thus to a closer correspondence to quasilinear theory. These results suggest that the standard map is not an ideal paradigm for real, physical systems.

Next, we consider the diffusion eqn due to the L-o mode with $\omega/\Omega = 2.6$, $\alpha = 80°$, and $\omega_p/\Omega = 0.3$. The value of threshold based on analysis is 0.42, and the wave amplitude necessary to accelerate 1% and 60% of the particles stochastically from zero energy is 0.4 and 0.75, respectively. The quantity $< \Delta\gamma > / < \Delta\gamma >_{QL}$ is well below unity for $\epsilon = 0.43$ and it does not reach unity until the wave amplitude has been increased to $\epsilon \sim 1.5$. For $\epsilon \gtrsim 1.5$, the $< \Delta\gamma > / < \Delta\gamma >_{QL}$ has small fluctuations about unity. The $< \Delta\gamma >_{QL}$ was obtained by using $H = 1$. Phase effects are important for the L-o mode and the ϵ_{thrs} depends strongly on the value of H which has a finite range even for $\gamma = 1$. The ϵ_{thrs} can change by more than a factor of 3 depending on the value of H. Thus, we must take into account the fraction of particles that are not stochastic at a given wave amplitude. The ratio of stochastic particles is $\sim 60\%$ at $\epsilon = 0.43$, $\sim 75\%$ at $\epsilon = 0.8$, $\sim 80\%$ at $\epsilon = 1.1$, $\sim 93\%$ at $\epsilon = 1.3$, and $\sim 99\%$ at $\epsilon = 1.5$. This is why $< \Delta\gamma > / < \Delta\gamma >_{QL}$ is below unity for $\epsilon \lesssim 1.5$. Let us denote the integrable particles by the subscript 'int' and the stochastic particles by the subscript 'st'. What we should really be plotting in Fig.4a is $< \Delta\gamma >_{st} / < \Delta\gamma >_{QL}$ and not $< \Delta\gamma > / < \Delta\gamma >_{QL}$. But $< \gamma >_{st} / < \gamma >_{QL} \sim \frac{(N_{int}+N_{st})}{N_{st}} < \gamma > / < \gamma >_{QL}$, where we have assumed $< \gamma >_{int} / < \gamma >_{QL} \ll 1$. Using the values of N_{st} cited above for various ϵ's, it then follows that $< \Delta\gamma >_{st} / < \Delta\gamma >_{QL}$ is indeed very close to unity. In short, the discrepancy between $< \Delta\gamma >$ and $< \Delta\gamma >_{QL}$ in Fig.4a for $\epsilon \lesssim 1.5$, is due to the fact that we have included integrable orbits in $< \gamma >$ but not in $< \Delta\gamma >_{QL}$. The fraction of stochastic particles can be easily calculated analytically by incorporating phase effects in the expression for the stochasticity threshold. We then find that stochastic particles are well described by the diffusion code.

The agreement between D and D_{QL} is again very good for a large range of wave amplitudes as shown in Fig.4b. This is encouraging considering that the theoretical analysis presented in this paper are at their worst for the parameters in Fig.4 where the phase effects are important and H

is not just confined to one value. Thus, we conclude that the diffusion formalism is quite robust and is highly accurate in predicting the time evolution of an ensemble of particles.

Acknowledgement

References

[1] A. A. Vedenov, E. P. Velikhov, and R.Z. Sagdeev, *Nucl. Fusion.* **1**, 82 (1961); *Nucl. Fusion Suppl.*, **2**, 465 (1962); W. E. Drummond, and D. Pines, *Nucl. Fusion Suppl.*, **3**, (1990).

[2] A. B. Rechester, and R. B. White, *Phys. Rev. Lett.*, **44**, 1586 (1980); A. B. Rechester, M.N. Rosenbluth, and R. B. White, *Phys. Rev. Lett.*, **A23**, 2664, (1981).

[3] T. H. Dupree, *Phys. Fluids*, **9**, 1773 (1966).

[4] B. V. Chirikov, *Phys. Rep.* **52**, 263 (1979).

[5] C. R. Menyuk, A. T. Drobot, K. Papadopoulos, and H. Karimabadi, *Phys. Rev. Lett.*, **58**, 2071 (1987); and *Phys. Fluids*, **31**, 3768 (1988); K. Akimoto, and H. Karimabadi, *Phys. Fluids.* **31**, 1505 (1988); H. Karimabadi, K. Akimoto, N. Omidi, and C. R. Menyuk, *Phys. Fluids B*, **2**, 606 (1990).

Figure Captions

Figure 1. Diffusion Coefficient. The parameters used are $\omega_p/\Omega = 0.3$, $\omega/\Omega = 1.97$, $\alpha = 80°$, and $\epsilon = 0.19$. The wave is a R-x mode. Only the diffusion coefficient between $\gamma = 1$ and $\gamma = 40$ is shown.

Figure 2 Time evolution of various quantities for $\omega/\Omega = 1.97$, $\omega_p/\Omega = 0.3$, $\alpha = 80°$, and $\epsilon = 0.19$. The wave is a R-x mode.

Figure 3. The variation of $< \Delta\gamma > / < \Delta\gamma >_{QL}$ and D/D_{QL} as functions of wave amplitude. The waves are R-x modes with $\omega/\Omega = 1.97$, $\alpha = 80°$, and $\omega_p/\Omega = 0.3$. The scale in the x-axis is linear but the scale from 0.19 to 0.99 being different than that from 0.99 to 10.

Figure 4. The variation of $< \Delta\gamma > / < \Delta\gamma >_{QL}$ and D/D_{QL} as functions of wave amplitude. The waves are L-o mode with $\omega/\Omega = 2.6$, $\alpha = 80°$, and $\omega_p/\Omega = 0.3$. The discrepancy between $< \Delta\gamma >$ and $< \Delta\gamma >_{QL}$ for $\epsilon \lesssim 1.5$ is due to the presence of integrable orbits. If we exclude the integrable orbits in calculating $< \Delta\gamma >$, we once again find an excellent agreement with the diffusion code. The fraction of integrable orbits can be determined *apriori* analytically. The scale in the x-axis is linear but the scale from 0.43 tp 1.5 is different than that from 1.5 tp 10.

55

FIGURE 1

FIGURE 2
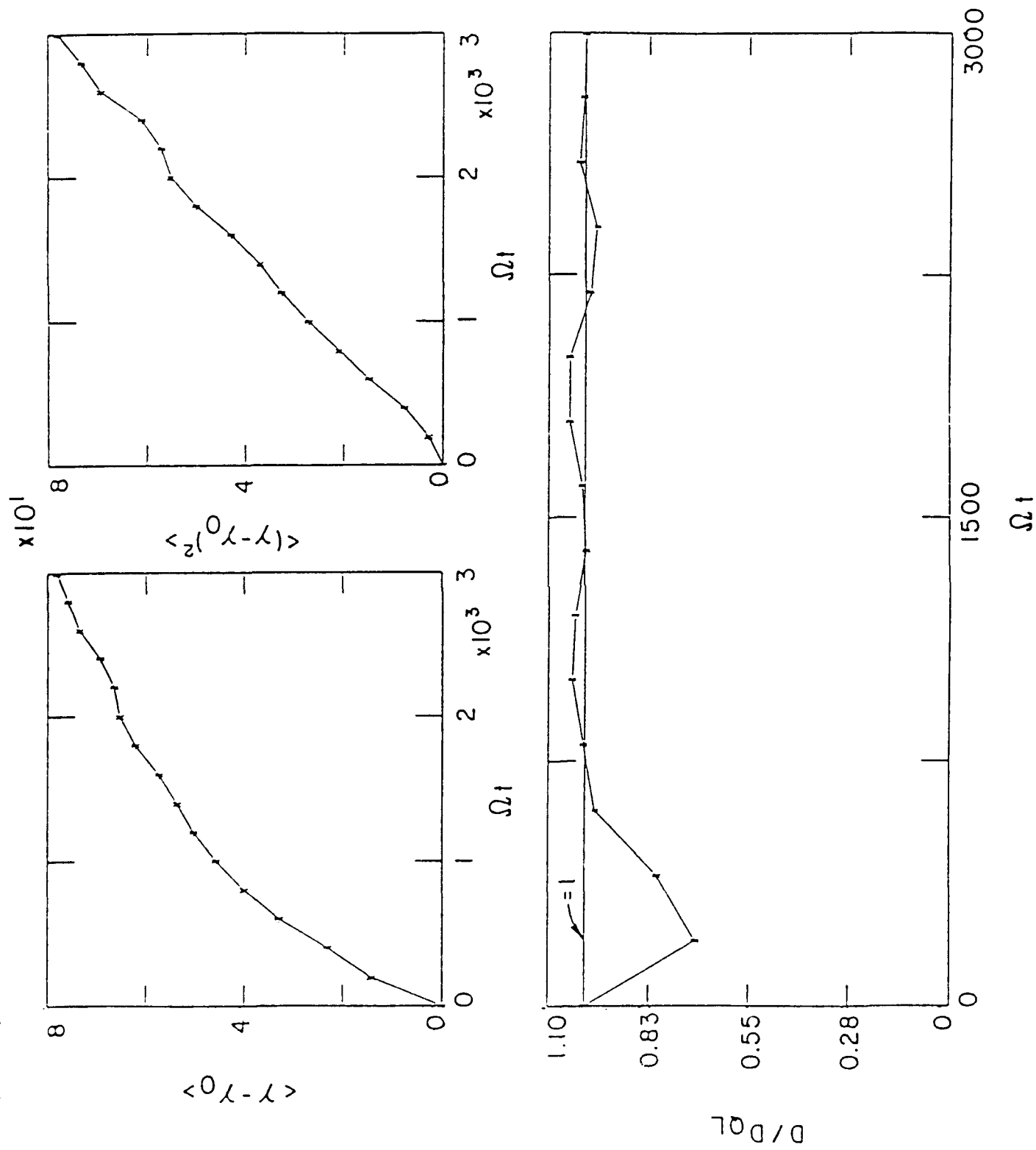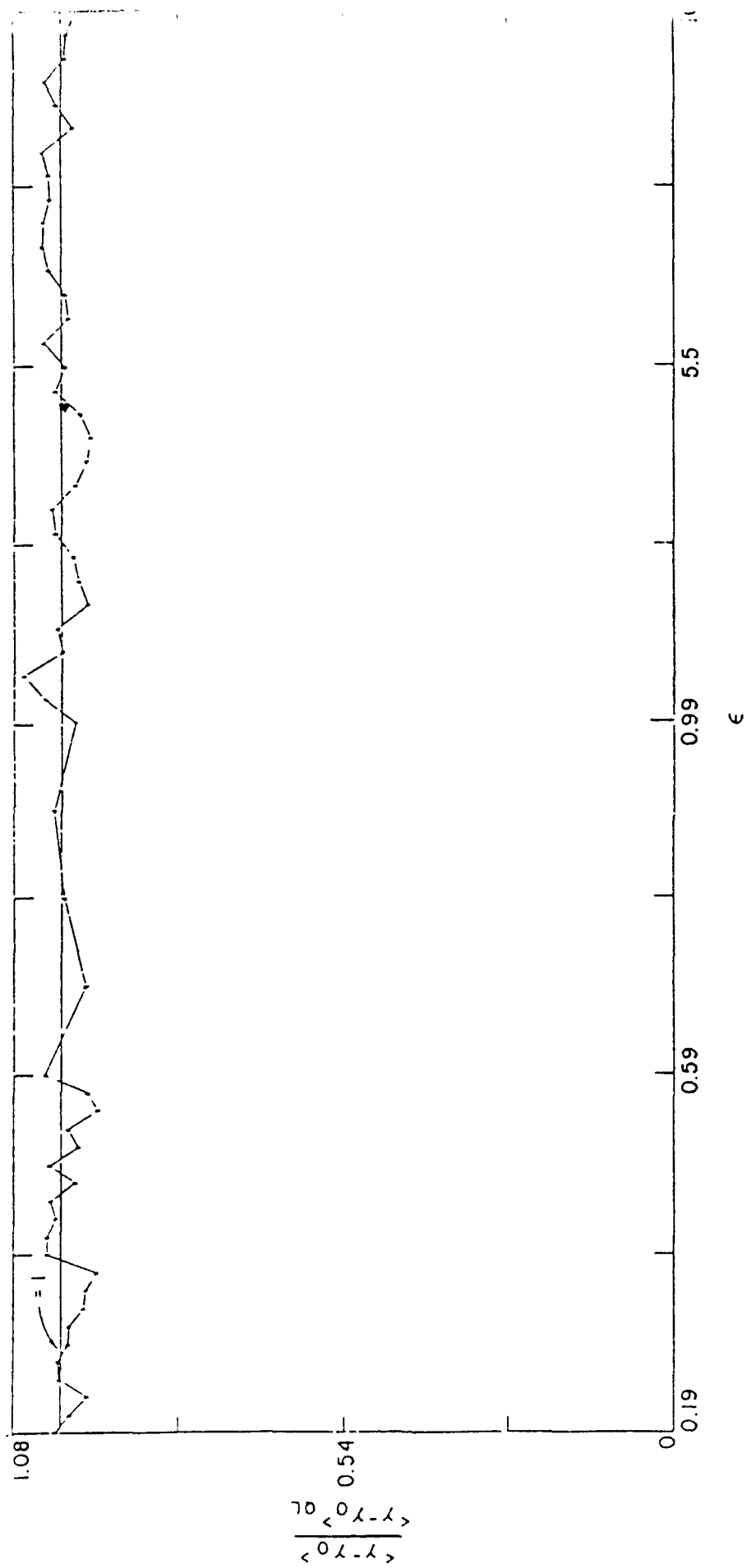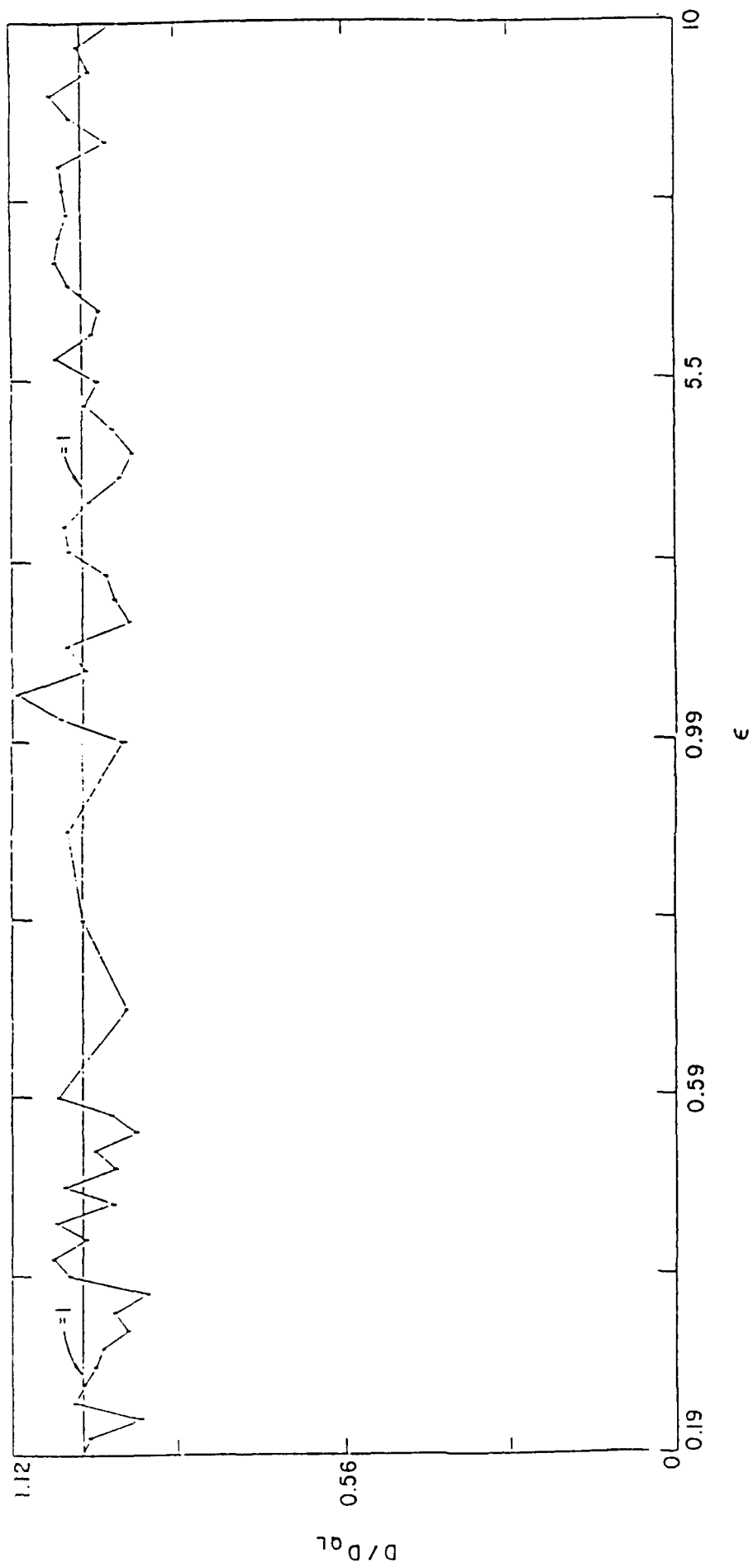
57

Figure 3a

$$\frac{\langle \gamma - \gamma_0 \rangle}{\langle \gamma - \gamma_0 \rangle_{OL}}$$
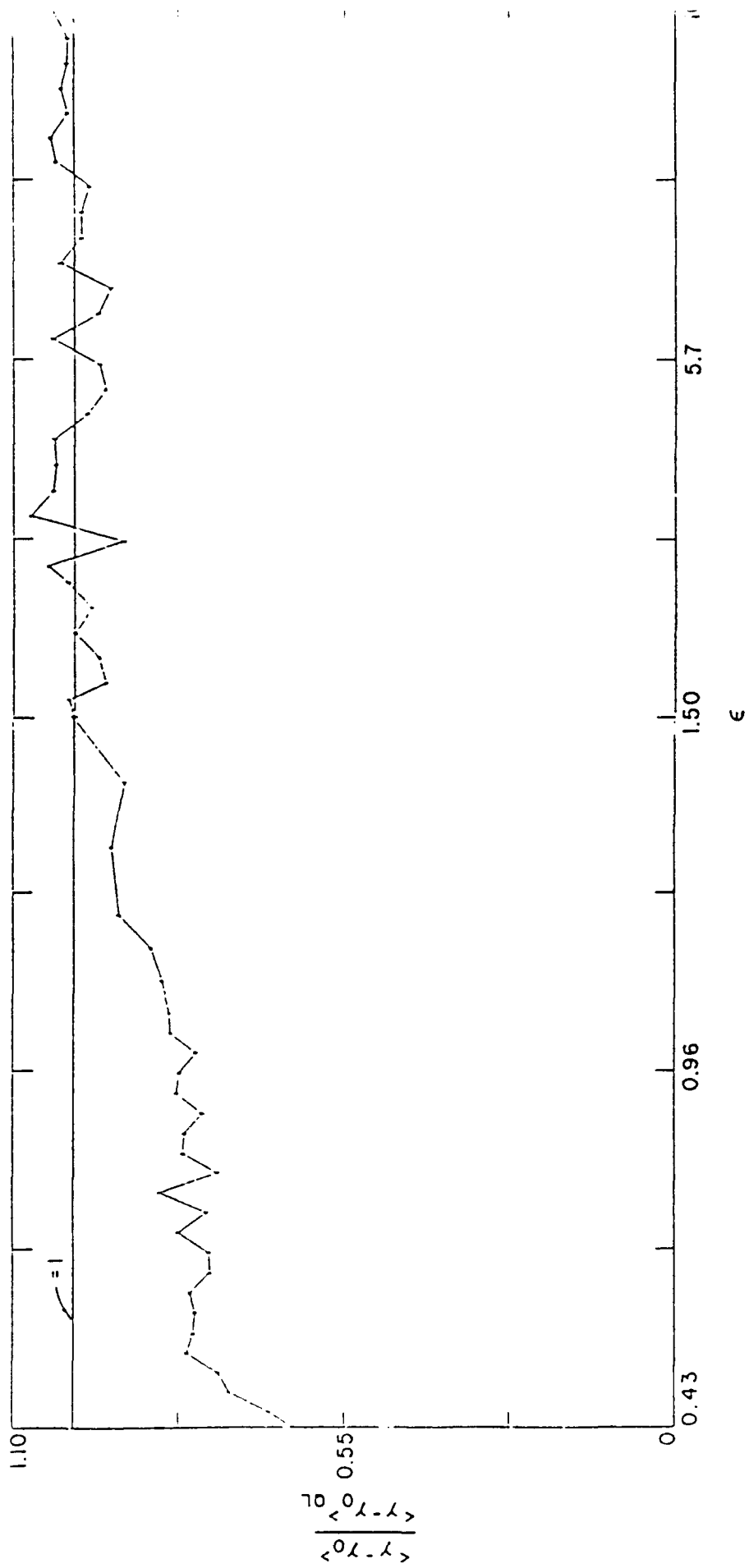
ϵ

58

Figure 3b

59

Figure 4a

60
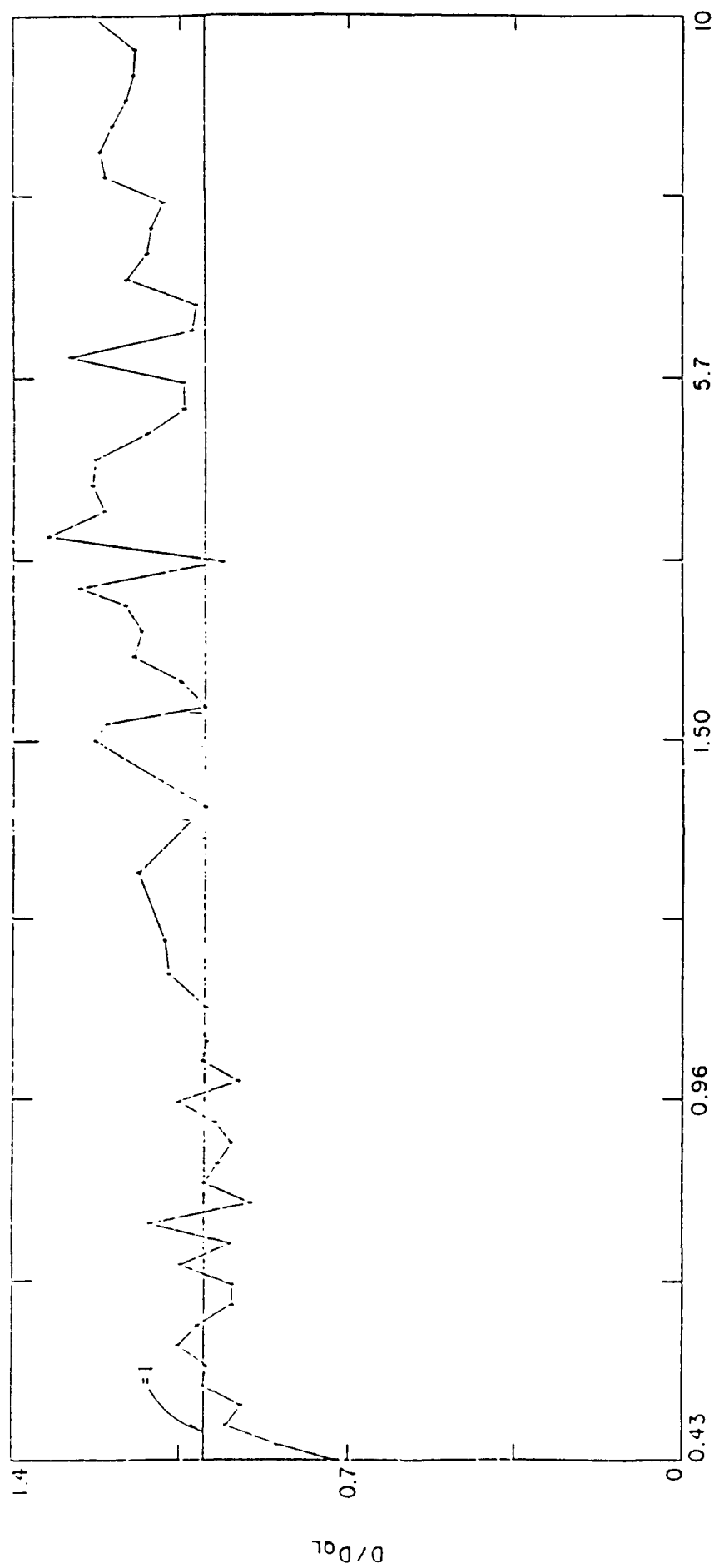
Figure 4b

61
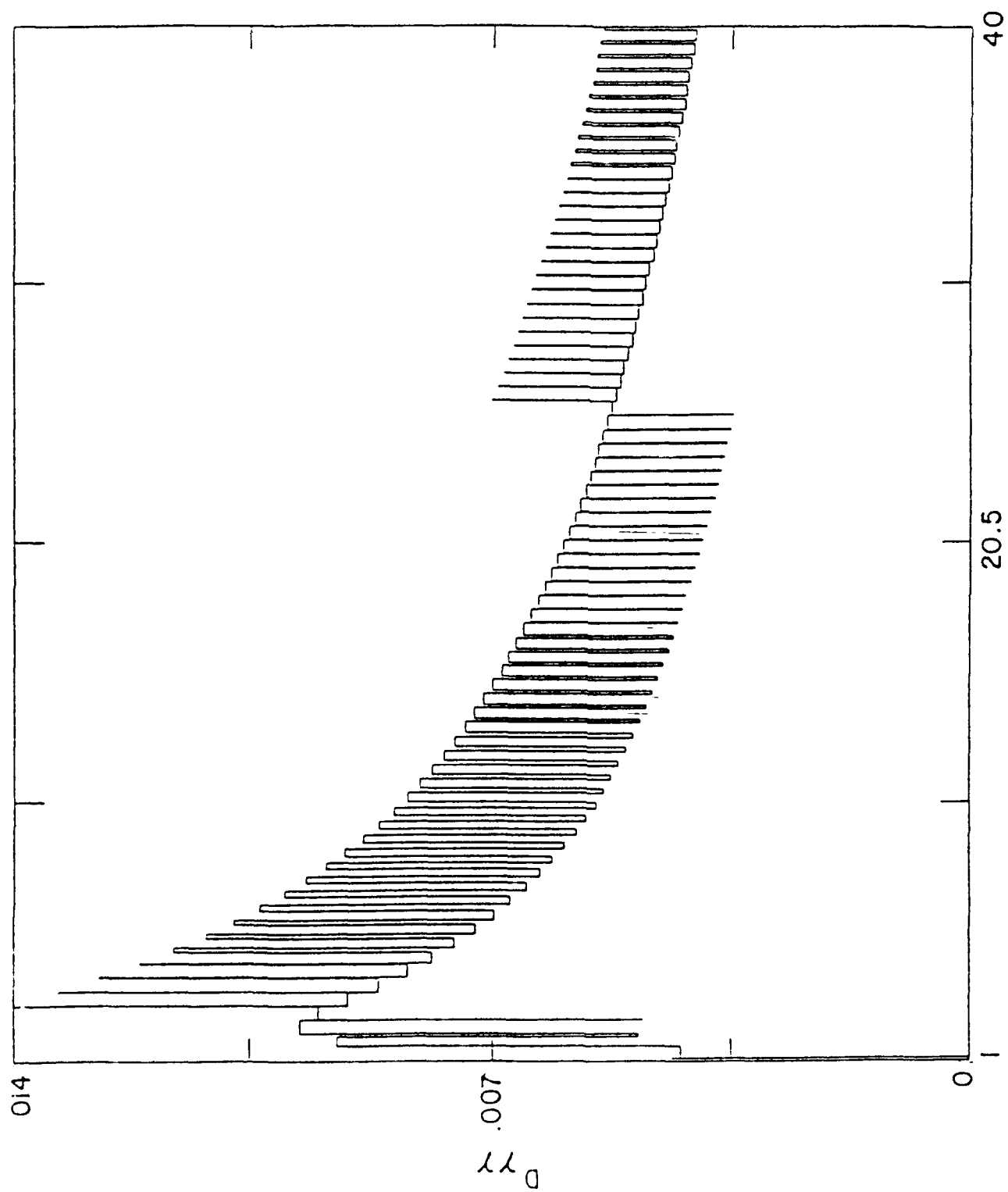
A Fast and Accurate Method of Calculating Particle Diffusion:
Application to the Ionosphere

H. Karimabadi

Institute of Geophysics and Planetary Physics,
University of California, Los Angeles, California 90024

C.R. Menyuk [a]

Science Applications International Corporation
1710 Goodridge Drive, McLean, Virginia 22102

Abstract

Electron acceleration by a wave propagating obliquely in a magnetized plasma is considered. For wave amplitudes above the stochasticity threshold, the motion of electrons is diffusive. A test of a simple diffusion formalism is presented. We reduce the diffusion equation to a 1-D form by transforming to a coordinate system that has the Hamiltonian as one of the axes. We present a model for the diffusion coefficient and solve the resulting diffusion equation by means of the finite element technique. The results are compared with numerical solutions of the orbits. Finally, we apply our results to the problem of electron diffusion in the lower ionosphere.

(a) Permanent Address: Department of Electrical Engineering, University of Maryland, Baltimore, Maryland 21228.

I. Introduction

The problem of charged particle acceleration by waves is of fundamental importance in plasma physics and plays a central role in the understanding of many processes in space physics. In an unmagnetized plasma, the motion of a charged particle interacting with a plane wave is very simple: there exists at most one resonance and the system is integrable. The trapping width is proportional to $\epsilon^{1/2}$ where ϵ is the wave amplitude. The particle motion can then become random only if there exist several waves with amplitudes and frequencies such that the trapping width of adjacent waves overlap. In other words, the condition for the particles to be stochastic is for the bounce frequency ω_b in the potential well of each wave to be larger than the spacing between the adjacent resonances $\omega_b \gg \Delta\omega$. The evolution of an ensemble of particles can then be described by the quasilinear (diffusion) equation [Vedenov, Velikhov, and Sagdeev, 1961; 1962; Zaslavsky, and Chirikov, 1972]. Conversely, when the wave amplitudes become large enough to satisfy the condition $\omega_b \gg N_w\Delta\omega$, then the stochasticity disappears as the effect of individual resonances would be washed out and the particle would see a single potential well with slowly varying parameters. Here N_w is the number of waves in the wave packet. Thus, the condition for the validity of the quasilinear theory is $N_w\Delta\omega \gg \omega_b \gg \Delta\omega$.

The presence of a static magnetic field changes the particle motion in two important ways: (1) particles can resonate with the harmonics of the gyrational motion, (2) resonances can occur even if the wave has a phase velocity larger than the speed of light. The resonance condition in a magnetized plasma is $\omega - k_\parallel v_\parallel = \ell\Omega/\gamma$, where $\ell = 0, \pm1, \pm2, ...$, and $\Omega = |q|B_o/mc$. The trapping width associated with each resonance is proportional to $\epsilon^{1/2}$. As long as $\epsilon \ll 1$ the neighboring resonances are well separated and the particle motion is periodic. At a critical value of the wave amplitude referred to as the stochasticity threshold [e.g., Lichtenberg and Lieberman, 1983], the adjacent resonances overlap and the motion becomes random or chaotic. The particle can then sample several resonances and gain large energies in the process. In this case, the motion of the particle can still be described by the quasilinear theory even though there is only one wave present.

The general problem of single particle motion under the influence of an obliquely propagating plane wave has been treated in a series of papers by Karimabadi and collaborators [Menyuk, et al., 1987; 1988; Akimoto and Karimabadi, 1989; Karimabadi, et al., 1990]. The main result of

these single particle studies has been the realization that for waves with $N_\parallel < 1$, the Hamiltonian surfaces become topologically open, thus allowing large particle acceleration. Here, $N_\parallel$ is the refractive index parallel to the magnetic field. In this paper, we derive a diffusion equation that describes the evolution of particle distribution function for wave amplitudes above the stochasticity threshold and $N_\parallel < 1$. The generalization of our work to the case of $N_\parallel > 1$ is trivial. We reduce the diffusion equation to 1-D by transforming to a coordinate system with the Hamiltonian as one of the axes. We then present a model for the diffusion coefficient and solve the diffusion equation using the finite element technique. This algorithm is found to be very fast and accurate. The solutions of the diffusion equation are compared with exact numerical solutions of the orbits. The conditions under which the diffusion formalism breaks down are discussed.

The techniques and algorithm expounded in this paper are quite general and are likely to find applications in many problems in space physics and astrophysics. We have already applied the above techniques successfully to the problem of particle acceleration in cometary shocks [Karimabadi, et al., 1989] and in supernova remnants [Karimabadi, 1988]. In section [VI], we briefly apply our results to the problem of remote acceleration of ionospheric electrons from ground based radio transmitters. Accelerated electrons could be used to create an artificial aurora, to probe the magnetosphere, and to measure the cross section of ionospheric constituents interacting with energetic electrons. We find the power needed for stochastic electron acceleration to be beyond the present day capabilities. We propose ways to overcome this problem. We present our conclusion in section [VII].

II. Test Particle Results

In this section we describe the formulation of the resonance overlap criterion which we use to determine the acceleration threshold. More details can be found in Karimabadi, et al. [1990].

In general, we assume that each electron is moving in a homogeneous magnetic field and a plane wave propagating obliquely to the magnetic field. This plane wave can have both electromagnetic and electrostatic components. We thus write the particle Hamiltonian as

$$H = \left[\left(c\vec{P} - q\vec{A} \right)^2 + m^2 c^4 \right]^{1/2} + q\Phi = mc^2 \gamma + q\Phi. \tag{1a}$$

where

$$\vec{A} = A_1 \frac{k_\parallel}{k} \sin \psi \, \hat{e}_x + A_2 \cos \psi \, \hat{e}_y - A_1 \frac{k_\perp}{k} \sin \psi \, \hat{e}_z + x B_0 \hat{e}_y \equiv \vec{A}_{em} + x B_0 \hat{e}_y, \tag{1b}$$

64

$$\Phi = \Phi_o \sin \psi, \tag{1c}$$

and

$$\psi = k_\perp x + k_\parallel z - \omega t. \tag{1d}$$

Although we are primarily interested in electron acceleration, we keep the charge q arbitrary in the derivation of the equations. We next use a series of canonical transformations and the techniques of Hamiltonian perturbation theory to reduce the Hamiltonian to the form

$$H \simeq H_0 + H_1. \tag{2}$$

The zero-order Hamiltonian is given by

$$H_0 = mc^2 \gamma_0 - \frac{\omega}{k_\parallel} p_\parallel, \tag{3a}$$

where

$$\gamma_0 = \left(1 + \frac{p_\perp{}^2}{m^2 c^2} + \frac{p_\parallel{}^2}{m^2 c^2} \right)^{1/2}. \tag{3b}$$

The quantities $p_\perp$ and $p_\parallel$ represent the momentum perpendicular and parallel to the magnetic field. The surfaces of constant H_o are elliptic in $p_\parallel - p_\perp$ space if $N_\parallel > 1$, hyperbolic if $N_\parallel < 1$ and parabolic if $N_\parallel = 1$. Equation (2) is derived by expanding in powers of the wave field; it is consistent with this expansion to take $p_\perp$ and $p_\parallel$ to be purely mechanical. The first-order Hamiltonian is given by

$$H_1 = \sum_{\ell=-\infty}^{\infty} Z_\ell \sin \left(k_\parallel z + \ell \theta \right), \tag{4}$$

where θ is the gyroangle and

$$Z_\ell = \frac{mc^2}{\gamma_o} \left\{ \epsilon_1 \left[\frac{q}{|q|} \frac{P_\parallel}{mc} \sin \alpha - \frac{q}{|q|} \frac{\Omega}{k_\perp c} \ell \cos \alpha \right] \right.$$
$$\left. J_\ell(k_\perp \rho) + \epsilon_2 \frac{P_\perp}{mc} J_\ell'(k_\perp \rho) + \frac{q}{|q|} \gamma_o \epsilon_3 J_\ell(k_\perp \rho) \right\}, \tag{5a}$$

with

$$\epsilon_1 = \frac{|q| A_1}{mc^2} = \frac{|q| E_1}{mc\omega}. \tag{5b}$$

65

$$\epsilon_2 = \frac{|q|A_2}{mc^2} = \frac{|q|E_2}{mc\omega}. \tag{5c}$$

$$\epsilon_3 = \frac{|q|\Phi_o}{mc^2} = -\frac{|q|E_3}{mcN\omega}. \tag{5d}$$

Here, the quantity α is the angle of wave propagation with respect to the magnetic field, q is the electric charge, and Ω is the magnitude of the nonrelativistic gyrofrequency. The explicit time dependence in the original Hamiltonian of Eq. (1a) has been absorbed into the z-coordinate of Eq. (4).

Resonances occur when $k_\| \dot{z} + \ell\dot{\theta} = 0$, or

$$\omega - \frac{k_\| P_\|}{m\gamma_o} - \frac{\ell\Omega}{\gamma_o} = 0, \tag{6}$$

a result which can also be obtained from standard, linear theory. It can be easily verified that the resonance surfaces are elliptic (hyperbolic) when the H-surface is hyperbolic (elliptic). Typically, for a given value of ℓ and H, there will be only one pair $(p_\perp, p_\|)$ which satisfies Eq. (6). It is this case which we are interested in treating. In some cases, it is possible for Eq. (6) to be satisfied for every point $(p_\perp, p_\|)$ on the Hamiltonian surface in phase space. In these cases, special methods of treatment are required [Karimabadi et al., 1990]. We will not discuss this issue in this paper.

If the wave amplitude is small, then an electron will be affected by at most one resonance. In this case, all but that single resonance's contribution to the Hamiltonian can be ignored, and the Hamiltonian becomes

$$H = H_o(p_\|, p_\perp) + Z_\ell \sin(k_\| z), \tag{7}$$

where z has been redefined to absorb $\ell\theta$. In this re-defined coordinate system, the resonance occurs at a point $(p_{\|r}, p_{\perp r})$ where $\dot{z} = 0$. Writing

$$H_o(p_\|, p_\perp) \simeq H_o(p_{\|r}, p_{\perp r}) + \frac{1}{2}\frac{\partial^2 H_o}{\partial p_\|^2}\bigg|_r (p_\| - p_{\|r})^2. \tag{8}$$

letting

$$M^{-1} \equiv \frac{\partial^2 H_o}{\partial p_\|^2}\bigg|_r = \left(1 - \frac{1}{N_\|^2}\right)\bigg/ m\gamma_o, \tag{9}$$

66

and absorbing the constant $H_o(p_{\|r}, p_{\perp r})$ into H, the Hamiltonian becomes

$$H = \frac{1}{2M}(p_\| - p_{\|r})^2 + Z_\ell \sin(k_\| z),\tag{10}$$

which is the pendulum Hamiltonian. The trapping half-width and the bounce frequency are then given by

$$\Delta p_\| = 2|MZ_\ell|^{1/2}.\tag{11}$$

and

$$\omega_b = k_\| \left|\frac{Z_\ell}{M}\right|^{1/2},\tag{12}$$

respectively. The trapping width in γ can be easily found from $\Delta p_\|$:

$$\Delta\gamma = \frac{\Delta p_\|}{mcN_\|}.\tag{13}$$

The trapping half-width given by (11) is independent of the initial phase. This is due to our approximation of the Hamiltonian near a resonance by the pendulum Hamiltonian. The phase dependence of the trapping half-width is mainly due to the $p_\|$ component of momentum and the electrostatic component of the wave. If $\epsilon \neq 0$, the phase dependence of the trapping half-width becomes increasingly important as $\alpha \to 90°$. The above analysis can be easily generalized to include the effect of phase on the trapping width [Ginet and Heinemann, 1990]. One then ends up with an equation for the trapping half-width that can in general only be solved numerically. This is not very useful to us and we use (11) in this paper.

It is important to note that the term "trapped" has a very specific meaning: it refers to orbits close enough to resonance condition so that the sum over all the harmonics can be replaced by a single term in the sum. The particles not very close to the resonance can still be accelerated, but the acceleration is much less effective.

In deriving (11) and (12), we have explicitly assumed that $\alpha \neq 90°$. For $\alpha = 90°$, most of the steps that led to (11) remain the same. The only difference comes in eliminating the time dependence in the Hamiltonian: the transformation $F_2 = p'_\|[z - \omega t/k_\|]$ is replaced by $F_2 = p'_t(-\omega t/k)$. It is then easy to show that the trapping width is still given by (13). The only difference is that for $\alpha = 90°$, $p_\|$ is a constant of motion and is determined a priori from the initial conditions. The sensitivity of the trapping width to $p_\|$ and thus to the initial phase at $\alpha \sim 90°$ is

67

not surprising since the term $\epsilon(\sin v)/N_{\parallel}$ in H becomes very large as $\alpha \to 90°$. The Hamiltonian of a particle initially at rest can then have a large range of values depending on the initial phase. For $\alpha \sim 90°$, $p_{\parallel}$ is still given by the solution of (3a) and (6) but with H_o replaced by H and $p_{\parallel}$ replaced by the canonical momentum. If $\epsilon_1 = 0$, the trapping width becomes less sensitive to the initial phase.

The separation on an H–surface between two adjacent primary resonances is

$$\delta p_{\parallel} = \frac{mc^2 \Omega k_{\parallel}}{\omega^2 - k_{\parallel}^2 c^2}. \tag{14}$$

The stochasticity threshold condition based on the overlap criterion [Chirikov, 1979] then reads

$$2\frac{\Delta P_{\parallel}}{\delta P_{\parallel}} = 4\,\omega_b/(\Omega/\gamma_o) \gtrsim 1. \tag{15}$$

As long as the resonances do not overlap, an electron in the neighborhood of the resonance ℓ can change in $p_{\parallel}$ by at most $2\Delta p_{\parallel}$. Once resonances overlap, the electron can jump from resonance to resonance and in this way gain large amounts of energy. We can determine in this way the threshold wave intensity to accelerate electrons originally at rest to 10 Mev or more.

III. The Diffusion Equation

There are two equivalent ways of deriving the diffusion equation. The first, where the effects of particle motion on the imposed fields are neglected, leads to the Fokker-Planck equation [Chandrasekhar, 1943; Romanov and Filippov, 1961; Sturrock, 1966]

$$\begin{aligned}
\frac{\partial f}{\partial t} &= -\frac{\partial}{\partial \vec{v}} \cdot (\langle \frac{\Delta \vec{v}}{\Delta t} \rangle f) + \frac{1}{2}\frac{\partial^2}{\partial v^2}(\langle \frac{(\Delta \vec{v})^2}{\Delta t} \rangle f) \\
&\equiv -\frac{\partial}{\partial \vec{v}} \cdot (Bf) + \frac{1}{2}\frac{\partial^2}{\partial v^2}(Df),
\end{aligned} \tag{16a}$$

where

$$B = \lim_{\Delta t \to \infty} \frac{\langle \Delta \vec{v} \rangle}{\Delta t}, \tag{16b}$$

$$D = \lim_{\Delta t \to \infty} \frac{\langle (\Delta \vec{v})^2 \rangle}{\delta t}, \tag{16c}$$

and where the brackets indicate an average over initial conditions. In the derivation of (16a), it is assumed that: (1) The change in velocity Δv in a time interval Δt is such that $\langle \Delta v \rangle$ and $\langle \Delta v^2 \rangle$

contain contributions linear in Δt; whereas, all higher products have expectation values that vary as a higher power of Δt and are therefore neglected. (2) The trajectory which a particle follows depends only on the instantaneous values of its physical parameters and is entirely independent of its whole previous history (Markovian assumption).

The second derivation of the diffusion equation is based on the quasilinear theory [Vedenov, Velikhov, and Sagdeev, 1961, 1962; Drummond, and Pines, 1962]. They conclude that:

$$\frac{\partial f}{\partial t} = \frac{\partial}{\partial v}(D\frac{\partial f}{\partial v}). \tag{17}$$

The diffusion equations (16a) and (17) are equivalent since the friction and diffusion coefficients in the Fokker-Planck equations are related by

$$B = \frac{1}{2}\frac{dD}{dv}. \tag{18}$$

The Hamiltonian (1a) is a function of $p_{\parallel}$ and $p_{\perp}$ and it is thus convenient to start with the relativistic diffusion equation in cylindrical coordinates

$$\frac{\partial f}{\partial t} = \frac{1}{p_{\perp}}\frac{\partial}{\partial p_{\perp}}\left[p_{\perp}(D_{\perp\parallel}\frac{\partial}{\partial p_{\parallel}} + D_{\perp\perp}\frac{\partial}{\partial p_{\perp}})f\right]$$
$$+ \frac{\partial}{\partial p_{\parallel}}\left[(D_{\parallel\parallel}\frac{\partial}{\partial p_{\parallel}} + D_{\parallel\perp}\frac{\partial}{\partial p_{\perp}})f\right], \tag{19}$$

where

$$D_{\parallel\parallel} = \int_0^\infty d\tau\langle\dot{p}_{\parallel}(t)\dot{p}_{\parallel}(t+\tau)\rangle, \tag{20a}$$

$$D_{\perp\perp} = \int_0^\infty d\tau\langle\dot{p}_{\perp}(t)\dot{p}_{\perp}(t+\tau)\rangle, \tag{20b}$$

$$D_{\parallel\perp} = D_{\perp\parallel} = \int_0^\infty d\tau\langle\dot{p}_{\perp}(t)\dot{p}_{\parallel}(t+\tau)\rangle. \tag{20c}$$

In (20), the angular brackets indicate an average over the initial coordinates:

$$\langle A\rangle \equiv k_{\parallel}\int_0^{2\pi/k_{\parallel}}\frac{dz_o}{2\pi}\int_0^{2\pi}A\frac{d\theta_o}{2\pi}. \tag{21}$$

Equation (19) is averaged over the cylindrical angle ϕ which becomes randomized on timescales much faster than the relaxation times of distributions in $p_{\parallel}$ and $p_{\perp}$.

69

Integrating over the unperturbed orbits we obtain

$$D_{\parallel\parallel} = \frac{\pi}{2}k_\parallel^2 \sum_{\ell=-\infty}^{\infty} Z_\ell^2 \delta\left(\omega - \frac{k_\parallel p_\parallel}{m\gamma} - \frac{\ell\Omega}{\gamma}\right) \equiv \sum_{\ell=-\infty}^{\infty} D_{\parallel\parallel_\ell}. \tag{22a}$$

$$D_{\perp\perp} = \frac{\pi}{2}(m\Omega)^2 \sum_{\ell=-\infty}^{\infty} \frac{\ell^2}{p_\perp} Z_\ell^2 \delta\left(\omega - \frac{k_\parallel p_\parallel}{m\gamma} - \frac{\ell\Omega}{\gamma}\right) \equiv \sum_{\ell=-\infty}^{\infty} D_{\perp\perp_\ell}. \tag{22b}$$

$$D_{\perp\parallel} = D_{\parallel\perp} = \frac{\pi}{2}k_\parallel m\Omega \sum_{\ell=-\infty}^{\infty} \frac{\ell}{p_\perp} Z_\ell^2 \delta\left(\omega - \frac{k_\parallel p_\parallel}{m\gamma} - \frac{\ell\Omega}{\gamma}\right) \equiv \sum_{\ell=-\infty}^{\infty} D_{\perp\parallel_\ell}. \tag{22c}$$

where $\delta(x)$ is the usual Dirac δ-function. These diffusion coefficients are not useful as they stand because in their derivation we did not take into account the decorrelation due to stochasticity. In order to overcome this problem, we use a modified form of resonance broadening theory [Dupree, 1966] as given below.

A. Diffusion Model

The δ-function in the diffusion coefficients came about when we substituted unperturbed orbits in the right hand side of (20), which then implies incorrectly that if the particle is in resonance with the wave, it will maintain resonance indefinitely. We showed in previous sections that the resonance width is indeed finite and is given by (11). The finiteness of the trapping width is due to the fact that $k_\parallel v_\parallel \neq \ell\Omega\dot{\gamma}/\gamma^2$, and, thus, the particle is shifted from exact resonance by the wave.

It can be easily shown that the decorrelation time or the shift in the resonance condition due to the finite trapping width is roughly $2\omega_b$ in the ℓ-th resonance. Thus, we replace the δ-function by a function $f(x)$, where

$$f(x) = \begin{cases} 1/4\omega_b, & \text{if } |x| \leq 2\omega_b \\ 0, & |x| > 2\omega_b \end{cases}$$

The quantity ω_b corresponds to the bounce frequency (12) in the ℓth resonance. Note that

$$\int_{-\infty}^{+\infty} f(x)dx = \int_{-\infty}^{+\infty} \delta(x)dx = 1.$$

This spread is equivalent through the order to which we are working to the spread in $p_\parallel$ calculated in (11).

B. Reduction to 1-D

Because H is a conserved quantity, the diffusion proceeds along a constant H-surface. It is then useful to replace the $(p_\parallel, p_\perp)$ coordinate system with the (H, γ) coordinate system, which

70

reduces the diffusion equation to one dimension. The details are given in the appendix and the diffusion equation reduces to

$$\frac{\partial f}{\partial t} = \frac{1}{\gamma}\frac{\partial}{\partial \gamma}\left(\gamma D_{\gamma\gamma}\frac{\partial f}{\partial \gamma}\right),$$

(23a)

where

$$D_{\gamma\gamma} = \frac{\pi}{8}\frac{\omega}{(1 - N_\parallel^2)^{1/2}}\sum_{\ell=-\infty}^{\infty}\left(\frac{Z_\ell}{mc^2}\right)^{3/2}\gamma^{1/2}.$$

(23b)

The sum is over regions of stochasticity. In other words, we first calculate a diffusion coefficient for each harmonic, and, then, in regions where resonances overlap, we sum the contribution due to each resonance. We stress that the problem is still two-dimensional. We have reduced the problem to one dimension along each H-surface, but we still have to consider solutions for many H-values if the initial distribution function spans more than one value of H.

The way in which we have defined $D_{\gamma\gamma}$ implies that its derivative is zero everywhere except on a countable set of points where it becomes infinite. Hence, the numerical evaluation of (23) requires great care. We deal with this difficulty by using a finite element discretization method in which case the problem should be characterized by a variational formulation. Below, we use the Ritz-Galerkin method [Muschietti, Appert and Vaclarik, 1982; Dhatti and Touzot, 1984] to give the diffusion equation an equivalent variational formulation.

C. Discretization of the Diffusion Code

We start by multiplying (23a) by γ and a wighting function $g(\gamma)$ and then integrate over the energy domain $\Gamma = (\gamma_{\min}, \gamma_{\max})$ to obtain

$$\int_\Gamma \gamma g(\gamma)\frac{\partial f}{\partial t}d\gamma = \left(\gamma D_{\gamma\gamma}g(\gamma)\frac{\partial f}{\partial \gamma}\right)\Big|_{\gamma_{\min}}^{\gamma_{\max}} - \int_\Gamma \gamma D_{\gamma\gamma}\frac{\partial g}{\partial \gamma}\frac{\partial f}{\partial \gamma}d\gamma.$$

(24)

Particle conservation implies that the first term on the right hand side of (24) is zero. Dividing the range $(\gamma_{\min}, \gamma_{\max})$ into N equal sized elements, the distribution function may be written

$$f = \sum_{j=1}^{N} f_j(t)\psi_j(\gamma),$$

(25)

where the $\psi_j(\gamma)$ are the basis functions for the finite elements, defined so that

$$\psi_i = \begin{cases} (\gamma - \gamma_{i-1})/(\gamma_i - \gamma_{i-1}), & \gamma_{i-1} \le \gamma \le \gamma_i \\ (\gamma_{i+1} - \gamma)/(\gamma_{i+1} - \gamma_i), & \gamma_i \le \gamma \le \gamma_{i+1}, \end{cases}$$

71

and is zero elsewhere, where (γ_{i-1}, γ_i) is the i-th element. We now use the v_i as the weighting elements in (25) and defining the elements of the matrices A and B

$$A_{ij} = \int_\Gamma \psi_i \psi_j \gamma \, d\gamma, \qquad (26a)$$

$$B_{ij} = -\int_\Gamma \frac{\partial \psi_i}{\partial \gamma} D_{\gamma\gamma} \gamma \frac{\partial \psi_j}{\partial \gamma} \, d\gamma, \qquad (26b)$$

where i and j range from $1 - N$, we obtain the equation

$$A \cdot \frac{\partial f}{\partial t} = B \cdot f. \qquad (27)$$

Time is discretized using a leapfrog scheme, and (27) is easily solved as both A and B are tridiagonal. Note that the matrices A and B are time independent as the fields are constant in time and thus these matrices need to be evaluated just once. The boundary conditions are that $D_{\gamma\gamma} = 0$ at the lower boundary and $f = 0$ at the upper boundary. We choose γ_{max} to be sufficiently large that no diffusion to this boundary occurs over the time scale of the simulation.

The diffusion coefficient $D_{\gamma\gamma}$ as given by (23b) is evaluated numerically as a function of γ as follows: First, we determine all the resonances that intersect the H-surface in the interval from γ_{min} to γ_{max} and calculate the trapping width for each resonance. We model the contribution of each resonance to the diffusion coefficient as a box having a width equal to the trapping width and a height given by the quantity inside the summation sign in (23b). So, there is a box centered around each resonance with known height and width. Next, we add the heights in regions where resonances overlap, otherwise leaving the boxes intact. The resulting diffusion coefficient is not smooth (Fig. 1) and is not differentiable. However, as evident from (24) and (26b), what is needed is the integral of $D_{\gamma\gamma}$ over each finite element which is well defined and easily obtained.

The stability condition for our code is $\Delta t \lesssim h^2 / D_{\gamma\gamma}$ where h is the grid spacing. In other words, the time step used in solving the diffusion equation should be smaller than the time it takes the particle to diffuse across the grid.

We have tested the code by running it for cases where the diffusion equation has analytic solutions and found the agreement between numerical and analytical results to be excellent. We have also found the number of particles to be typically constant to better than one part in 10^{-5}.

Before we compare the solutions of the diffusion code with exact orbit calculations, it is important to check the accuracy of our analytical expressions for the trapping width and stochasticity threshold. This is done below.

IV. Threshold Calculation

Here we are interested in determining the conditions under which the electrons in the ionosphere can be accelerated to large energies from rest. The analytical threshold is based on the overlap condition, and there is no guarantee that at the overlap amplitude the resonances extend down to $\gamma = 1$. Thus, the quantity we are interested in is not the amplitude at which the first two resonances overlap but the amplitude at which the first three resonances overlap with the stochastic region in phase space reaching down to $\gamma = 1$. We require the overlap of the first three resonances because the waves we are considering have $N \sim 1$ and for such waves the trapping width is an increasing function of the harmonic number up to some critical ℓ beyond which the trapping width drops off exponentially. We have found empirically that if the first three resonances overlap, the remaining resonances will overlap as well. Thus, the overlap of the first three resonances with the additional constraint that trapping width(s) reach down to $\gamma = 1$ ensures global stochasticity in the phase space region of interest.

The experimental value of wave amplitudes for which zero energy particles can be stochastically accelerated are determined by solving the orbits of 256 particles, all with initial $\gamma = 1$ and initial phases uniformly distributed between 0 and 2π. The orbits are typically solved up to $\Omega t = 1000$ and the maximum energy γ_{max} reached for each particle during this time interval is plotted as a function of the initial phase, as shown in Fig. 2. This method yields a quantitative measure of the fraction of particles that are stochastic. In other contexts, the surface of section technique is useful in determining the level of chaos in phase space; however, since each phase corresponds to a different value of H, many surface of section plots are needed to determine the phase dependence and, thus, this is not practical for us.

The comparison of the analytical and numerical conditions are given below for various plasma parameters and wave modes.

(i) R-x mode, $\omega_p/\Omega = 0.3$

First, we consider the R-x mode in a plasma with $\omega_p/\Omega = 0.3$, $\alpha = 80°$ and a range of wave frequencies from $\omega/\Omega = 1.09$ to 7. A typical route to global chaos in this parameter regime is illustrated in Fig. 2. For $\epsilon = 0.14$ which is below the stochasticity threshold, the particle orbits are integrable and the gain in energy is limited. The γ_{max} oscillates as a function of the initial phase (Fig. 2a) with different phases corresponding to different values of H. The dependence of the γ_{max} on the initial phase means that the stochasticity threshold is also dependent on the phase. As the wave amplitude is increased to $\epsilon = 0.155$, a very small fraction of particles are stochastically accelerated (Fig. 2b). At $\epsilon = 0.27$, more than 90% of the particles are stochastic (Fig. 2d). The remaining 10% of the particles are locally stochastic (weakly chaotic) but are limited by KAM surfaces to low energies. There are, however, a small fraction of particles $\sim 5\%$ near $\psi = \pi/2$ that remain integrable even after the wave amplitude has been increased to $\epsilon = 0.5$. The γ_{max} is in fact smallest at $\psi = \pi/2$ as evident in Fig. 2a.

It is important to note that particles can gain energy without being trapped. The energy gain of a particle starting with zero energy is determined by how far the particle is from a resonance and how strong that resonance is. The different initial phases correspond to different H values, and the distance of the particle from the resonance as well as the strength of that resonance, changes as a function of H. For the R-x mode and the parameters of this section, the spread in H due to different phases is small. The phase effects are much more important for L-o mode as we show shortly. For particles near $\psi = \pi/2$, the particles are far from resonance and the KAM surfaces separating the particles from resonance persist to high wave amplitudes.

As the simulated value for the stochasticity threshold at a given frequency, we choose two amplitudes $\epsilon_{1\%}$ and $\epsilon_{90\%}$ which correspond to amplitudes for which 1% and 90% of the particles first become stochastic, respectively. We use $\epsilon_{90\%}$ rather than $\epsilon_{100\%}$ because as shown in Fig. 2, there can be a large gap between $\epsilon_{90\%}$ and $\epsilon_{100\%}$, while the gap between $\epsilon_{1\%}$ and $\epsilon_{90\%}$ is much smaller. In other words, only 90% of the particles are easily accelerated in the parameter regime above.

At all frequencies in Fig. 3, except $\omega/\Omega = 1.09$, the particles reach energies above $\gamma > 3$ in $\Omega t = 1000$ after they become stochastic. We may thus determine what fraction of the particles

74

are stochastic. Another check is to solve the orbits up to $\Omega t = 3000$ and check whether they were accelerated beyond γ_{max} at $\Omega t = 1000$. These two tests yielded similar results in all cases. For $\omega/\Omega = 1.09$, the index of refraction is small and even the stochastic particles could not be accelerated easily above $\gamma = 3$. At this frequency, we determined that $\gamma > 2$ is a good condition for stochasticity.

The comparison of the analytical and simulated values of stochasticity threshold is shown in Figs. 3a and 3b. The theoretical threshold is indicated by the solid curve. The stochasticity threshold ϵ_{thrs} is seen to increase with frequency. The value of $\epsilon_{1\%}$ does not vary much, whereas the value of $\epsilon_{90\%}$ increases rapidly as a function of frequency. The analytical threshold is in better agreement with $\epsilon_{1\%}$ than $\epsilon_{90\%}$ for most of the frequency range below $\omega/\Omega \sim 5$ with the situation reversing at higher frequencies. The overlap condition for stochasticity is a crude and simple way of estimating the condition for stochasticity and it is not surprising that the simulated threshold values deviate from the analytical results. The fact that the wave amplitudes are rather large ($\epsilon_{thrs} \gtrsim 0.1$) also contributes to the error. An additional factor of π in the stochasticity threshold which is often invoked to take into account the effects of higher order resonances (Chirikov, 1979) does not seem appropriate for our case, and it would in fact make the differences between the analytical and simulated values more drastic.

At low frequencies, the gap between $\epsilon_{1\%}$ and $\epsilon_{90\%}$ is small and thus the transition to global chaos is more abrupt as is evident from Fig. 3c. The gap widens at higher frequencies and for $\omega/\Omega \gtrsim 4$ it becomes difficult to accelerate more than 80% of the particles.

Next, we consider the variation of ϵ_{thrs} as a function of propagation angle α for the same parameters as in Fig.3 and $\omega/\Omega = 2$. Both the analytical and simulated ϵ are seen in Fig. 4 to first drop rapidly and then flatten out as a function of α. The rapid drop of ϵ_{thrs} is not surprising since the system is integrable at $\alpha = 0°$. The analytical threshold in this case overestimates the threshold condition by roughly a factor of 2. The analytical estimate for the overlap of the first three resonances but not extending to $\gamma = 1$ are slightly below $\epsilon_{1\%}$. Had we replaced the factor of 4 in (15) by a factor of 2π, the agreement between the analytical and simulated values of ϵ_{thrs} would have much better for the parameters of Fig. 4. Even though there exist theoretical arguments for the presence of this factor, it does not work for all frequencies.

(ii) R-x mode, $\omega_p/\Omega = 2$

Next, we consider the plasma parameters corresponding to the dayside ionosphere $\omega_p/\Omega = 2$, and $\alpha = 80°$. For this parameter regime only 80% of particles are easily accelerated and there exists a rather large gap between $\epsilon_{80\%}$ and $\epsilon_{90\%}$. As a result, we have plotted $\epsilon_{80\%}$ rather than $\epsilon_{90\%}$ in Fig. 5a. The value of γ_{max} is very small near $\psi = \pi/2$ and $3\pi/2$ and particles with initial phases close to these values remain integrable even for very large wave amplitudes. The analytical threshold lies mostly between $\epsilon_{1\%}$ and $\epsilon_{80\%}$. The threshold amplitudes tend to be higher than those in case (i). This is mainly due to the smaller indices of refraction. The number of overlapping resonances and the trapping width are strong functions of N. For $N < 1$, the trapping width increases as a function of harmonic number up to some critical value ℓ_{crit} beyond which it drops off exponentially. The smaller N, the smaller ℓ_{crit} and thus the fewer the number of overlapping resonances. Since the index of refraction at a given frequency is smaller for $\omega_p/\Omega = 2$ compared to that for $\omega_p/\Omega = 0.3$, fewer resonances overlap and the diffusion is weaker for $\omega/\Omega = 2$. Thus, it is easier to accelerate electrons in the nightside ionosphere.

(iii) L-o mode, $\omega_p/\Omega = 0.3$

Figure 6 illustrates the transition to chaos for $\omega/\Omega = 2.6$ and $\alpha = 80°$. As mentioned earlier, the phase dependence of the γ_{max} is more important for the L-o mode than it is for the R-x mode. This is particularly true at large angles where the term $\epsilon(\sin\psi)/N_\parallel$ in the Hamiltonian becomes significant. In Fig. 6a all the orbits are integrable and the minimum acceleration is seen to occur at $\psi = 0$, π and 2π. As the wave amplitude is changed from 0.35 to 0.5, only $\sim 60\%$ of the particles become stochastic. The particles between $\psi \sim 0$ to π remain mostly integrable. It is not until ϵ has been raised to ~ 1 that $\sim 50\%$ of the particles between $\psi \sim 0 \to \pi$ become stochastic. The phases between ~ 0 to π correspond to positive H values. Recalling that $p_\parallel \propto (\ell\Omega/\omega - H)$ and $\Delta\gamma \propto p_\parallel^{1/2}$, it is easily seen that the trapping width is larger and the ϵ_{thrs} smaller for negative H values.

The behavior shown in Fig. 6 is typical of what happens at other frequencies in this parameter regime. Thus, we use $\epsilon_{1\%}$ and $\epsilon_{60\%}$ as the experimental estimates for ϵ_{thrs}. The comparison of the analytical and experimental values of ϵ_{thrs} are shown in Fig. 7a. The analytical value of ϵ_{thrs} changes dramatically as a function of frequency whereas the experimental values vary slowly with

frequency. The analytical value of ϵ_{thrs} is seen to be highly inaccurate for $\omega/\Omega \lesssim 2$ and $\omega/\Omega \gtrsim 5$ due to the importance of the phase effects for the L-o mode. If we replace H_o by H and $p_{\parallel_r}$ by the canonical momentum in (15), we find much better agreement with the experimental values as we will show shortly.

The ratio of $\epsilon_{60\%}$ to $\epsilon_{1\%}$ fluctuates between ~ 1.15 to 2.15 as evident from Fig. 7b. This ratio gets smaller at higher frequencies in contrast to case (i). The ϵ_{thrs} values are typically larger than those for the R-x mode in Fig. 3 in agreement with the previous predictions [Karimabadi et al., 1990].

Finally, the variation of ϵ_{thrs} with the propagation angle α is shown in Fig. 8. The variation of ϵ_{thrs} with angle has the general form of that for the R-x mode. The theoretical estimates are in reasonable agreement with experimental results for α between $10°$ and $80°$. For $\alpha \gtrsim 80°$, the theoretical threshold (15) appears to be inaccurate. As we mentioned earlier, this is due to the fact that at large angles the phase dependent term in H due to L-o mode becomes very large. There is a simple way of modifying (15) to account for the phase dependence: replace H_o by H and $p_{\parallel_r}$ by the canonical momentum. Thus, depending on the initial phase, we would have a different value of H which we then use in (15). The accuracy of this procedure is tested in Fig. 9. We find a good agreement with the experimental result. The agreement is surprisingly good considering the crude way that we have incorporated the phase effects into the expression for the trapping width.

The acceleration of particles starting at rest generally requires larger wave amplitudes than those starting with a finite energy. The Bessel functions in the trapping width go to zero if evaluated at $\gamma = 1$, and there are usually persistent KAM surfaces that separate such particles from the nearby resonance. The analytical results are however in reasonably good agreement with the experimental results in spite of the complexity of the dynamics at low energies.

V. Test of the Quasilinear Theory

In order to test the quasilinear theory, we have solved the diffusion equation for many different parameters and compared the results with exact orbit calculations. We take the initial particle distribution function to be a delta function centered at $\gamma = 1$. In the exact orbit calculations, we follow the orbits of 256 particles, all with initial $\gamma = 1$ and phases distributed uniformly between 0 and 2π, up to $\Omega t = 3000$. This corresponds roughly to the relevant length scale for ionospheric

heating [Menyuk. *et al.*, 1988]. The resulting distribution function is very bumpy due to the small number of particles used. To obtain smooth distributions, many more particles would have to be used—an approach which is both both impractical and unnecessary. Instead, we compare the moments of the two distribution functions. The small number of particles which we use is sufficient in this case to yield an accurate result. In the following, we use the quantities $\langle \gamma - \gamma_o \rangle \equiv \langle \Delta\gamma \rangle$ and $\langle (\gamma - \gamma_o)^2 \rangle \equiv \langle (\Delta\gamma)^2 \rangle$ to make the comparison, where γ_o is the initial γ of the particles and the brackets indicate an average over the initial conditions:

$$\langle (\gamma - \gamma_o)^2 \rangle = \frac{\int_1^\infty (\gamma - \gamma_o)^2 f(\gamma, t) d\gamma}{\int_1^\infty f(\gamma, t) d\gamma}. \tag{28}$$

Note that $D_{\gamma\gamma} \propto \langle (\Delta\gamma)^2 \rangle$. The test of the quasilinear theory is presented below.

(i) R-x mode, $\omega/\Omega = 1.97$

First, we consider the diffusion due to a R-x mode with $\omega/\Omega = 1.97$, $\alpha = 80°$ and $\omega_p/\Omega = 0.3$. The value $\omega_p/\Omega = 0.3$ corresponds roughly to the nighttime ionosphere at 130 km [Gurevich, 1978]. The theoretical and numerical ϵ_{thrs} are 0.19 and 0.143 respectively.

We carry out our comparison for wave amplitudes ranging from 0.19 to 10. The variation of several quantities as functions of time are shown in Fig. 10 for $\epsilon = 0.19$. The quantity $\langle (\Delta\gamma)^2 \rangle$ is seen to follow a linear increase in time in accord with the underlying assumptions built into the Fokker-Planck equation. The particles have not had enough time to sample all the available resonances and as a result the quantity $\langle (\Delta\gamma)^2 \rangle$ increases with time. Once the particles reach the energies beyond which $D_{\gamma\gamma}$ becomes very small, the $\langle (\Delta\gamma)^2 \rangle$ flattens out as a function of time and diffusion stops. For the parameters of Fig. 10, the flattening out does not happen until $\Omega t \gg 3000$.

The quantity D/D_{QL} which is the ratio of the exact orbit calculation of $\langle (\Delta\gamma)^2 \rangle$ to that obtained from the diffusion code, deviates significantly from unity at early times (Fig. 10c) but settles down close to its asymptotic value for $\Omega t \gtrsim 750$. This is expected since from Eqs. 16b and 16c, it follows that the diffusion formalism is strictly valid for times long compared with correlation time scales. Similar results are also seen at higher amplitudes as is apparent in Figs. 11 and 12.

The deviation of particle motion from the predicted quasilinear diffusion at early times can occur due to at least two effects: First, there can exist small but finite islands of stability within an otherwise stochastic phase space. A particle running close to such an island can get temporarily

78

trapped. Such stickiness in phase space can obviously have an effect on the diffusion of the particles. As we mentioned earlier, the trapping width increases as a function of harmonic number and in the transition to global chaos, the border of chaos lies at the lowest energies. Since we start the particles at $\gamma = 1$, and the stickiness is most important at the border of chaos which is also at $\gamma \sim 1$, the particles often experience some initial stickiness; however, once the particles reach the higher energies, they diffuse freely. Thus, there exists a finite time before all the particles can diffuse freely. The second source of deviation from the predicted quasilinear behavior is that the particles may initially sample a few resonances in which case the motion is closer to a coherent acceleration than diffusion. The first effect results in a retardation in the diffusion and the second effect leads to diffusion larger than D_{QL}. The balance between these two effects determines D/D_{QL} at early times. For $\Omega t \gtrsim 750$, the above two effects become much less important.

The Fig. 10d-e, show the evolution of $\langle z \rangle$ and $\langle z \rangle_{\gamma \gtrsim 10}$ in time, where $\langle z \rangle$ is the average distance in the z-direction travelled by the particles whereas $\langle z \rangle_{\gamma \gtrsim 10}$ is the average z-distance travelled by only those particles that attained $\gamma_{\max} \gtrsim 10$ during the length of the run. As the wave amplitude is increased, more of the particles can reach $\gamma_{\max} = 10$ and the evolution of $\langle z \rangle$ and $\langle z \rangle_{\gamma \gtrsim 10}$ become more similar as shown in Figs. 11 and 12. For parameters of this section, nearly all of the particles are accelerated in the positive z-direction. We can estimate the variation of z with time from (2): $\gamma - \gamma v_z/(cN_\parallel) \sim 1$ or

$$v_z = (\gamma - 1)N_\parallel c/\gamma. \tag{29}$$

We have used $H_\circ = 1$. As γ increases,

$$v_z \to N_\parallel c. \tag{30}$$

Note that the value of v_z is fixed independent of the wave amplitude. The line of $v_z = N_\parallel c$ is also plotted in Fig. 10d-e. The simple estimate (30) represents an upper bound on $\langle z \rangle$ in this case. Equation (30) becomes increasingly accurate at higher wave amplitudes where particles are accelerated faster and to larger energies as evident from Figs. 11 and 12. The particles with $\gamma \gtrsim 10$ cover a distance in z from 0 to 18 km in a time of $\Omega t = 2000$ and for $\epsilon = 0.10$. This range is increased to 0 - 21 km and 0 - 36 km for $\epsilon = 3.99$ and $\epsilon = 10$, respectively. Equation (30) predicts that all particles move in the positive z-direction, consistent with the numerical results.

The fraction of particles having $\gamma \gtrsim 10$ is plotted in Fig. 10e. The theoretical curve follows the experimental curve very closely especially at later times. The same is also true at other wave amplitudes as shown in Figs. 11 and 12.

Next we plot values of $\langle\Delta\gamma\rangle/\langle\Delta\gamma\rangle_{QL}$ and D/D_{QL} at $\Omega t = 3000$ for a range of wave amplitudes from $\epsilon = 0.19$ to 10. Here, $\langle\Delta\gamma\rangle$ and $\langle\Delta\gamma\rangle_{QL}$ are the average (over the initial condition) of $\Delta\gamma$ as obtained from numerical solutions of orbits and the diffusion code, respectively. The results are shown in Fig. 13. The quasilinear theory appears to be quite adequate in describing the particle motion over this rather large range in wave amplitude. For $\epsilon \gg 10$, the particle motion approaches the integrable regime of unmagnetized plasma in which case the diffusion equation would no longer be valid. The deviation of D/D_{QL} from unity as a function of wave amplitude has a sporadic behavior and does not seem to follow a nice oscillating pattern. In short, we have found no evidence for oscillations of D/D_{QL} as a function of wave amplitude, in contrast to what was found by Rechester and White [1980] in their studies of the standard mapping. Furthermore, the fluctuation amplitude of D/D_{QL} is much smaller than that seen in their work. The presence of resonances of different sizes clearly leads to averaging beyond that which is found in the standard map and thus to a closer correspondence to quasilinear theory. These results suggest that the standard map is not an ideal paradigm for real, physical systems.

(ii) L-o mode, $\omega/\Omega = 2.6$

Next, we consider the diffusion due to the L-o mode with $\omega/\Omega = 2.6$, $\alpha = 80°$ and $\omega_p/\Omega = 0.3$. The theoretical threshold is 0.42 and the numerical thresholds $\epsilon_{1\%}$ and $\epsilon_{60\%}$ are 0.4 and 0.75, respectively.

The evolution of the various quantities as functions of time are shown in Figs. 14 through 16. The quantity $\langle(\Delta\gamma)^2\rangle$ follows a more or less linear increase in time as before.

The diffusion is larger than D_{QL} at early times as shown in Fig. 14c even though for $\epsilon = 0.427$ less than 50% of the particles are stochastic. Similar behavior is also seen at higher wave amplitudes (Figs. 15c, 16c). This is mainly due to the fact that at early times some particles are coherently accelerated by a few resonances. As before, for $\Omega t \gtrsim 750$, the D/D_{QL} settles down close to its final value. For $\epsilon = 0.427$, the asymptotic value of D/D_{QL} is below unity (Fig. 14c). This is due to the fact that at this wave amplitude less than 60% of the particles are stochastic. As the wave

amplitude is increased, more of the particles become stochastic and eventually D/D_{QL} becomes larger than unity as shown in Figs. 15c and 16c.

The evolution of $\langle z \rangle$ and $\langle z \rangle_{\gamma \gtrsim 10}$ in time are shown in Fig. 14d for $\epsilon = 0.427$. A good majority of the particles are now travelling in the negative z–direction and the analytical estimate (30) agrees reasonably well with $\langle z \rangle_{\gamma \gtrsim 10}$ but not with $\langle \gamma \rangle$. This is expected since for $\epsilon = 0.427$ less than 60% of the particles are stochastic and (30) is strictly valid for high energy particles. Furthermore, as we have already shown, for the L-o mode the phase effects become important and in estimating v_z, it is the full Hamiltonian H and not H_o that has to be used:

$$v_z = (\gamma - H/mc^2 + \frac{q}{|q|}\frac{\epsilon_1}{N_\parallel}\sin\alpha\sin\psi)\frac{N_\parallel}{\gamma}. \tag{31}$$

Now, v_z can be either negative or positive depending on ψ and H. Notice that $\langle z \rangle_{\gamma \gtrsim 10}$ is actually larger in Fig. 14e than it is in Figs. 15e and 16e. This is a result of the high energy particles moving in the positive z–direction when $\epsilon = 0.427$; whereas, when $\epsilon = 3.9$ and 10, the high energy particles move large distances in both the positive and negative z–directions, and, thus, averaging yields smaller values z-values. When $\epsilon = 0.427$, the particles having $\gamma \gtrsim 10$ cover a range in z from 0 to 27 km in $\Omega t = 3000$; whereas, for $\epsilon = 3.9$ and 10, the range in z is -25 to 40 km and -30 to 43 km, respectively.

The fraction of particles with $\gamma \gtrsim 10$ as obtained from the diffusion code and exact orbit calculations are shown in Figs. 14e, 15e and 16e. The agreement between the two methods seems very good for $\Omega t \gtrsim 1000$.

Finally, we examine the behavior of $\langle \Delta\gamma \rangle / \langle \Delta\gamma \rangle_{QL}$ and D/D_{QL} as functions of wave amplitude. This is shown in Fig.17 where we have plotted $\langle \Delta\gamma \rangle / \langle \Delta\gamma \rangle_{QL}$, and D/D_{QL} at $\Omega t = 3000$ for a range of wave amplitudes. The quantity $\langle \Delta\gamma \rangle / \langle \Delta\gamma \rangle_{QL}$ is well below unity for $\epsilon = 0.43$ and it does not reach unity until the wave amplitude has been increased to $\epsilon \sim 1.5$. For $\epsilon \gtrsim 1.5$, the $\langle \Delta\gamma \rangle / \langle \Delta\gamma \rangle_{QL}$ has small fluctuations about unity. The $\langle \Delta\gamma \rangle_{QL}$ was obtained by using $H = 1$. However, as we showed earlier, the phase effects are important for the L-o mode and the ϵ_{thrs} depends strongly on the value of H which has a finite range even for $\gamma = 1$. The ϵ_{thrs} can change by more than a factor of 3 depending on the value of H (see e.g., Fig. 9). Thus, we must take into account the fraction of particles that are not stochastic at a given wave amplitude. The ratio of stochastic particles is $\sim 60\%$ at $\epsilon = 0.43$, $\sim 75\%$ at $\epsilon = 0.8$, $\sim 80\%$ at $\epsilon = 1.1$, $\sim 93\%$ at $\epsilon = 1.3$, and $\sim 99\%$ at $\epsilon = 1.5$.

This is why $\langle\Delta\gamma\rangle/\langle\Delta\gamma\rangle_{QL}$ is below unity for $\epsilon \lesssim 1.5$. Let us denote the integrable particles by the subscript 'int' and the stochastic particles by the subscript 'st'. What we should really be plotting in Fig. 17a is $\langle\Delta\gamma\rangle_{st}/\langle\Delta\gamma\rangle_{QL}$ and not $\langle\Delta\gamma\rangle/\langle\Delta\gamma\rangle_{QL}$. But $\langle\gamma\rangle_{st}/\langle\gamma\rangle_{QL} \sim \langle\gamma\rangle(N_{int} + N_{st})/N_{int}\langle\gamma\rangle_{QL}$, where we have assumed $\langle\gamma\rangle_{int}/\langle\gamma\rangle_{QL} \ll 1$. Using the values of N_{st} cited above for various ϵ's, it then follows that $\langle\Delta\gamma\rangle_{st}/\langle\Delta\gamma\rangle_{QL}$ is indeed very close to unity. In short, the discrepancy between $\langle\Delta\gamma\rangle$ and $\langle\Delta\gamma\rangle_{QL}$ in Fig. 17a for $\epsilon \lesssim 1.5$, results from the inclusion of integrable orbits in $\langle\gamma\rangle$ but not in $\langle\Delta\gamma\rangle_{QL}$. The fraction of stochastic particles can be calculated analytically by incorporating phase effects in (15) as we did in Fig. 9. We then find that stochastic particles are well described by the diffusion code.

Similarly, the agreement between D and D_{QL} is very good. This result is encouraging, considering that the theoretical analysis presented in this paper are at their worst for the parameters of this section where the phase effects are important and H is not just confined to one value. Thus, we conclude that the diffusion formalism is quite robust and is highly accurate in predicting the time evolution of an ensemble of particles.

VI. Application to the Ionosphere

In this section, we assess the plausibility of accelerating the electrons in the ionosphere using ground based transmitters.

There are three requirements for the effective acceleration of particles: (1) the wave amplitude must be larger than ϵ_{thrs}; (2) particles must remain in the system (ionosphere) long enough to diffuse to high energies; and (3) the acceleration mechanism should be insensitive to details of the initial particle distribution.

If condition (1) can be met, then condition (3) is also satisfied since the stochastic particle acceleration, in contrast to any coherent mechanism, is quite robust. First, we consider the power needed in order to achieve $\epsilon \gtrsim \epsilon_{thrs}$ in the ionosphere. As we showed earlier, the lowest ϵ_{thrs} occurs for the R-x mode in the nighttime ionosphere ($\omega_p/\Omega = 0.3$) in the frequency range $\omega/\Omega \sim 1.0 - 2$. The threshold can be as low as 0.08 at $\alpha \sim 50°$ and $\epsilon \sim 0.1$ at $\alpha \sim 80°$. At such low wave amplitudes, only a small fraction $\lesssim 5\%$ of particles can be accelerated. Fortunately, the transition to global chaos is abrupt in this parameter regime and once ϵ is raised to ~ 0.14, more than 90%

of the particles become stochastic. Thus, the minimum wave amplitude for stochastic particle acceleration by waves with $N_\parallel < 1$ is between $\epsilon \sim 0.08 - 0.14$.

The stochasticity threshold is in general much lower ($\epsilon \sim 10^{-4} - 10^{-3}$) for waves having $N_\parallel > 1$, but the Hamiltonian surfaces are closed in such cases, only a few resonances are available, and the acceleration is much smaller than in cases where $N_\parallel < 1$.

The power flux is related to the wave amplitude by [Menyuk, et al., 1988]:

$$P \simeq 30 \left(\epsilon \frac{\omega}{\Omega} \right)^2 W/cm^2. \tag{32}$$

Thus, a power flux in the range $\sim 0.7 - 2.3 \ W/cm^2$ is required to accelerate the zero energy electrons to large energies in the ionosphere. Let us for the moment suppose that such a power flux can be achieved. We then estimate the size of the acceleration region. The main motion of the particle is in the $z-$direction and the particles execute Larmor motion in the perpendicular motion with $r_L = v_\perp \gamma / \Omega$. Using (30) and setting $z \sim r_L$, we obtain $\gamma v_\perp / c \sim N_\parallel \Omega t$. For the parameters in Fig. 10 and for $\Omega t = 3000$, we have $\gamma v_\perp / c \sim \gamma \sim 512$. Thus, the escape of the particles occurs in the $z-$direction. Even though the evolution of $< z >_\gamma \gtrsim 10$ in time is insensitive to the wave amplitude, more particles can be accelerated in less time at larger wave amplitudes. For $\epsilon \simeq 0.1 - 0.2$, the typical distance that is required for accelerating a significant number of particles to $\gamma \gtrsim 10$ is of the order of $10 - 20$ km as shown in Fig. 10. Thus, considering a region of ionosphere 10 km $\times$ 20 km, the total power required is $\sim 1.4 \times 10^{12} - 4.6 \times 10^{12}$ W. If we launch 1 msec pulses with a duty cycle of 1 per minute, we find an average power of $\sim 10^7 - 10^8$ W. These values are beyond the present-day capabilities.

In view of our findings, we are forced to consider ways to reduce the stochasticity threshold. There are several possibilities: (1) Preaccelerate the electrons. This involves a two-step process. First, the particles are accelerated to weakly relativistic energies and then the rf waves are applied. Since the ϵ_{thrs} is lower at higher energies, we could make the particles stochastic for lower rf amplitudes. The dependence of ϵ_{thrs} on energy is, however, weak and this technique can at most lower the amplitude required by a factor of 2. (2) Apply several waves at closely spaced frequencies. The problem is that if the wave amplitudes are too far below the ϵ_{thrs} value of a single wave, the resulting diffusion would be limited and slow. (3) The magnetic field in the ionosphere is well represented by a magnetic dipole. Thus, a more realistic application to the ionosphere requires

taking into account the inhomogeneity of the magnetic field. It is well known that even a weak inhomogeneity in the magnetic field can lower the ϵ_{thrs} by as much as 2 orders of magnitude. Physically, the change in B_o is equivalent to having several resonances for a given harmonic number. Thus, the resonances are more tightly packed and the overlap occurs at smaller amplitudes than in the uniform field limit. In order to have a strong enough diffusion, however, the wave amplitude cannot be much smaller than in the uniform field limit.

Finally, the self-consistent effects are expected to play a role once a significant number of particles are accelerated. The study of self-consistent effects as well as mode conversion are currently underway, and preliminary results were reported by Akimoto and Karimabadi (1989).

VII. Conclusions

In this work, we have carried out a detailed comparison of the theoretical stochasticity threshold with exact orbit calculations. We reduced the diffusion equation to a one-dimensional form by transforming to a coordinate system where the Hamiltonian surface is one of the axes. We then constructed a model for the diffusion coefficient and wrote a finite element code that solves the diffusion equation. This code has been carefully compared with a particle code, and it shows excellent agreement over a wide range of frequencies and wave amplitudes. We applied our results to the problem of radio-frequency acceleration of the electrons in the ionosphere. We found that the powers needed are beyond present-day technology. We then discussed several ways to overcome this problem.

Finally, we emphasize that the method of reducing the diffusion equation to one dimension and the code that we have developed are quite powerful and are expected to find many applications. We are currently applying the above techniques to the problem of particle acceleration in planetary shocks.

Appendix A: Diffusion Equation Along the H-surface

In this appendix, we show how the diffusion equation can be reduced to a one-dimensional form by choosing a coordinate system that has H as one of the axes. A given H-surface is given by:

$$H_o = mc^2 \gamma_o - p_\| \omega / k_\|. \tag{A1}$$

We can rewrite the equation for H_o as

$$a_H \left(\frac{P_\|}{mc} + \frac{b_H}{a_H} \right)^2 - \frac{P_\perp^2}{m^2 c^2} = \frac{b_H^2}{a_H} + 1 - H_o^2, \tag{A2a}$$

where

$$a_H = \frac{1}{N_\|^2} - 1, \tag{A2b}$$

$$b_H = \frac{H_o}{N_\|}, \tag{A2c}$$

The H-surfaces are not confocal since both a_H and b_H depend on H. Thus, a confocal orthogonal transformation cannot be made. In fact there is no simple transformation from $(p_\|, p_\perp)$ to an orthogonal coordinate system with the H-surface as one of the axes. Fortunately, the orthogonality condition is not necessary, and, as we now show, any component of the diffusion tensor not parallel to the H-surface is zero.

Let us consider the diffusion equation under the transformation from $(p_\|, p_\perp)$ to (H, g) where g is arbitrary for the moment. We start with (19) rewritten in tensor notation:

$$\frac{\partial f}{\partial t} = \frac{1}{R} \frac{\partial}{\partial p_i} \left(R D_{ij} \frac{\partial f}{\partial p_j} \right), \tag{A3}$$

where $R = p_\perp$ is the Jacobian of the transformation from Cartesian to cylindrical coordinates. From the chain rule, we have

$$\frac{\partial}{\partial p_i} = \frac{\partial y_k}{\partial p_i} \frac{\partial}{\partial y_k}. \tag{A4}$$

where $y_1 = H$ and $y_2 = g$. Using this in (A3), yields

$$\frac{\partial f}{\partial t} = \frac{1}{R} \frac{\partial y_k}{\partial p_i} \frac{\partial}{\partial y_k} \left(R D_{ij} \frac{\partial y_\ell}{\partial p_j} \frac{\partial f}{\partial y_\ell} \right)$$

$$= \frac{\partial}{\partial y_k} \left(\frac{\partial y_k}{\partial p_i} D_{ij} \frac{\partial y_\ell}{\partial p_j} \frac{\partial f}{\partial y_\ell} \right) - R D_{ij} \frac{\partial y_\ell}{\partial p_j} \frac{\partial f}{\partial y_\ell} \frac{\partial}{\partial y_k} \left(\frac{1}{R} \frac{\partial y_k}{\partial p_i} \right), \tag{A5}$$

or

$$\frac{\partial f}{\partial t} = \frac{\partial}{\partial y_k}\left(\bar{D}_{k\ell}\frac{\partial f}{\partial y_\ell}\right) - RD_{ij}\frac{\partial y_\ell}{\partial p_j}\frac{\partial f}{\partial y_\ell}\frac{\partial}{\partial y_k}\left(\frac{1}{R}\frac{\partial y_k}{\partial p_i}\right).$$

where $\bar{D}_{k\ell}$ is the new diffusion tensor and is given by

$$\bar{D}_{k\ell} = \frac{\partial y_k}{\partial p_i}D_{ij}\frac{\partial y_\ell}{\partial p_j}.$$

Writing out the various components of the diffusion tensor explicitly, we have

$$D_{HH} = \sum_\ell\left[D_{\|\|_\ell}\left(\frac{\partial H}{\partial p_\|}\right)^2 + 2D_{\perp\|_\ell}\frac{\partial H}{\partial p_\|}\frac{\partial H}{\partial p_\perp} + D_{\perp\perp_\ell}\left(\frac{\partial H}{\partial p_\perp}\right)^2\right], \qquad (A8a)$$

$$D_{gg} = \sum_\ell\left[D_{\|\|_\ell}\left(\frac{\partial g}{\partial p_\|}\right)^2 + 2D_{\perp\|_\ell}\frac{\partial g}{\partial p_\|}\frac{\partial g}{\partial p_\perp} + D_{\perp\perp_\ell}\left(\frac{\partial g}{\partial p_\perp}\right)^2\right], \qquad (A8b)$$

$$D_{Hg} = \sum_\ell\left[D_{\|\|_\ell}\frac{\partial H}{\partial p_\|}\frac{\partial g}{\partial p_\|} + D_{\perp\|_\ell}\left(\frac{\partial H}{\partial p_\|}\frac{\partial g}{\partial p_\perp} + \frac{\partial g}{\partial p_\|}\frac{\partial H}{\partial p_\perp}\right) + \right.$$
$$\left. D_{\perp\perp_\ell}\frac{\partial H}{\partial p_\perp}\frac{\partial g}{\partial p_\perp}\right], \qquad (A8c)$$

and

$$D_{Hg} = D_{gH}. \qquad (A8d)$$

The derivatives are evaluated at the crossing points of a given H–surface and the resonance curves. In particular, we find

$$\frac{\partial H}{\partial p_\|} = -\frac{\Omega}{\omega}\frac{\ell}{p_\perp N_\|}\frac{\partial H}{\partial p_\perp}. \qquad (A9)$$

It follows that D_{HH} is identically zero. Furthermore, using the relation (A9) and substituting (22) in (A8c), we find that D_{Hg} is identically zero independent of the form of g. So, the new coordinate system need not be orthogonal. The fact that $D_{Hg} = D_{HH} = 0$ is hardly surprising since both D_{Hg} and D_{HH} involve integrals over the quantity $\dot{H}$ which is zero.

A useful choice for g is the relativistic factor γ. The surfaces of constant γ define circles in momentum space. The old variables are realted to the new variables by

$$\frac{p_\|}{mc} = (\gamma - \frac{H}{mc^2})N_\|, \qquad (A10a)$$

$$\frac{p_\perp}{mc} = \left[\gamma^2 - 1 - N_\|^2(\gamma - \frac{H}{mc^2})^2\right]^{1/2}. \qquad (A10b)$$

86

and the Jacobian of the transformation in dimensionless units is given by

$$R = \gamma N_\parallel,$$

(A11)

which is valid for $\alpha \neq 90°$. Replacing g by γ, and using (A8) through (A11) in (A6) and (A7), we obtain the diffusion equation (23a) and diffusion coefficient (23b).

References

1. K. Akimoto and H. Karimabadi. *Phys. Fluids.* BF1, 2530 (1989).

2. K. Akimoto and H. Karimabadi. *Phys. Fluids.* 31, 1505 (1988).

3. S. Chandrasekhar. *Rev. Mod. Phys.*, 15, 1 (1943).

4. B. V. Chirikov, *Phys. Rep.* 52, 263 (1979).

5. G. Dhatti, and G. Touzot. *The Finite Element Displayed* (John Wiley and Sons. New York. 1984).

6. W.E. Drummond, and D. Pines, *Nucl. Fusion Suppl.*, 3, 1049 (1962).

7. T. H. Dupree, *Phys. Fluids* 9, 1773 (1966).

8. G. Ginet, M. Heinemann. *Phys. Fluids*, 3, (1990).

9. H. Karimabadi, *Ph.D. Thesis*, University of Maryland, 1988.

10. H. Karimabadi, C. R. Menyuk, P. Sprangle and L. Vlahos, *Ap. J.*, 316, 462 (1987).

11. H. Karimabadi, N. Omidi, and K. Akimoto, *EOS*, 70, 284 (1989).

12. H. Karimabadi, K. Akimoto, N. Omidi, and C. R. Menyuk, *Phys. Fluids B*, 2, 606 (1990).

13. A. J. Lichtenberg and M. A. Lieberman, *Regular and Stochastic Motion* (Springer-Verlag, New York, 1983).

14. C. R. Menyuk, A. T. Drobot, K. Papadopoulos, and H. Karimabadi. *Phys. Rev. Lett.* 58, 2071 (1987); and *Phys. Fluids* 31, 3768 (1988).

15. L. Muschietti, K. Appert, and J. Vaclavik. *Phys. Fluids.* 24, 151 (1981).

16. A. B. Rechester, and R. B. White, *Phys. Rev. Lett.* 44, 1586 (1980).

17. Y. A. Romanov, and G.F. Filippov, *Sov. Phys. JETP*, 13, 87, (1961).

18. P. A. Sturrock, *Phys. Rev.*, 141, 186 (1966).

19. A. A. Vedenov, E. P. Velikhov, and R.Z. Sagdeev, *Nucl. Fusion.* 1, 82 (1961); *Nucl. Fusion Suppl.*, 2, 465 (1962).

20. E. Villalón and W. J. Burke, *Phys. Fluids*, 30, 3695 (1987).

21. G. M. Zaslavsky, and B. V. Chirikov, *Sov. Phys. Usp.*, 14, 549 (1972).
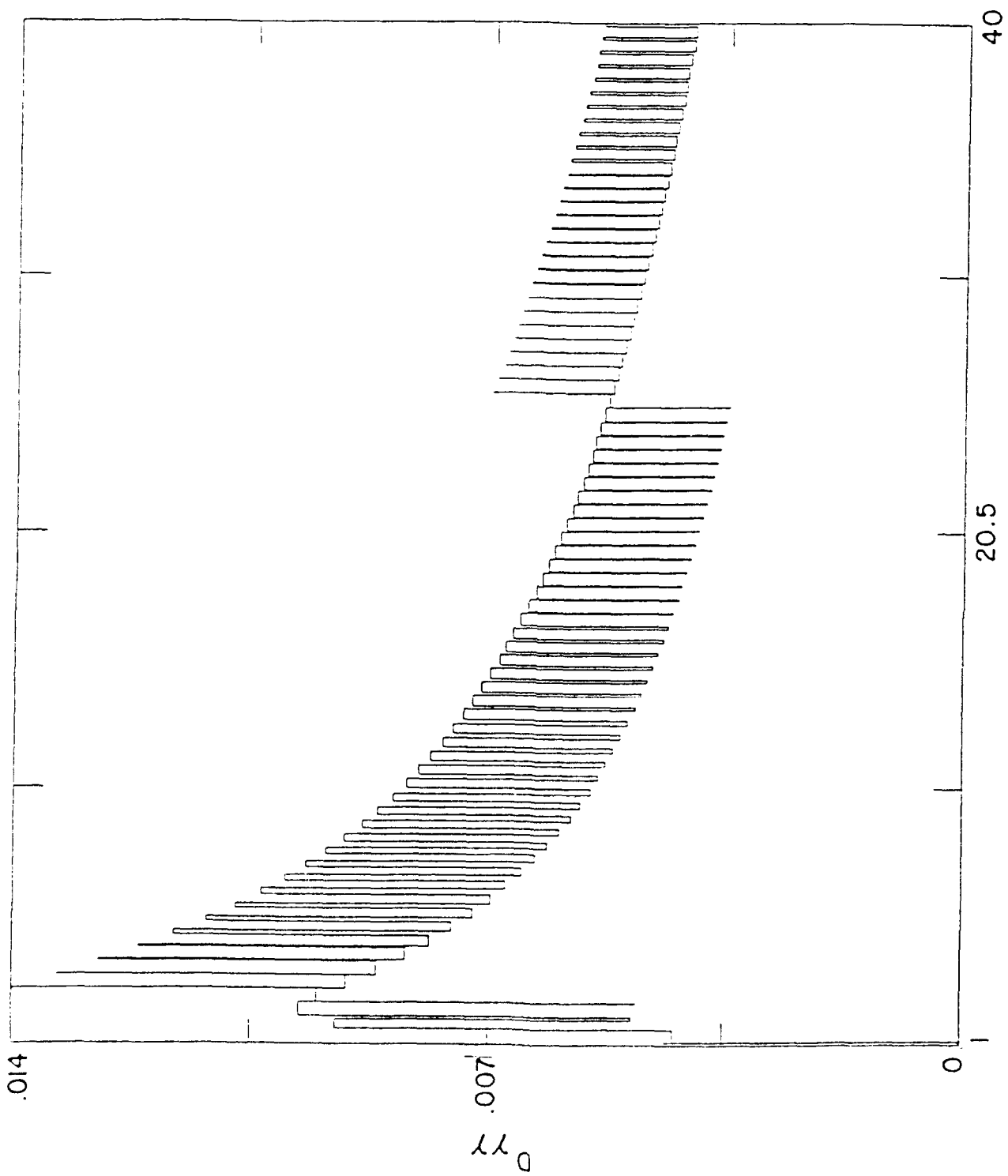
Figure 1a

Figure 1b

COUNTS OF OVERLAPS

γ

Figure 2a

91
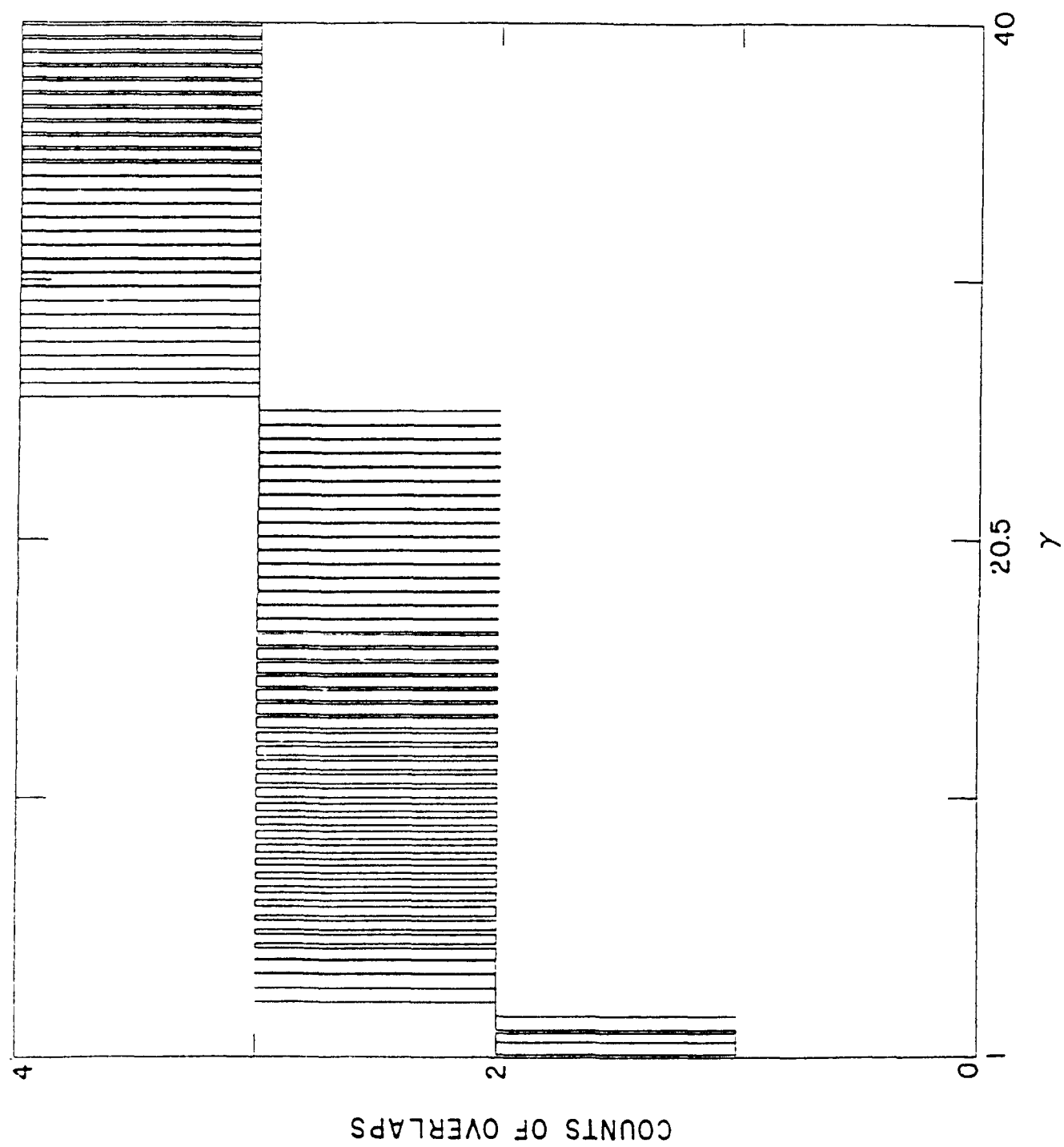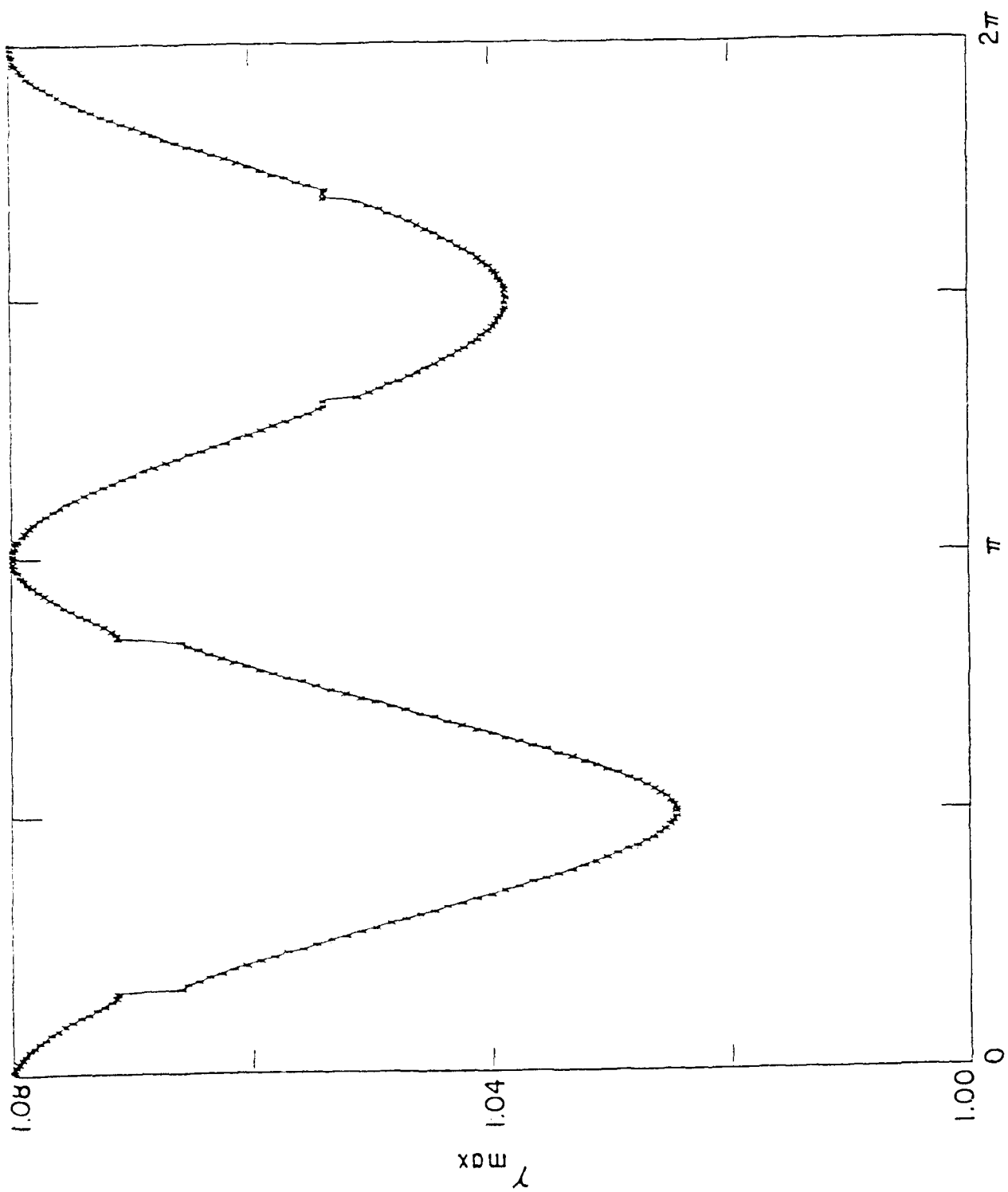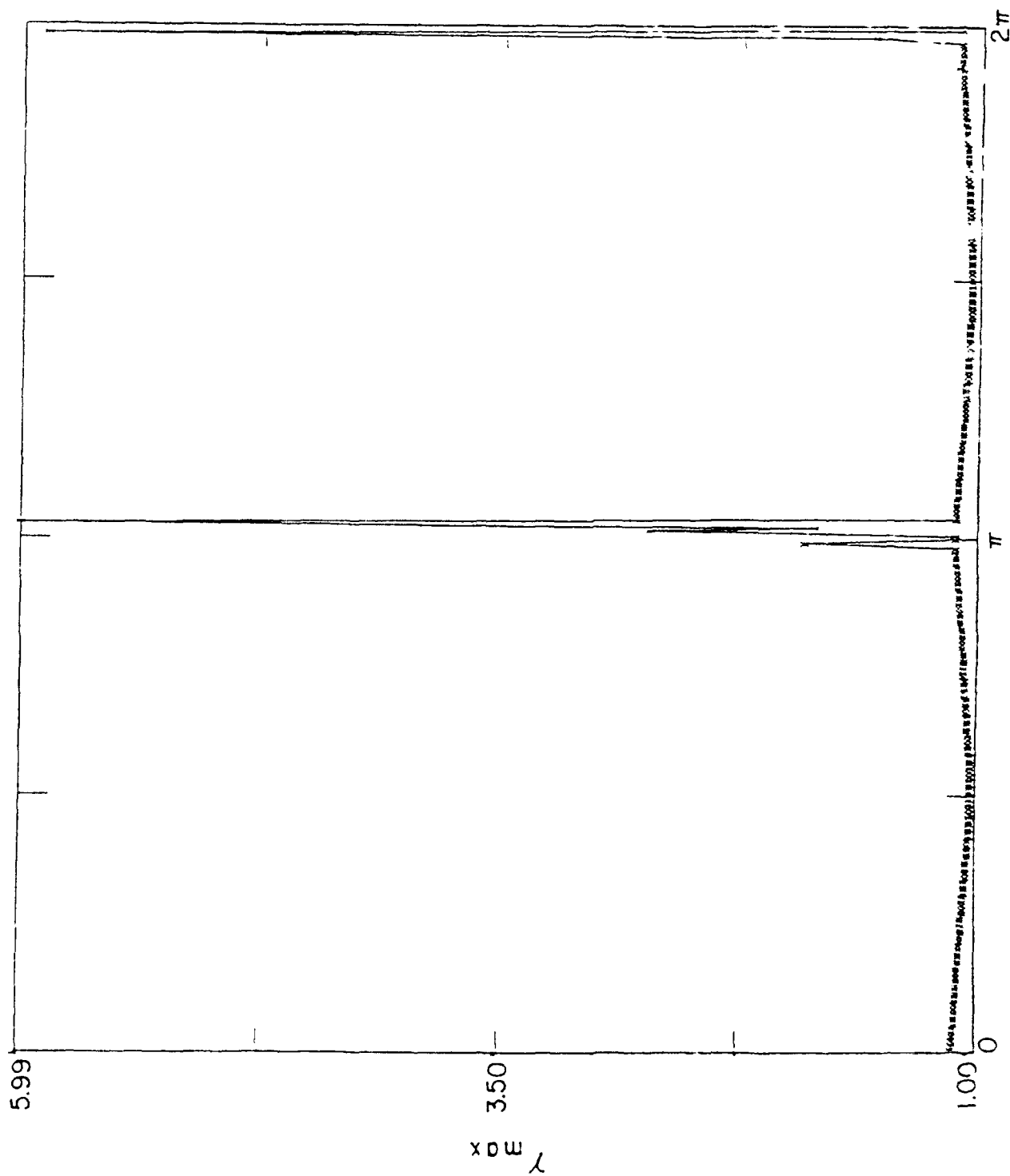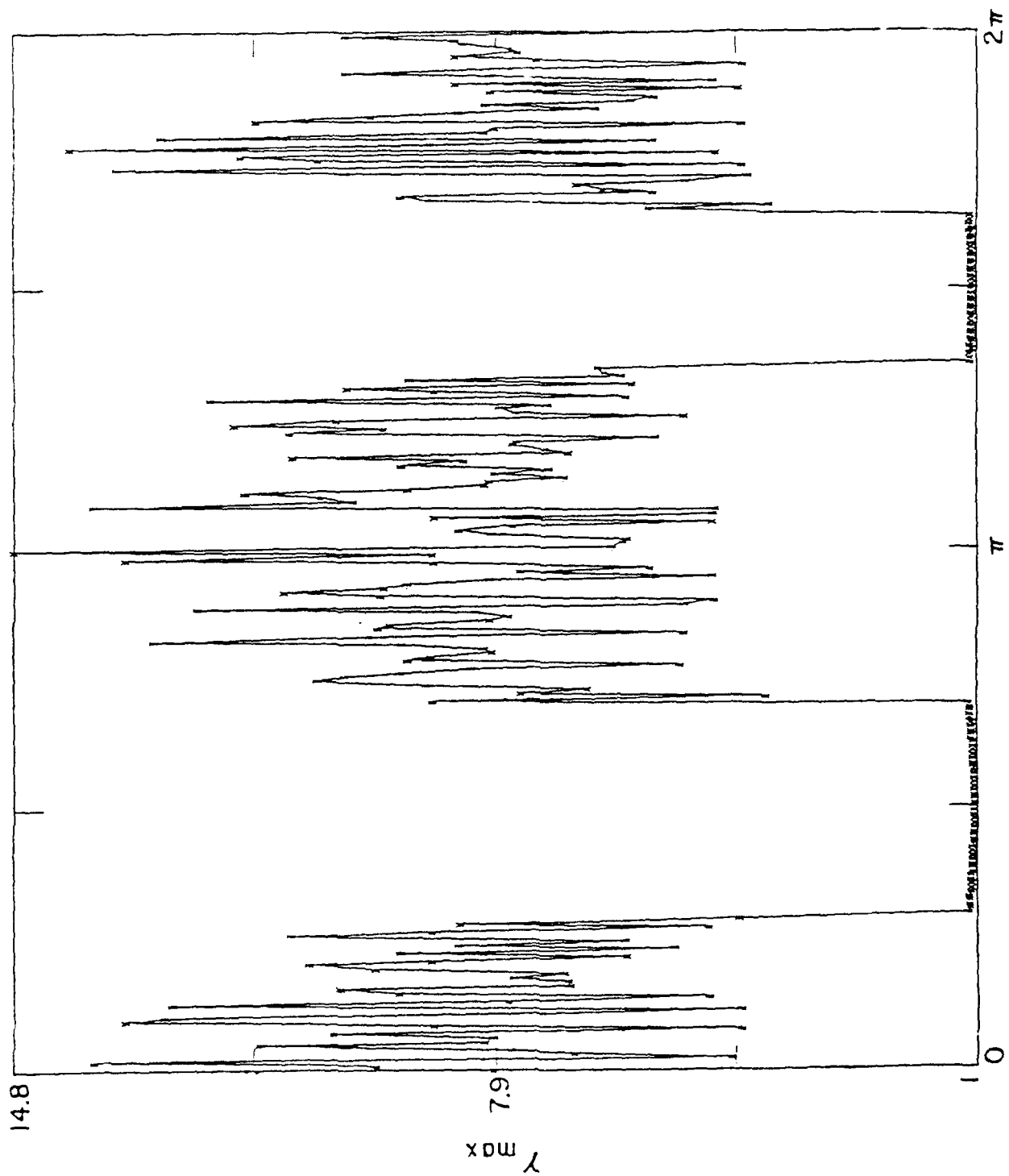
Figure 2b

Figure 2c
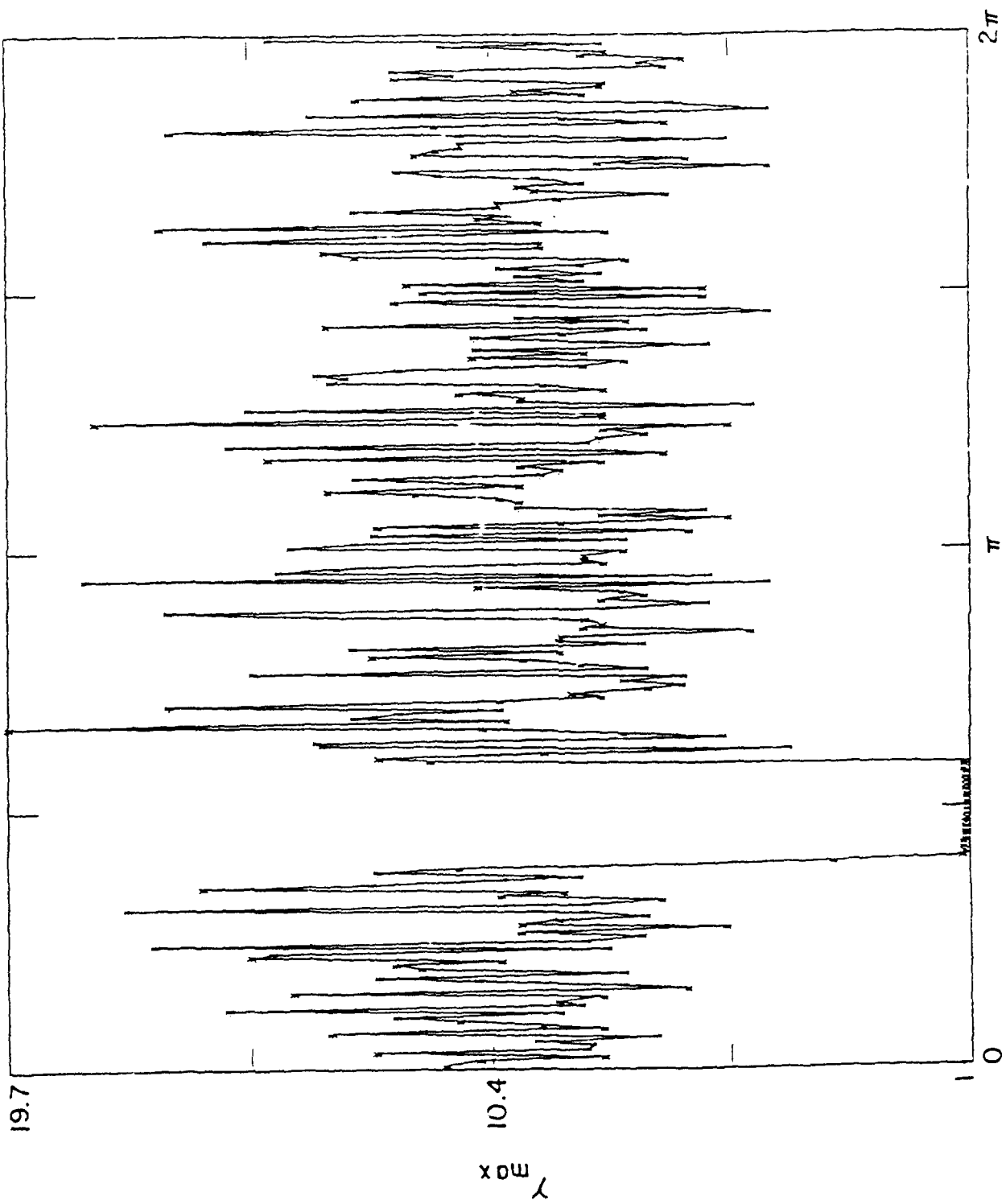
Figure 2d
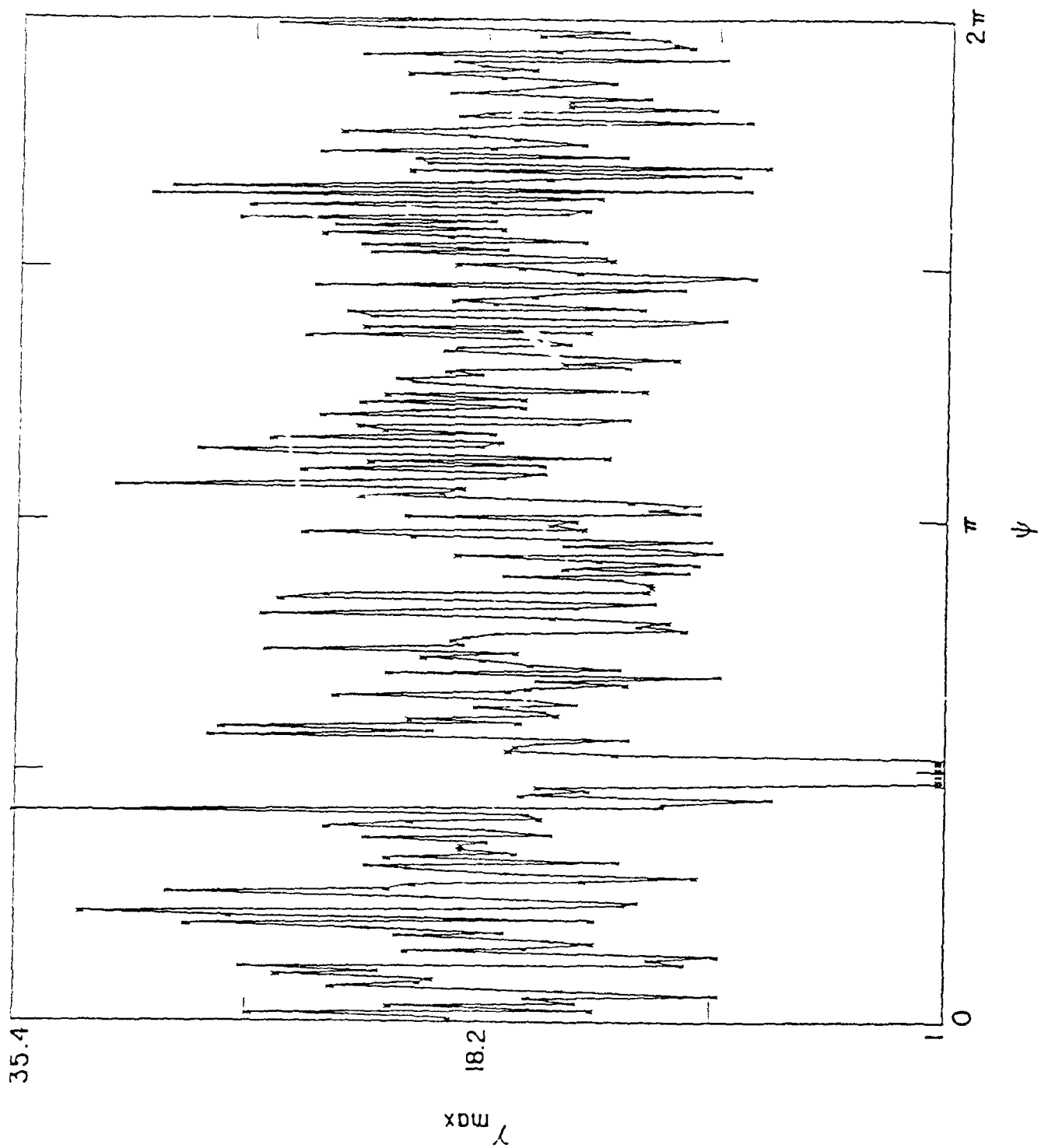
Figure 2e
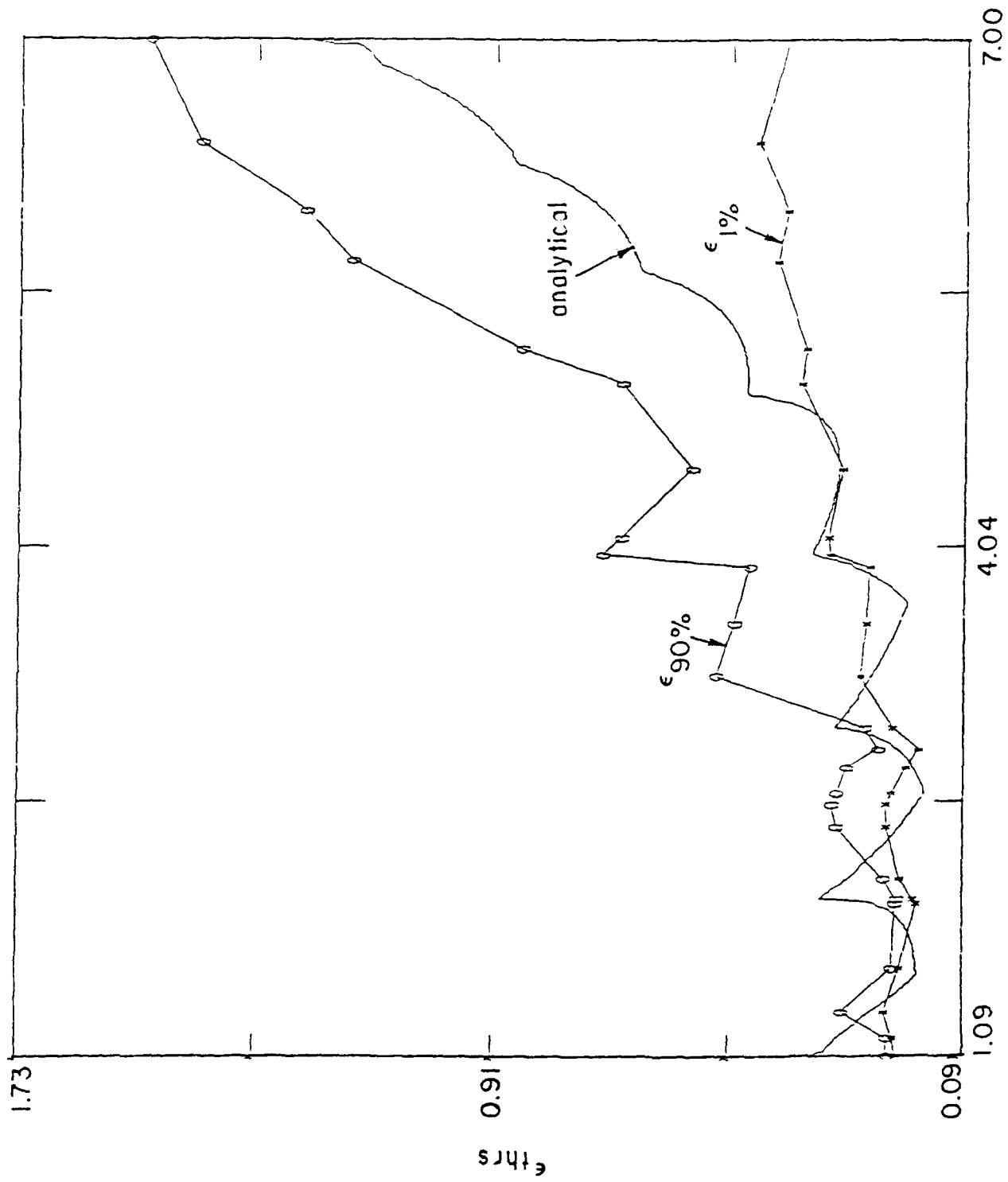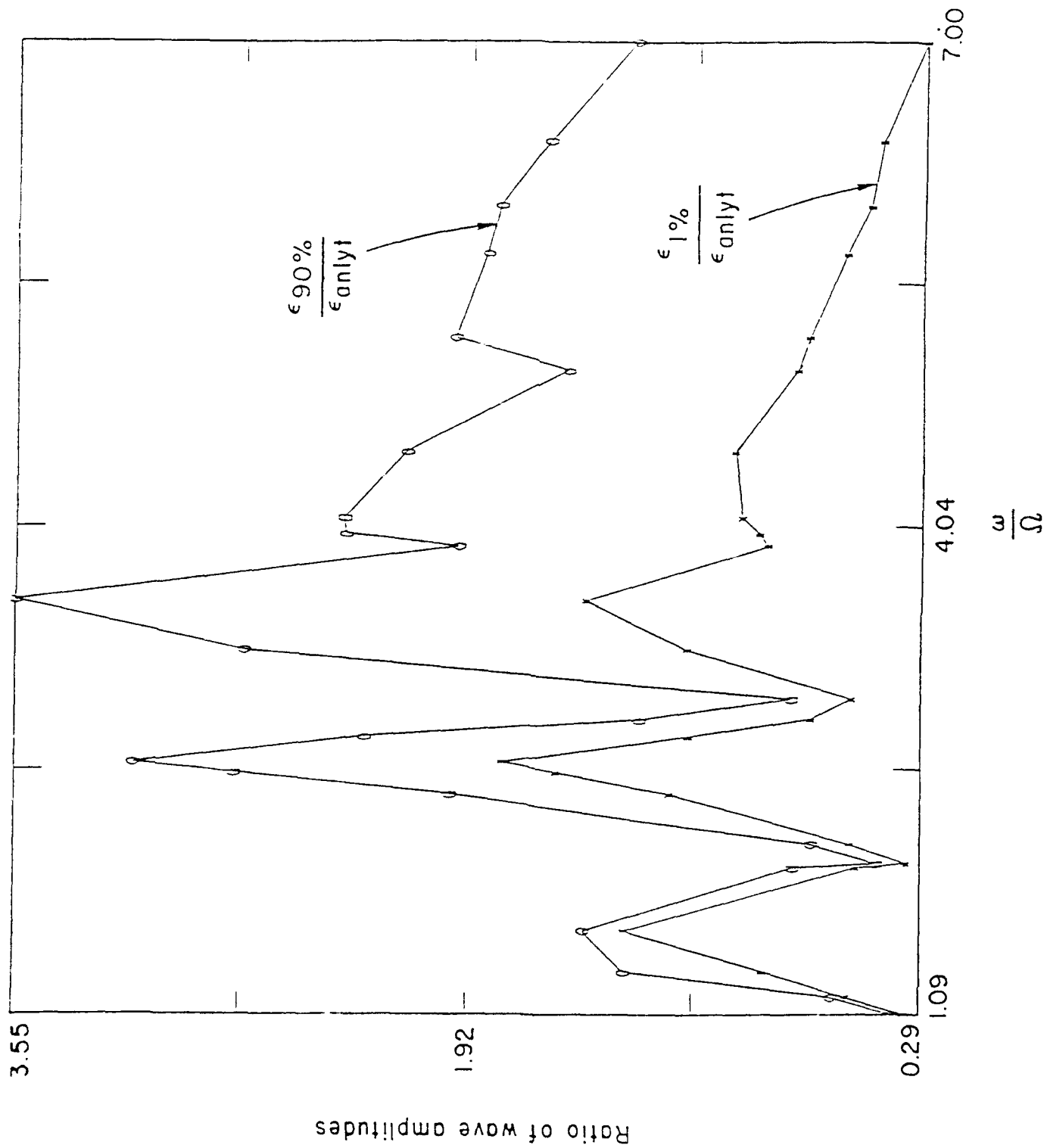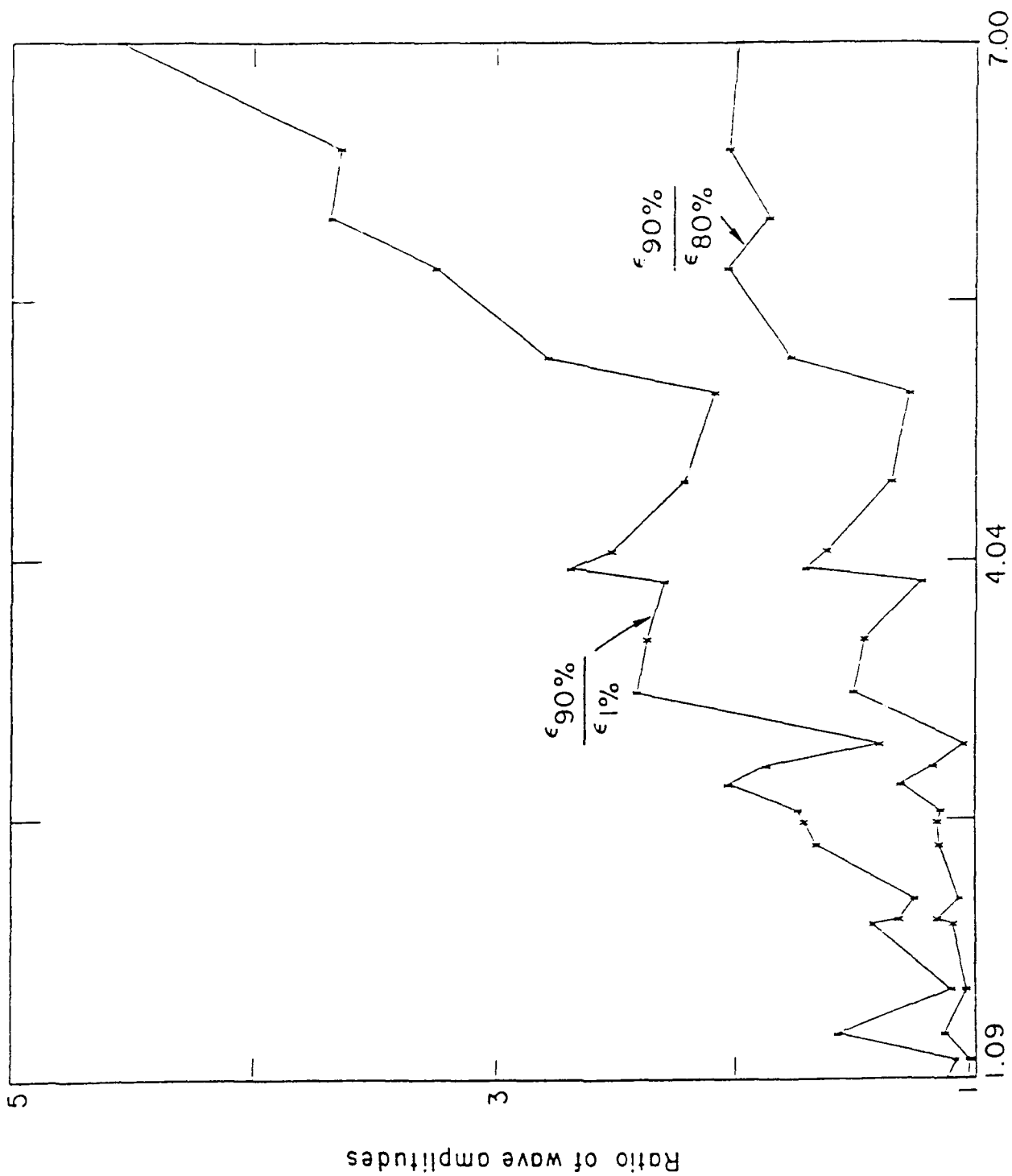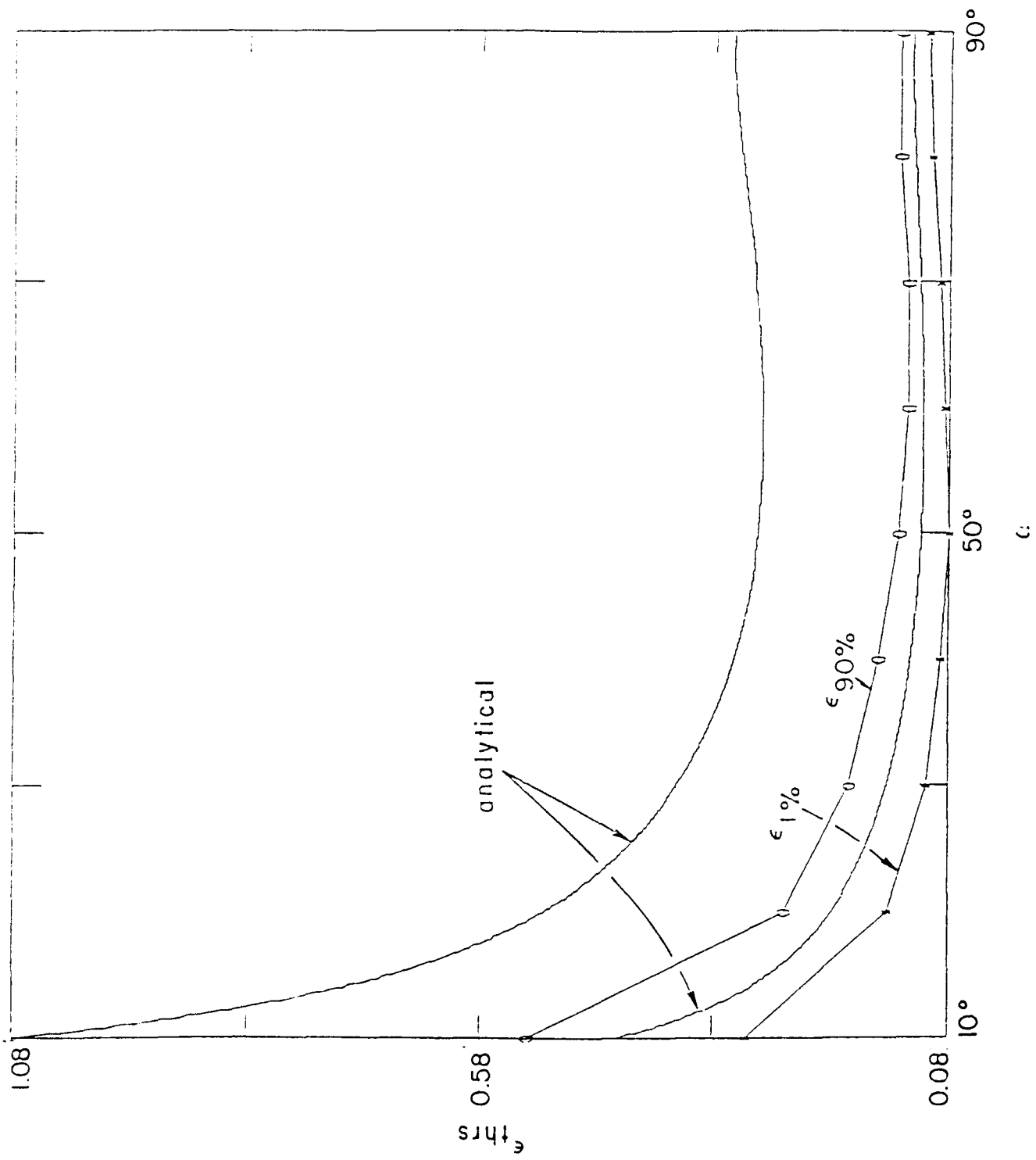
γ_{max}

35.4

18.2

0   π 2π

ψ

95

Figure 3a

96

Figure 3b

97

Ratio of wave amplitudes

$\frac{\omega}{\Omega}$

Figure 3c

38

Figure 4

Figure 5

100

Figure 6a

101

Figure 6b

102

Figure 6c

103

Figure 6d

γ_{max}

ψ

33.8

17.4

0

π

2π

104

Figure 7a

105

Figure 7b

$$\frac{\omega}{\Omega}$$
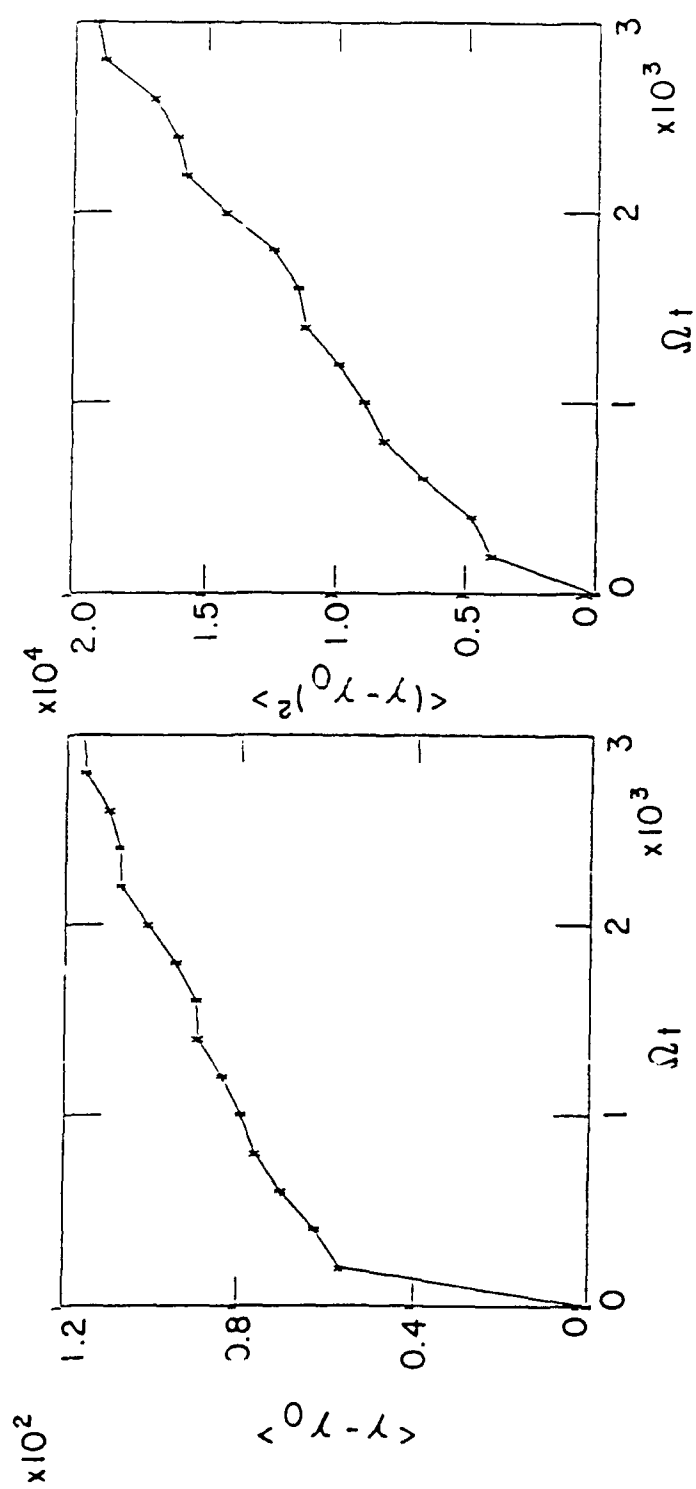
$\epsilon_{60\%} / \epsilon_{1\%}$

a

Figure 8

107
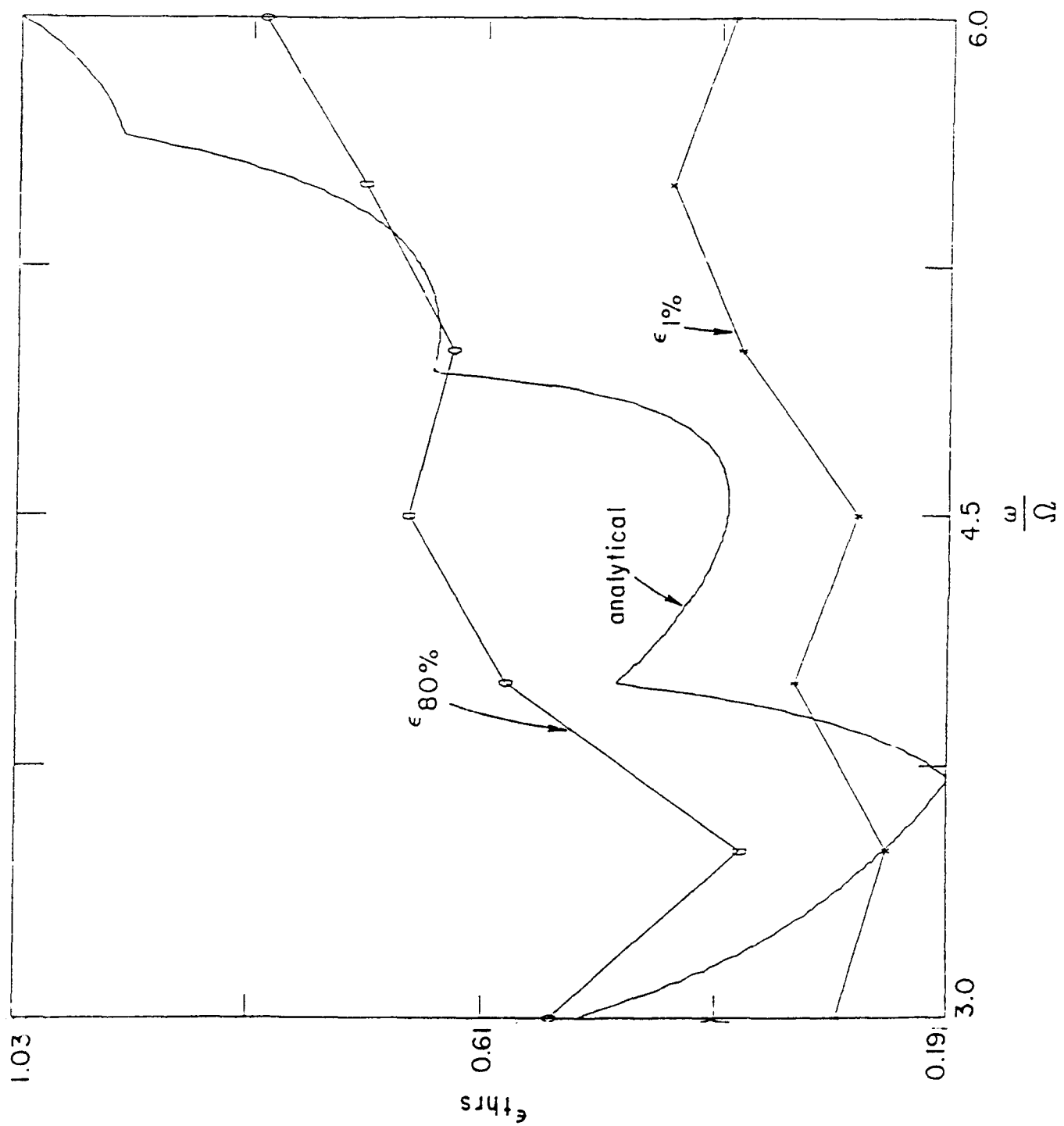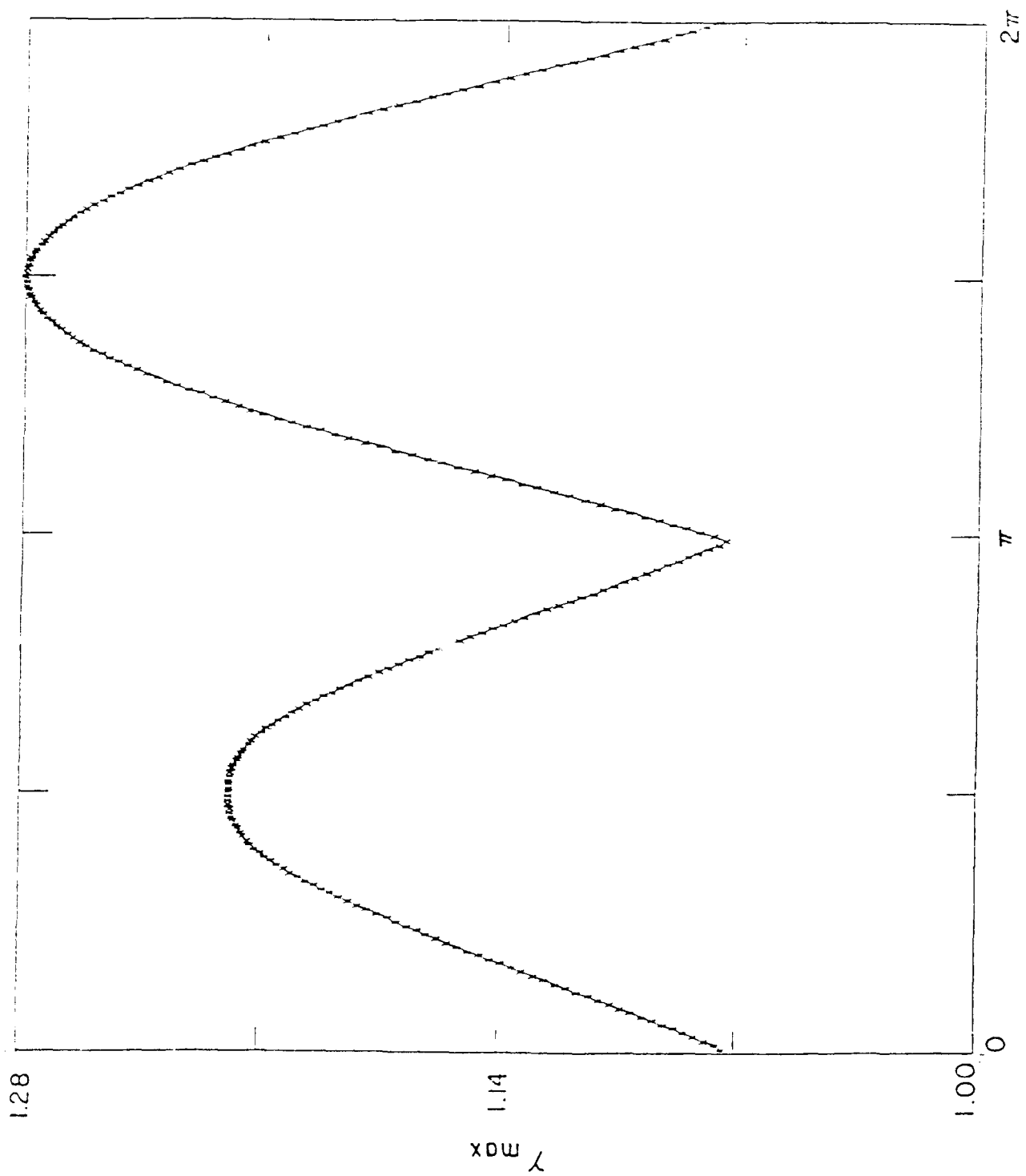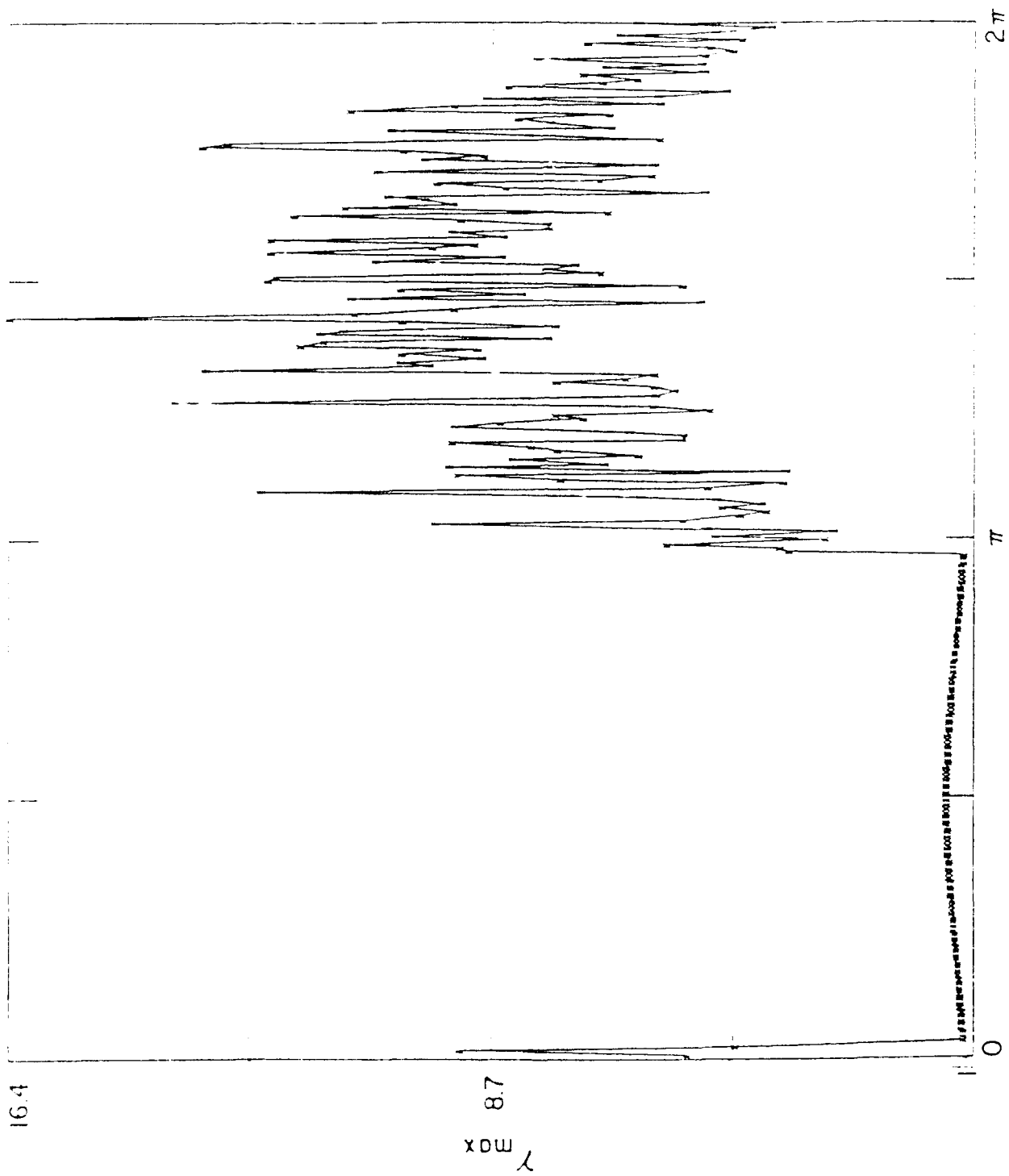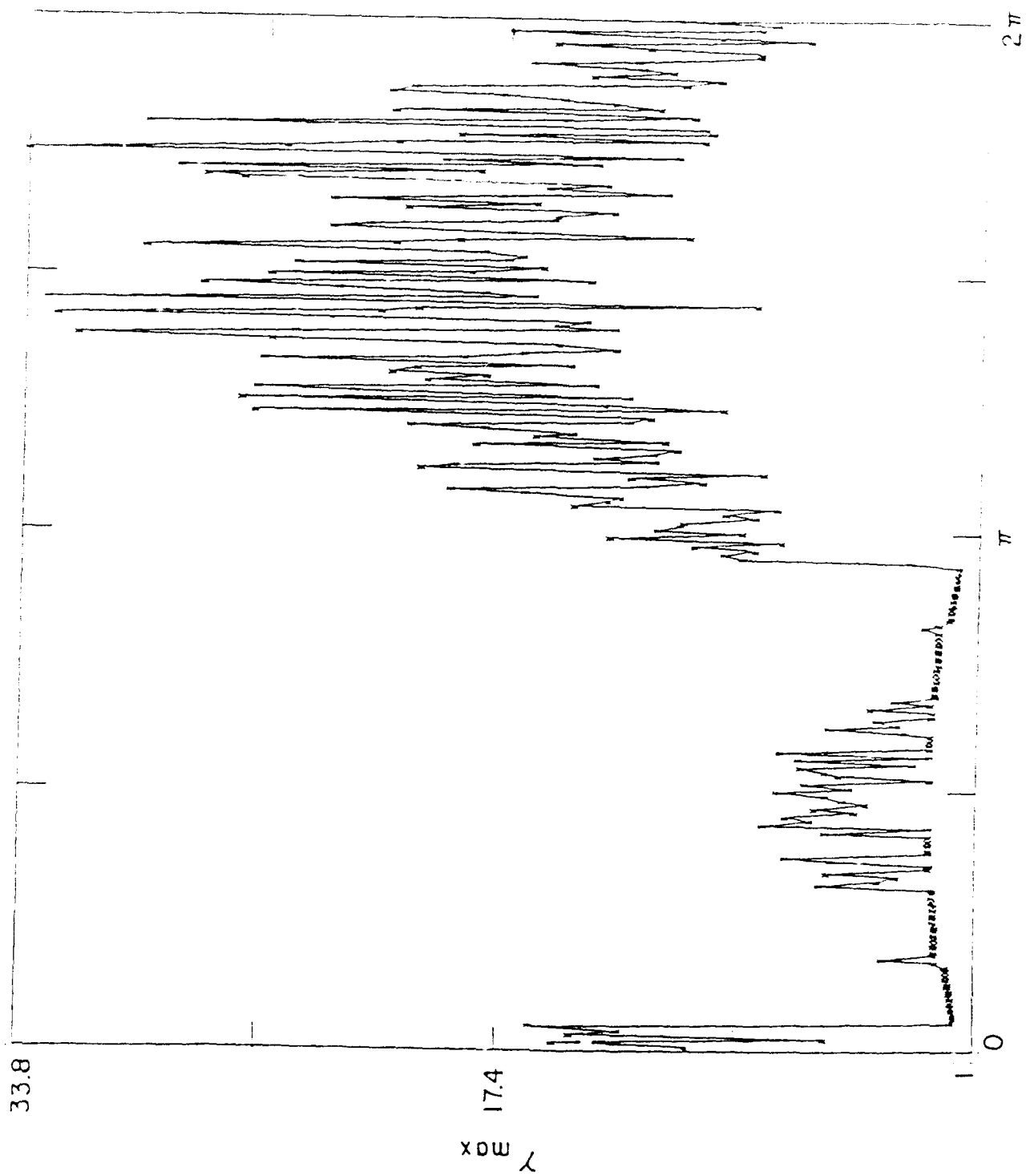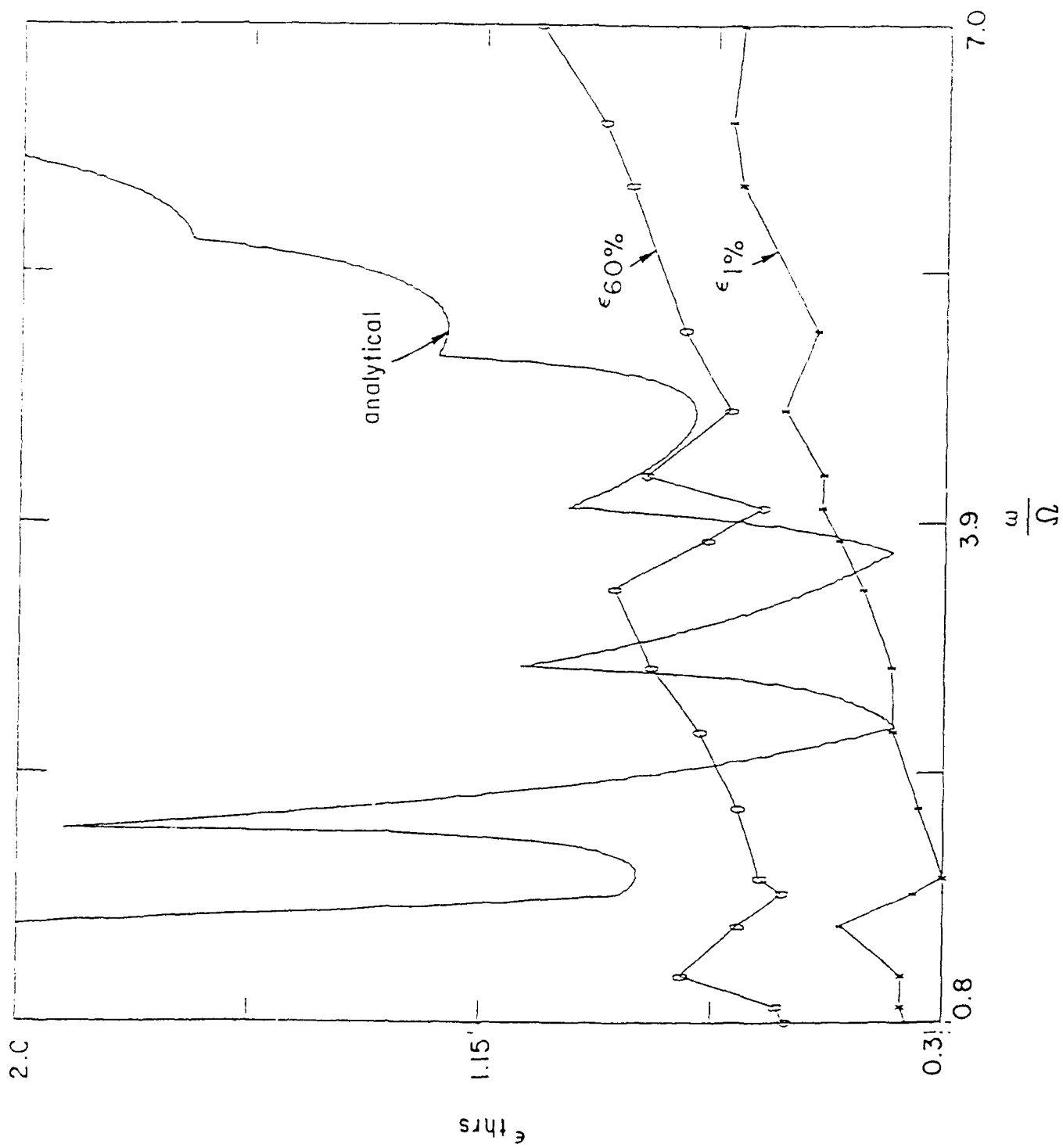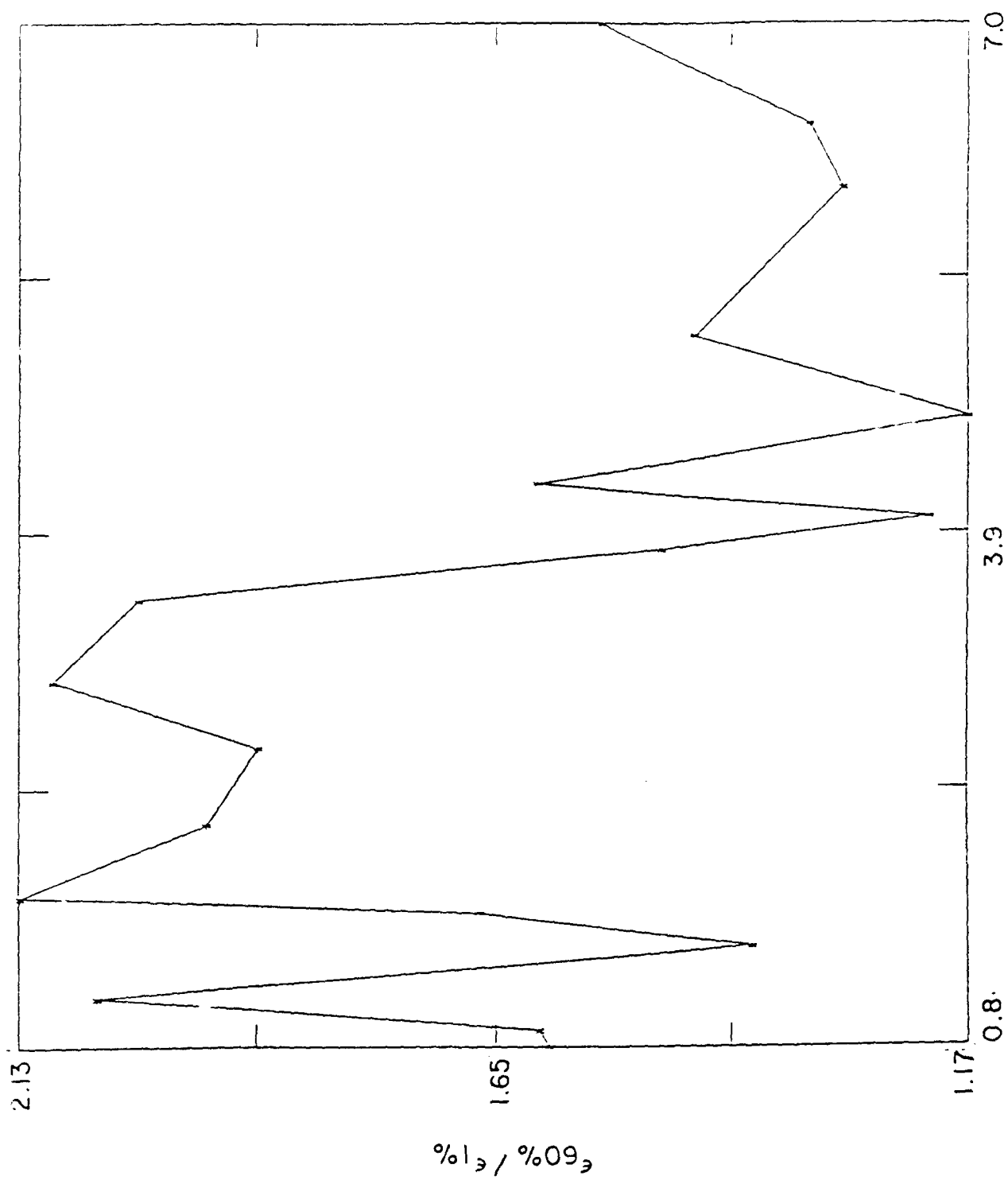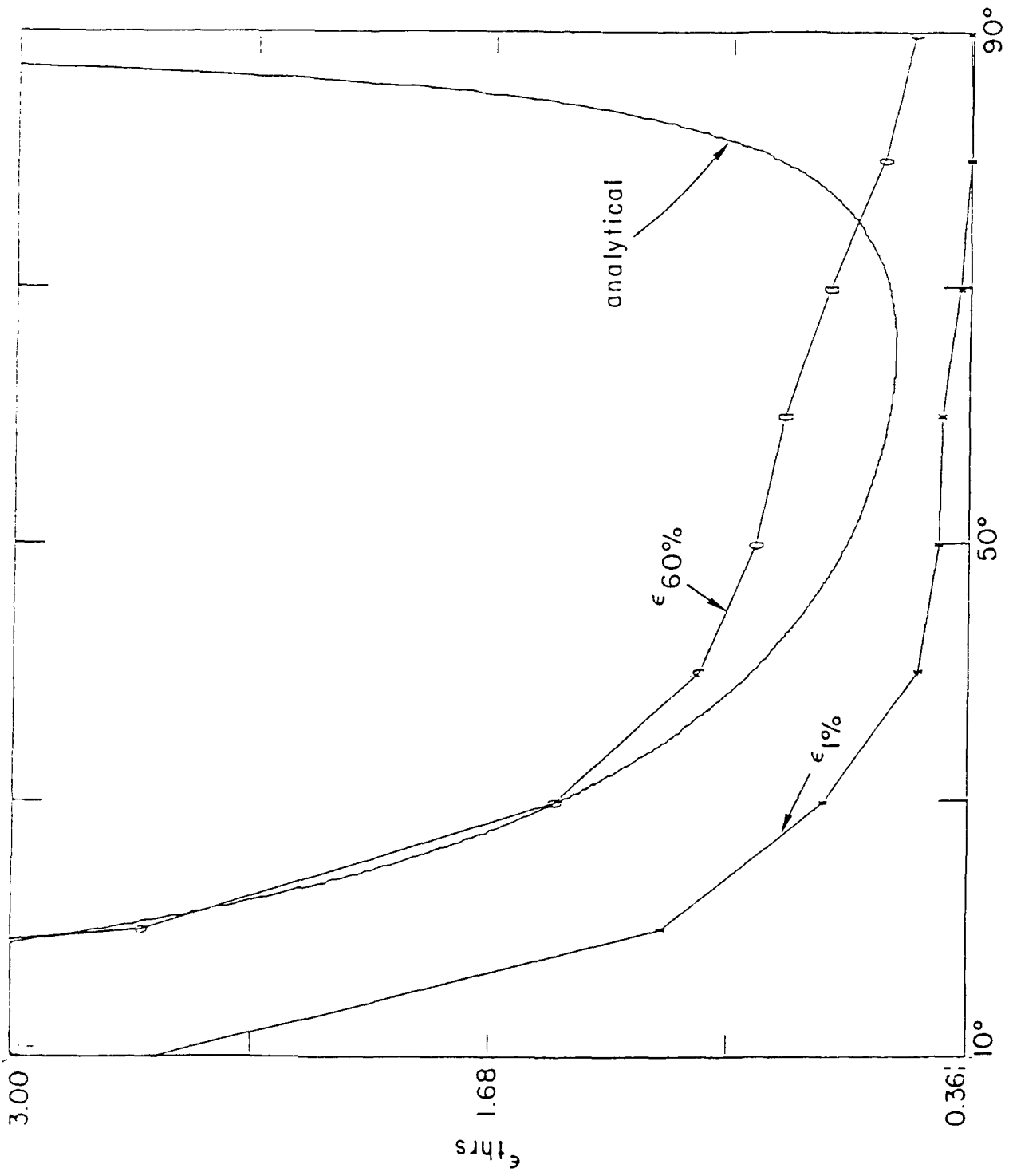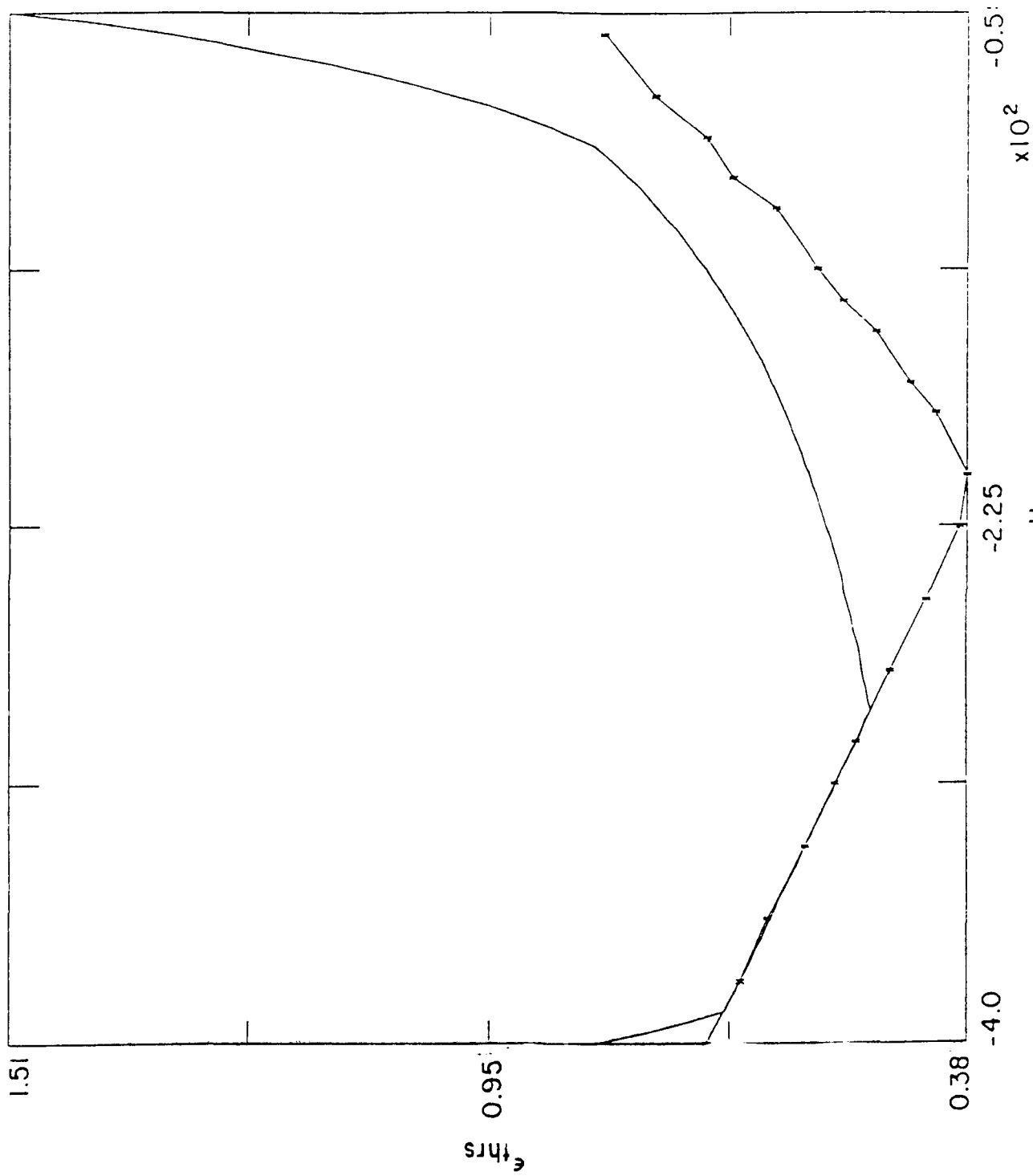
Figure 9

Figure 10a-c

109
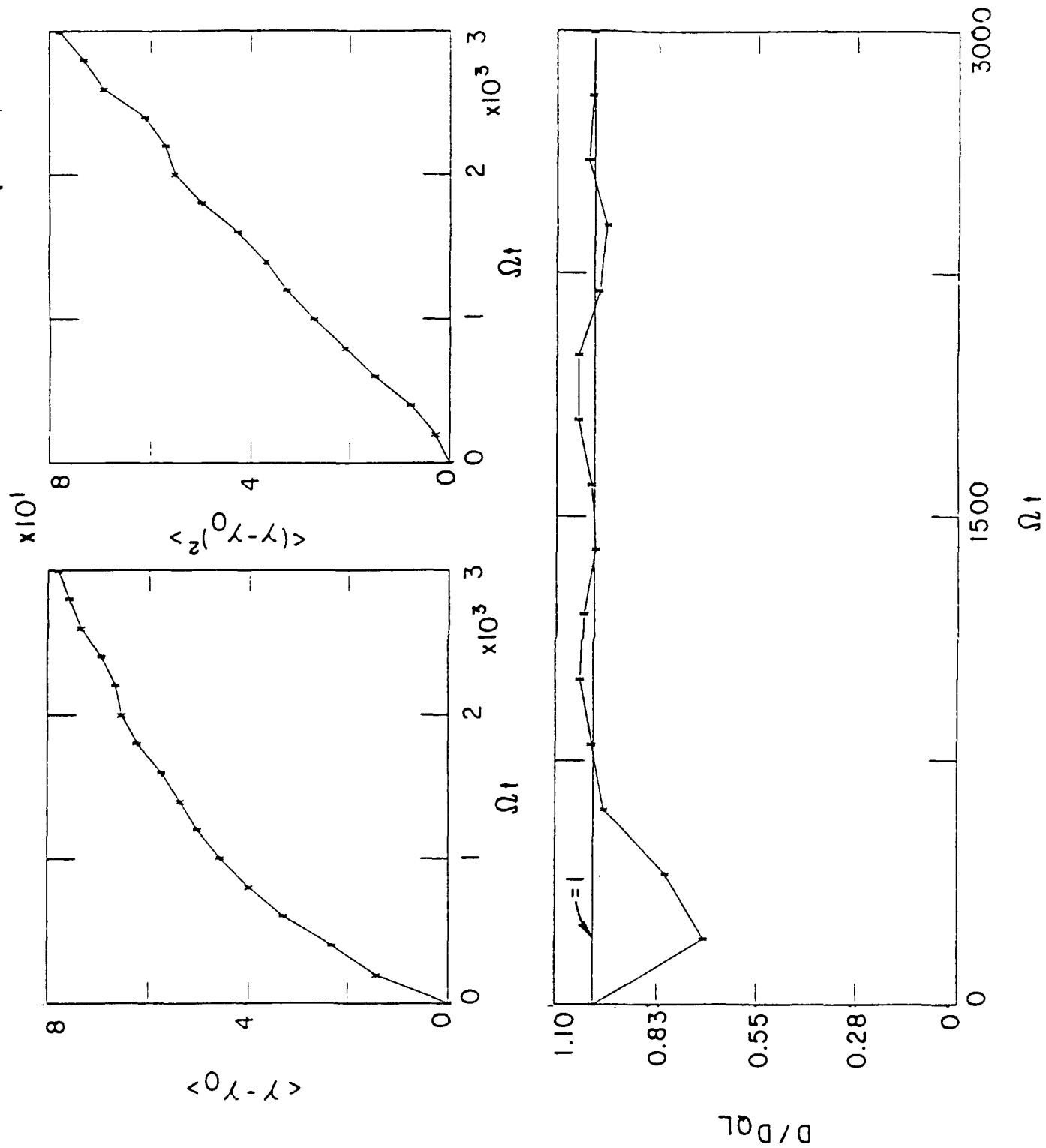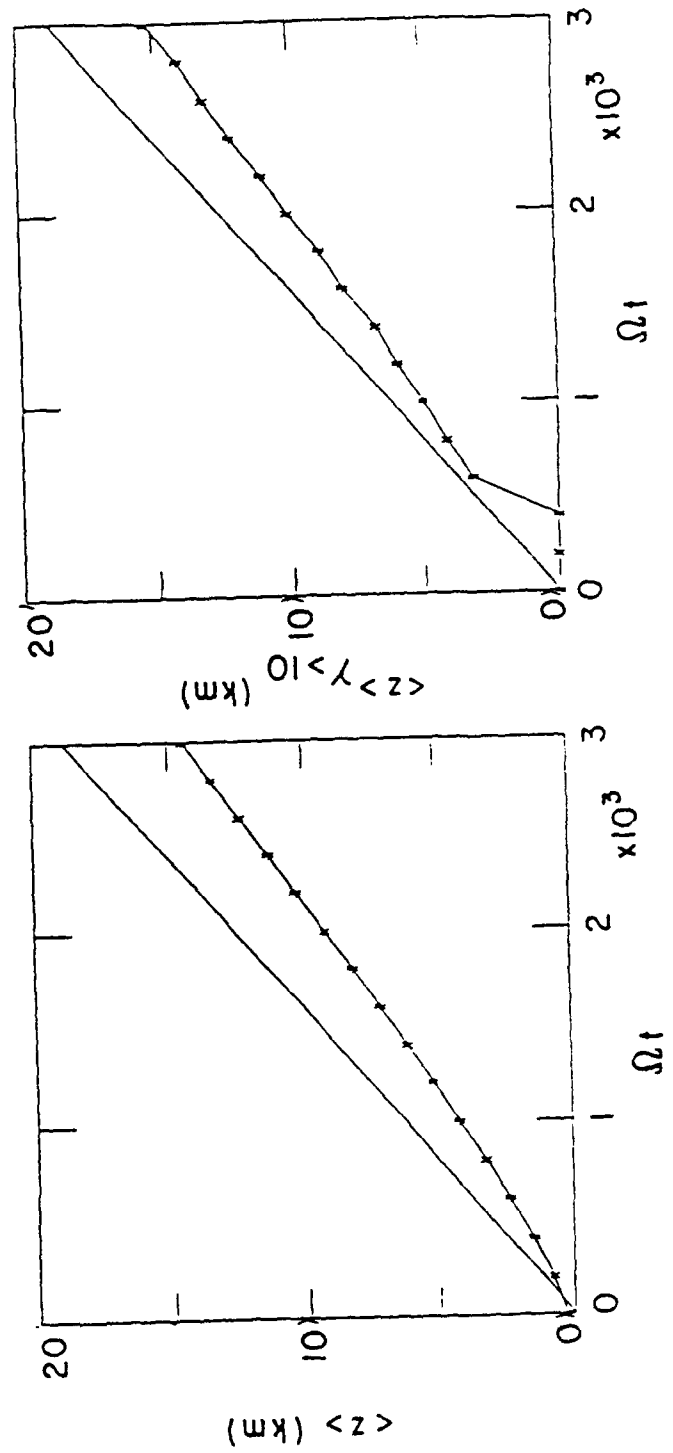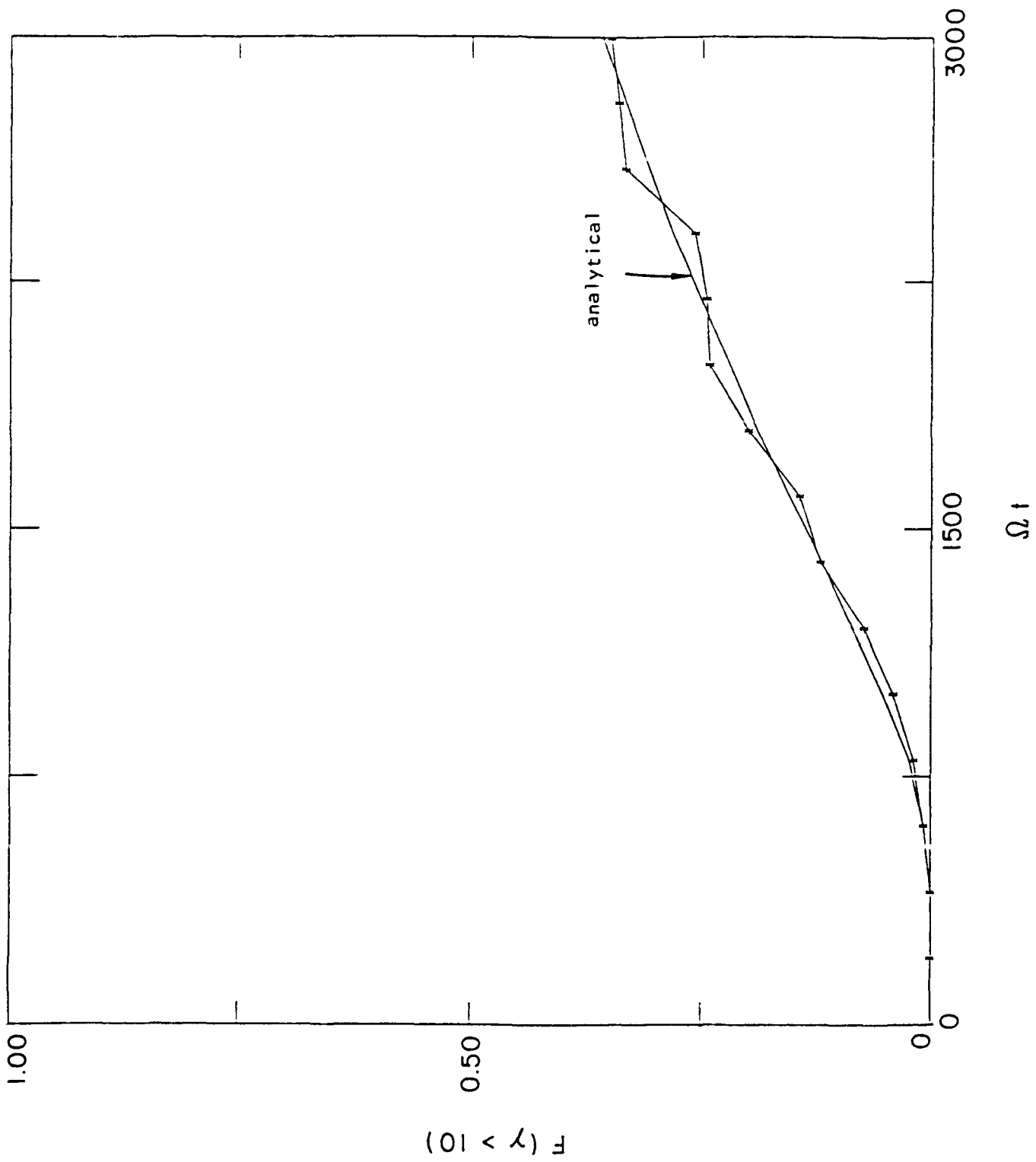
Figure 10d-e

Figure 10f

Figure 11a-c

112
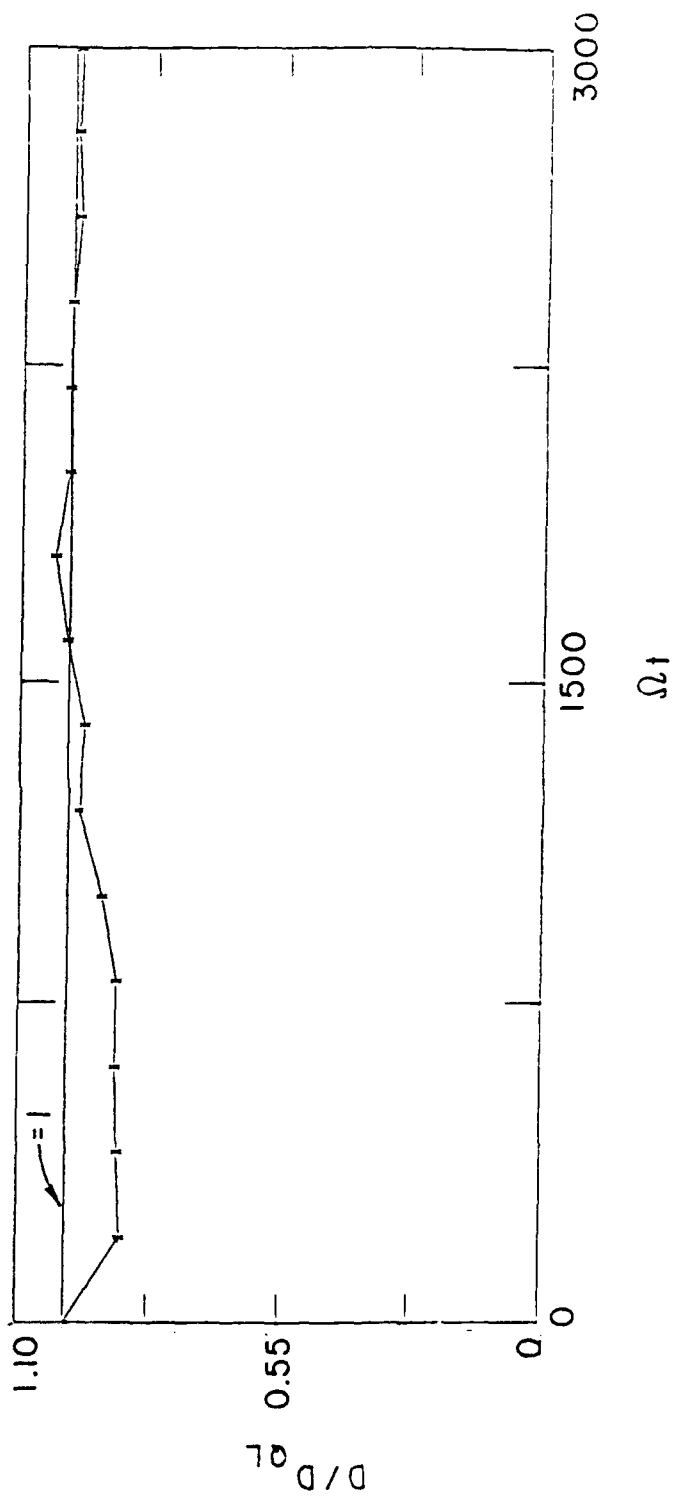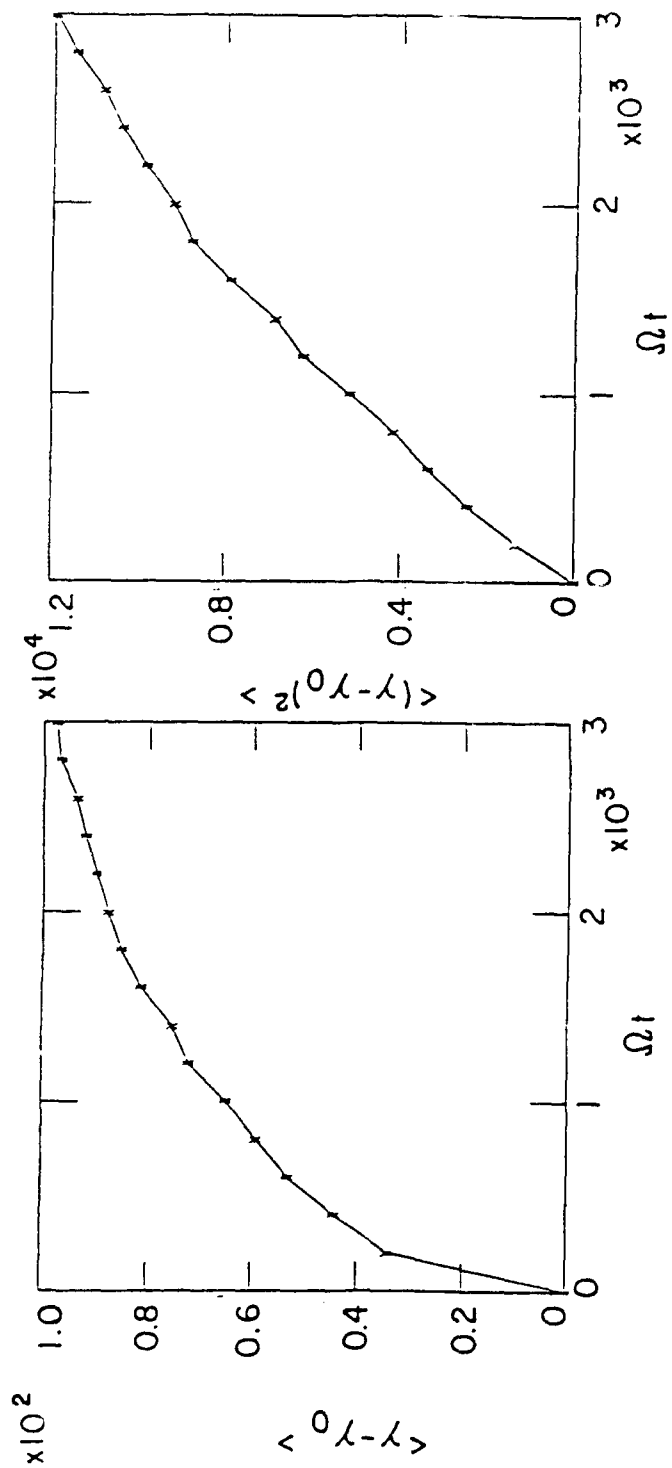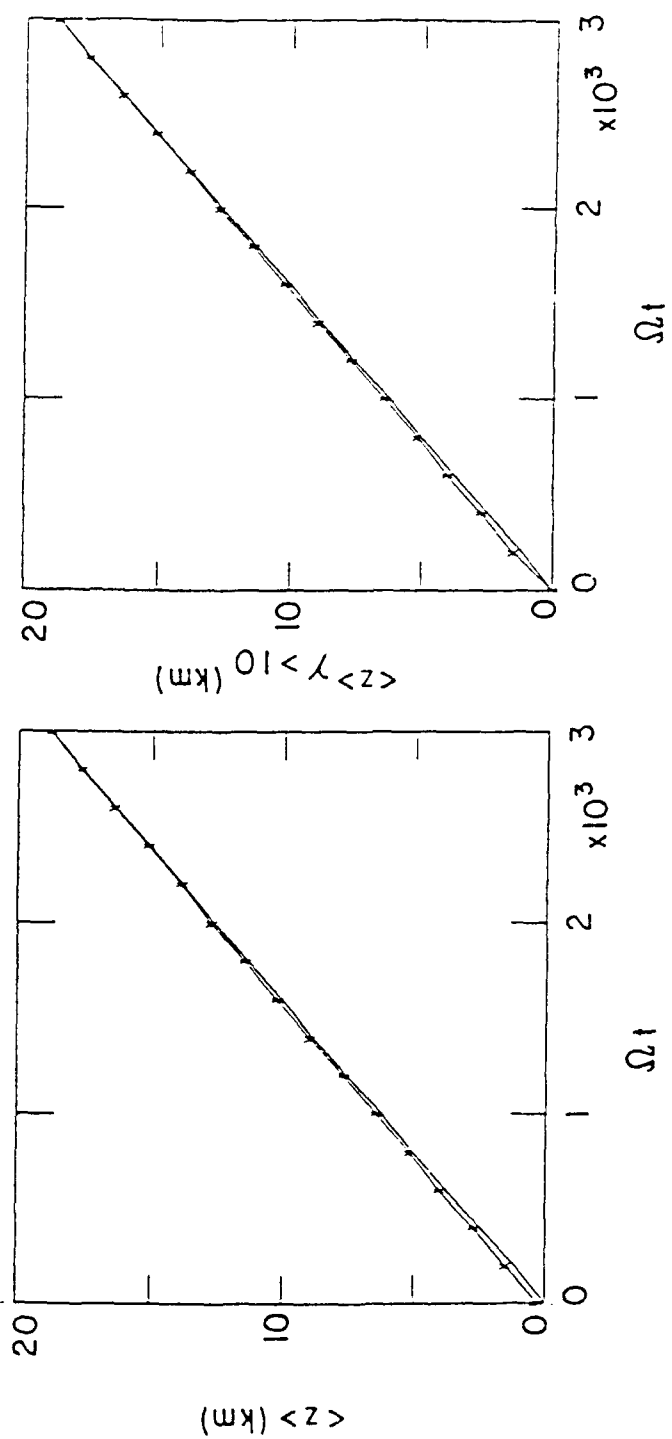
Figure 11d-e

Figure 11f

F (γ > 10)

Ωt

Figure 12a-c

115

Figure 12d-e

116

Ωt

Figure 12f

$F(\gamma > 10)$

117

Figure 13a

Figure 13b

D/D_{OL}

ϵ

1.12

0.56

0

0.19   0.59   0.99   5.5   10

611
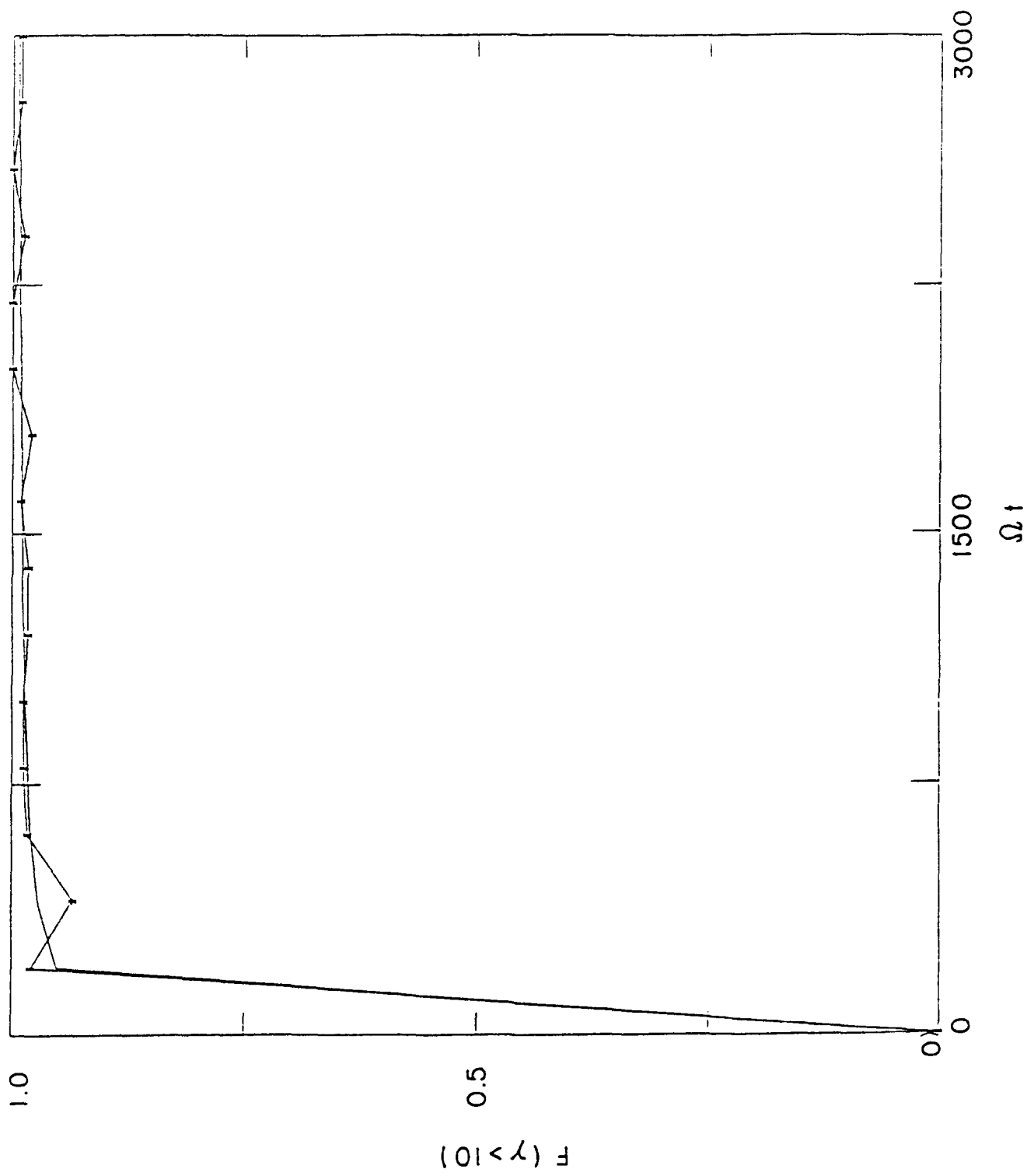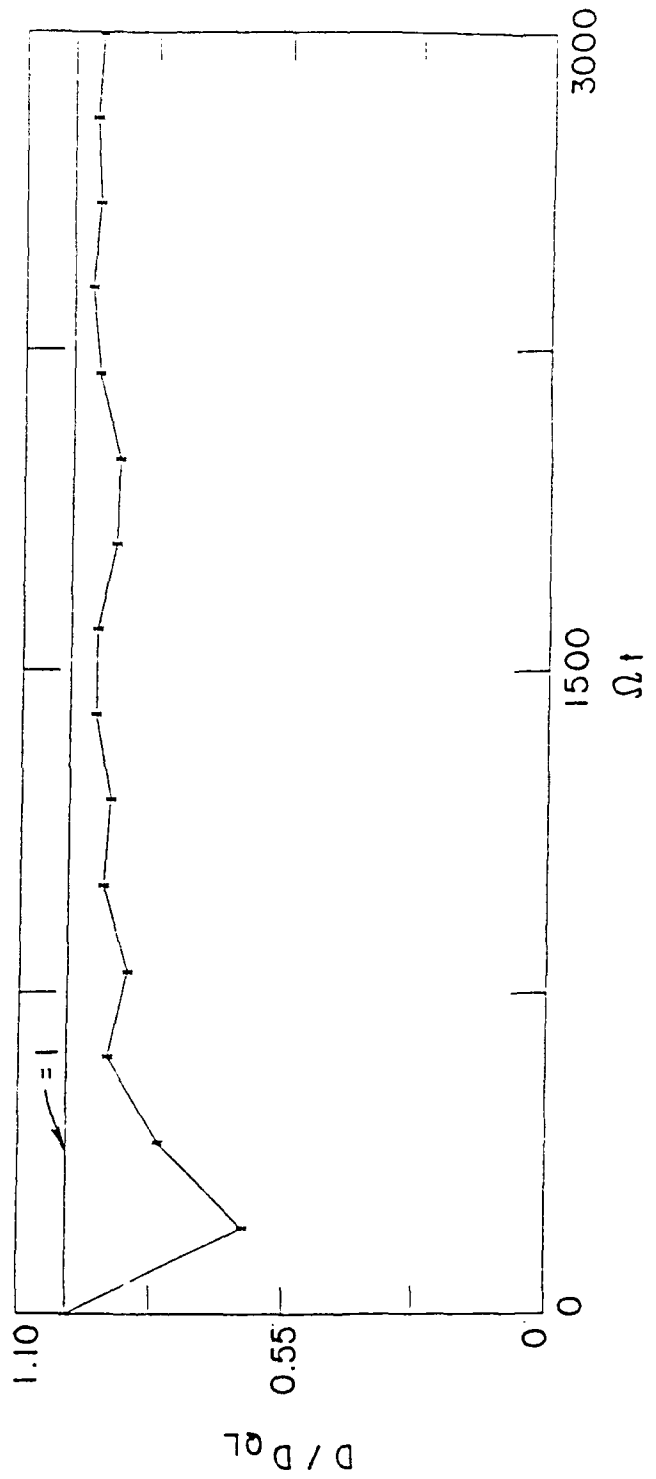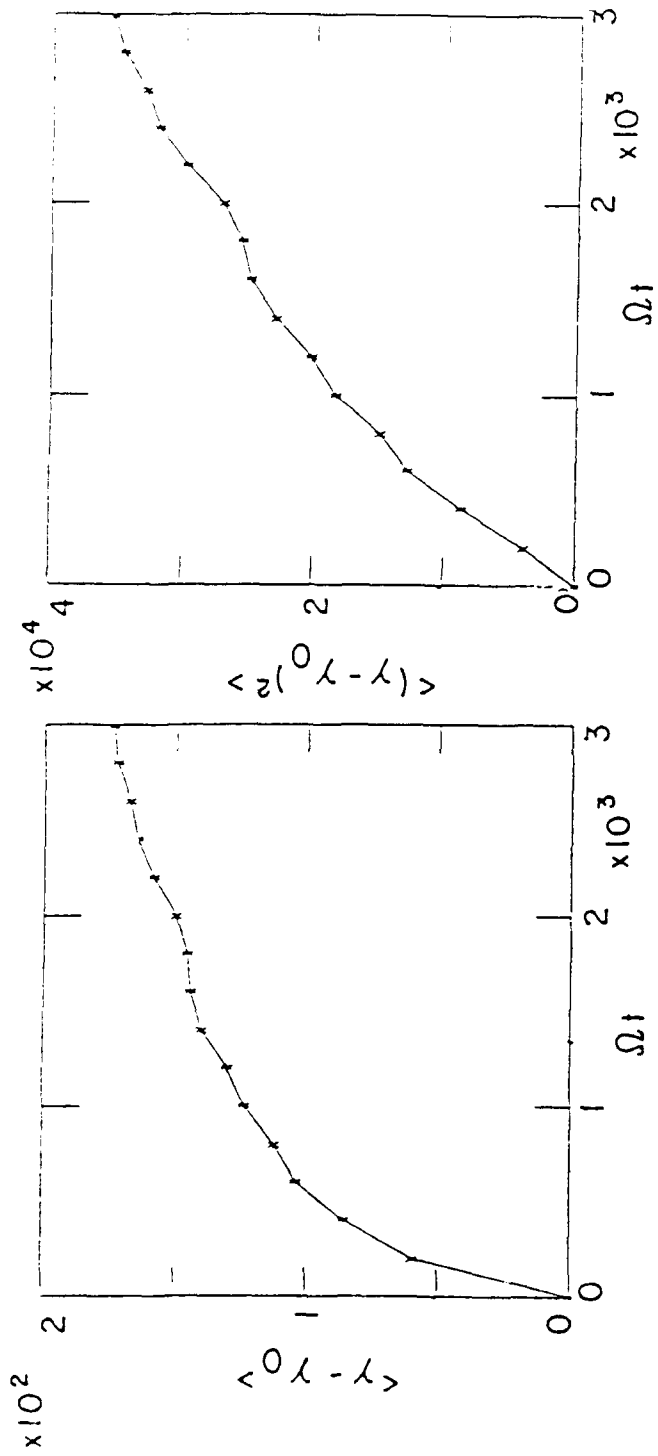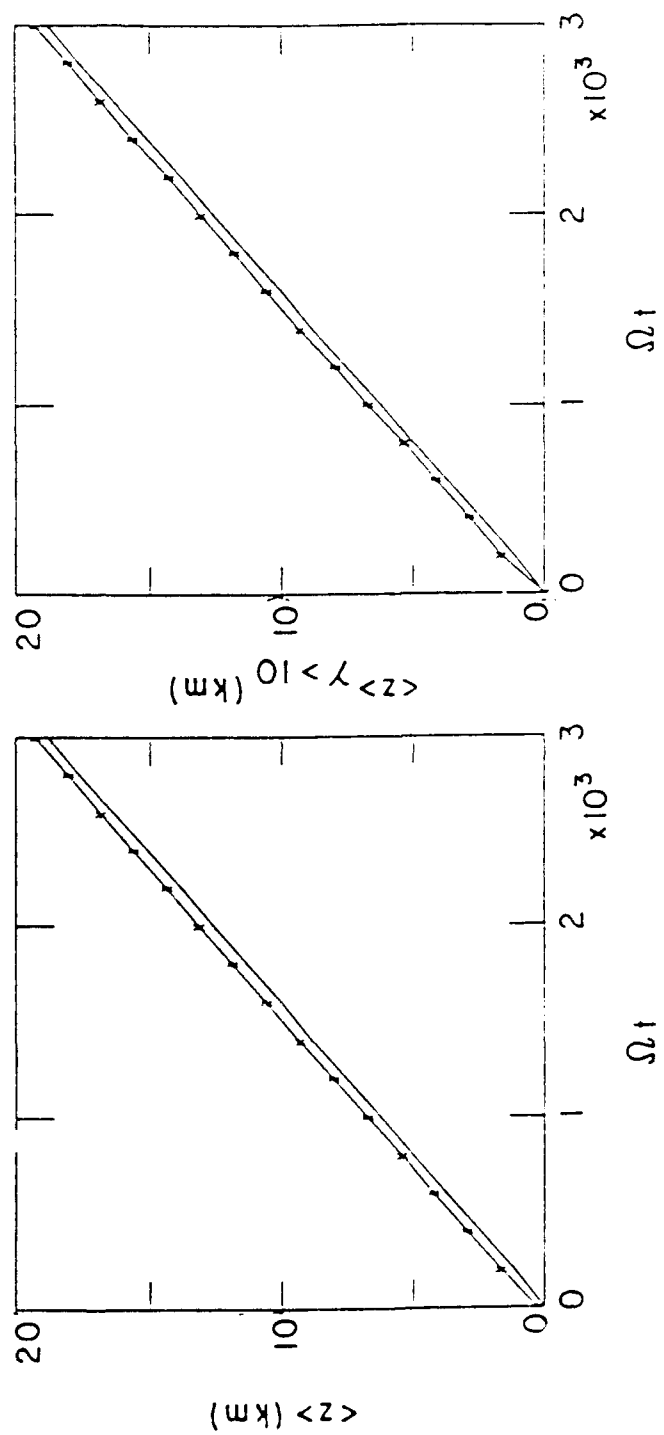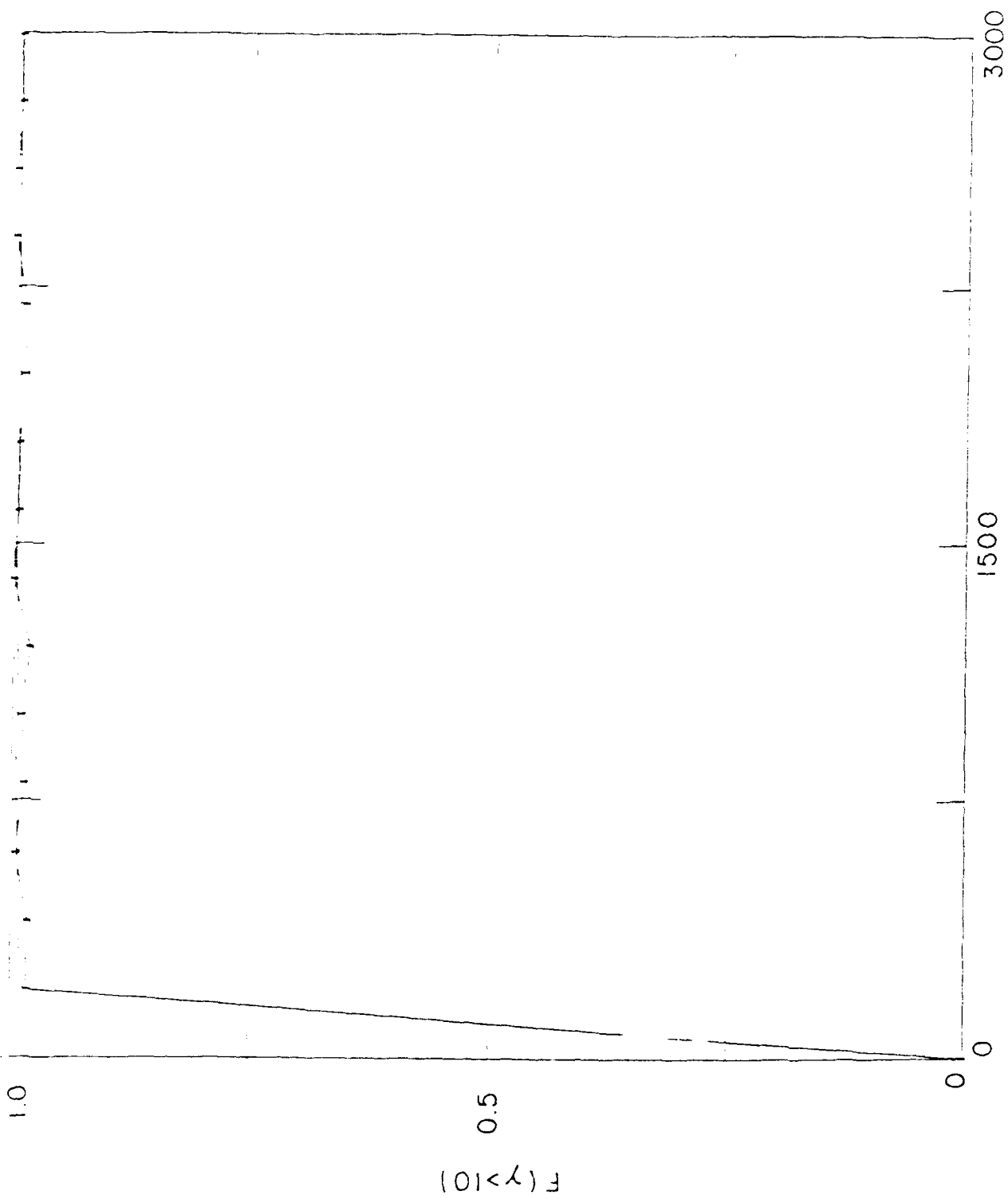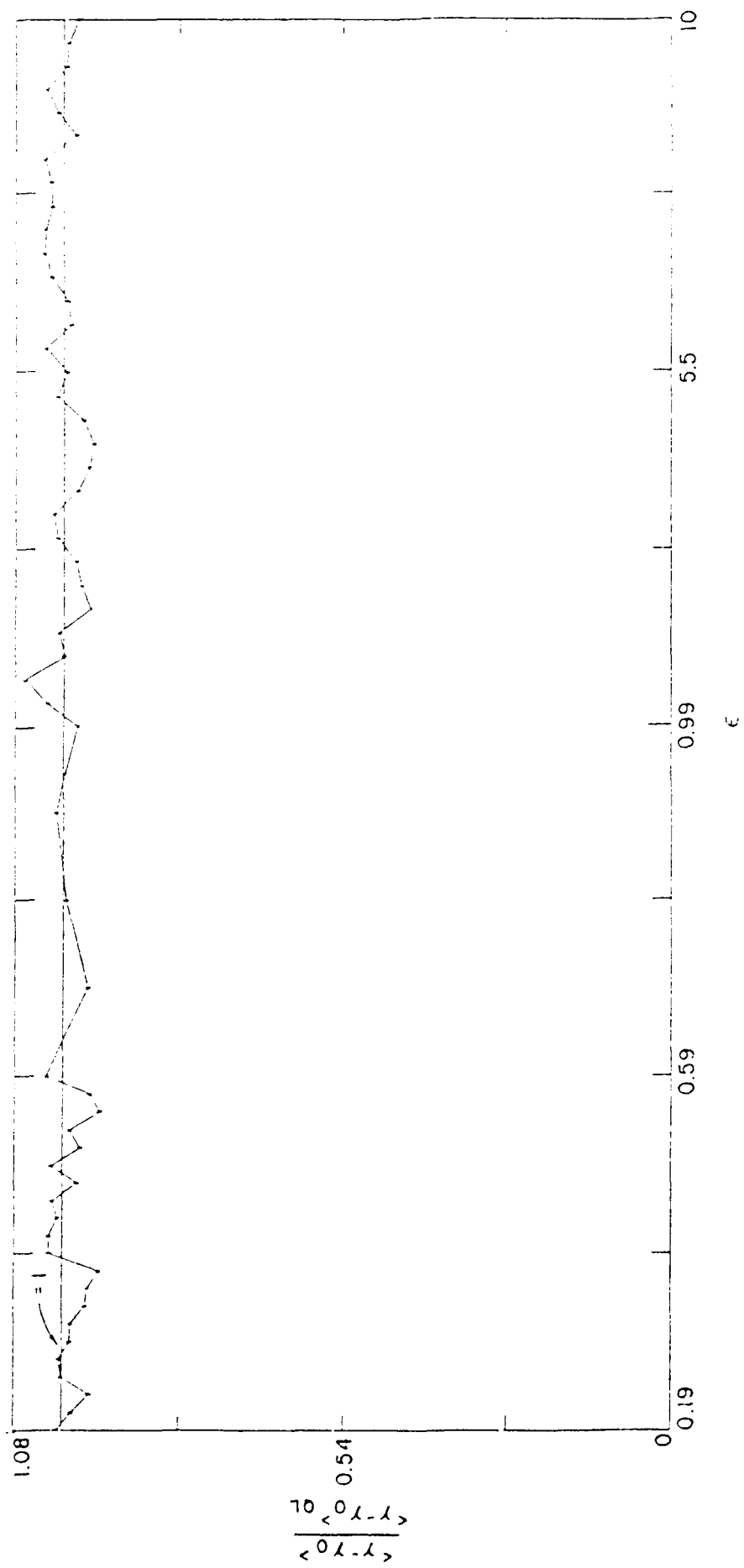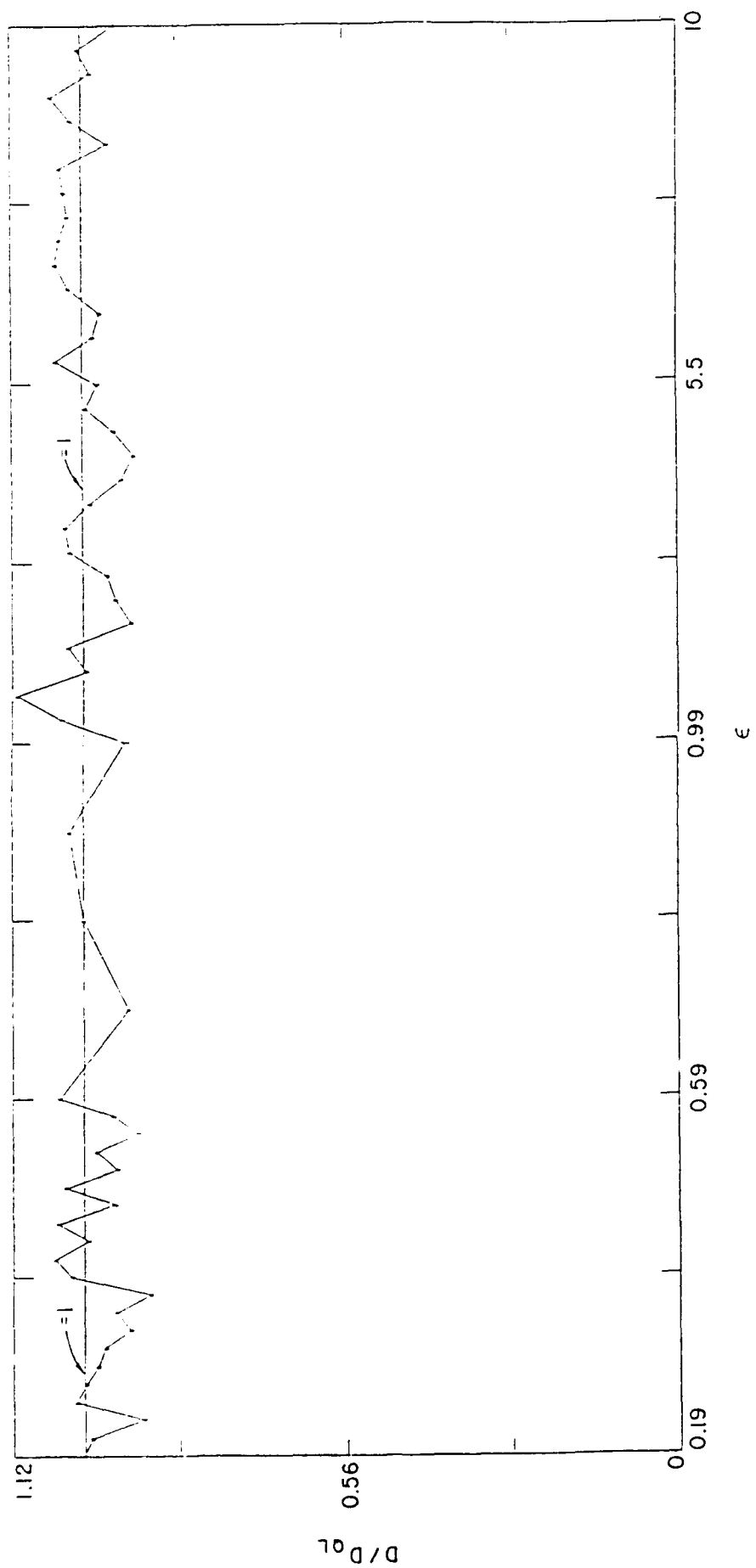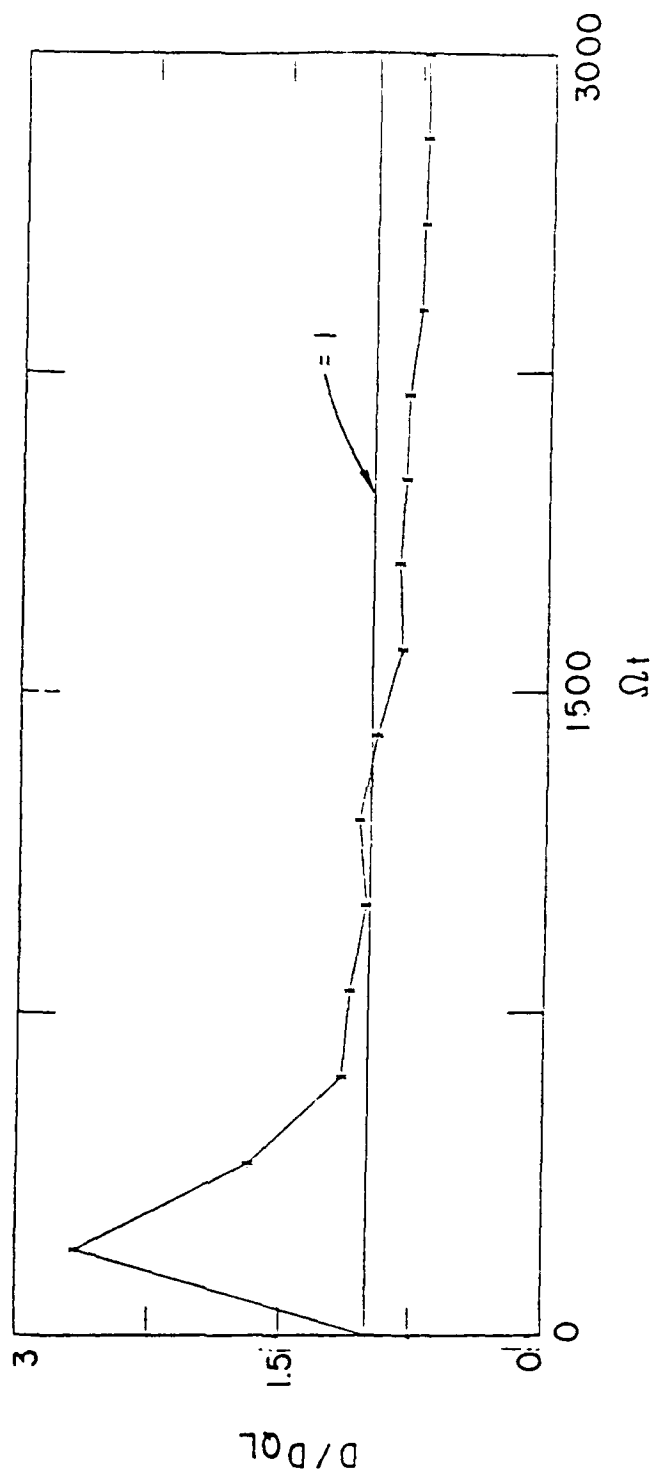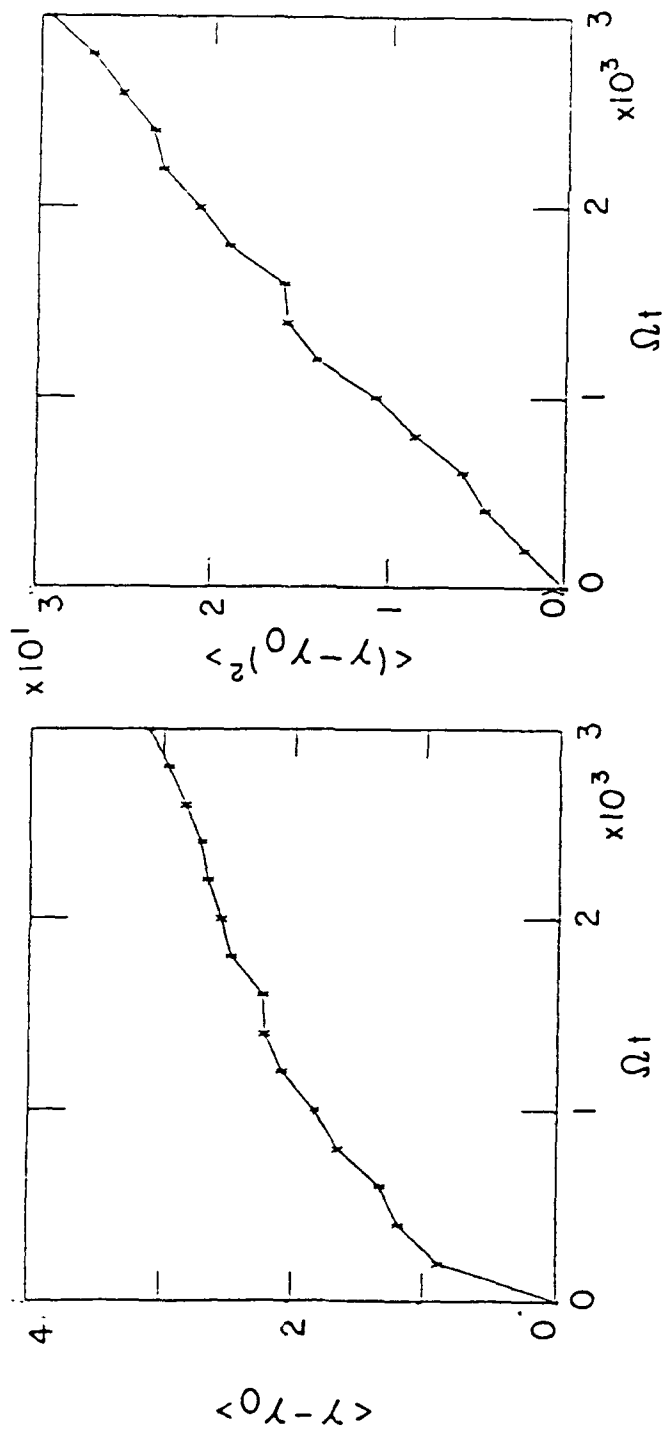
Figure 14a-c

Figure 14d-e

121

Figure 14f

F(γ>10)

Ωt

122

Figure 15a-c

123
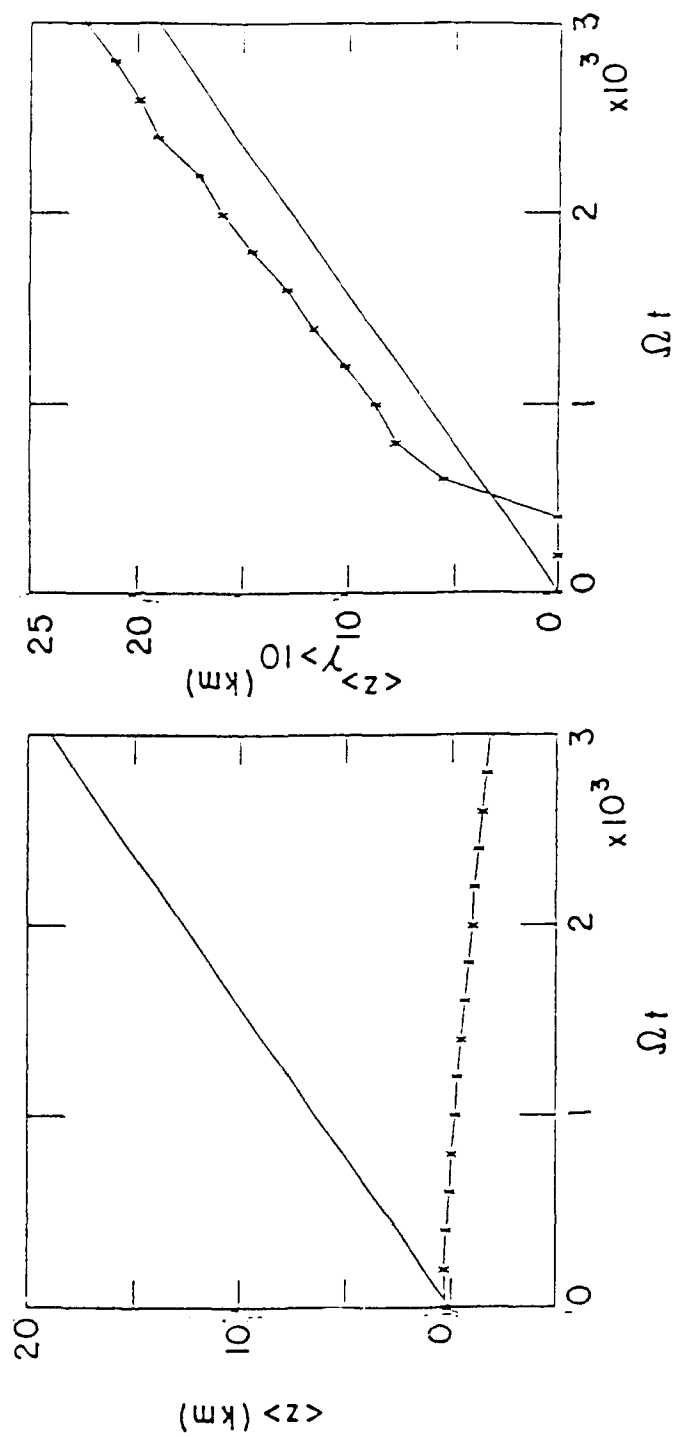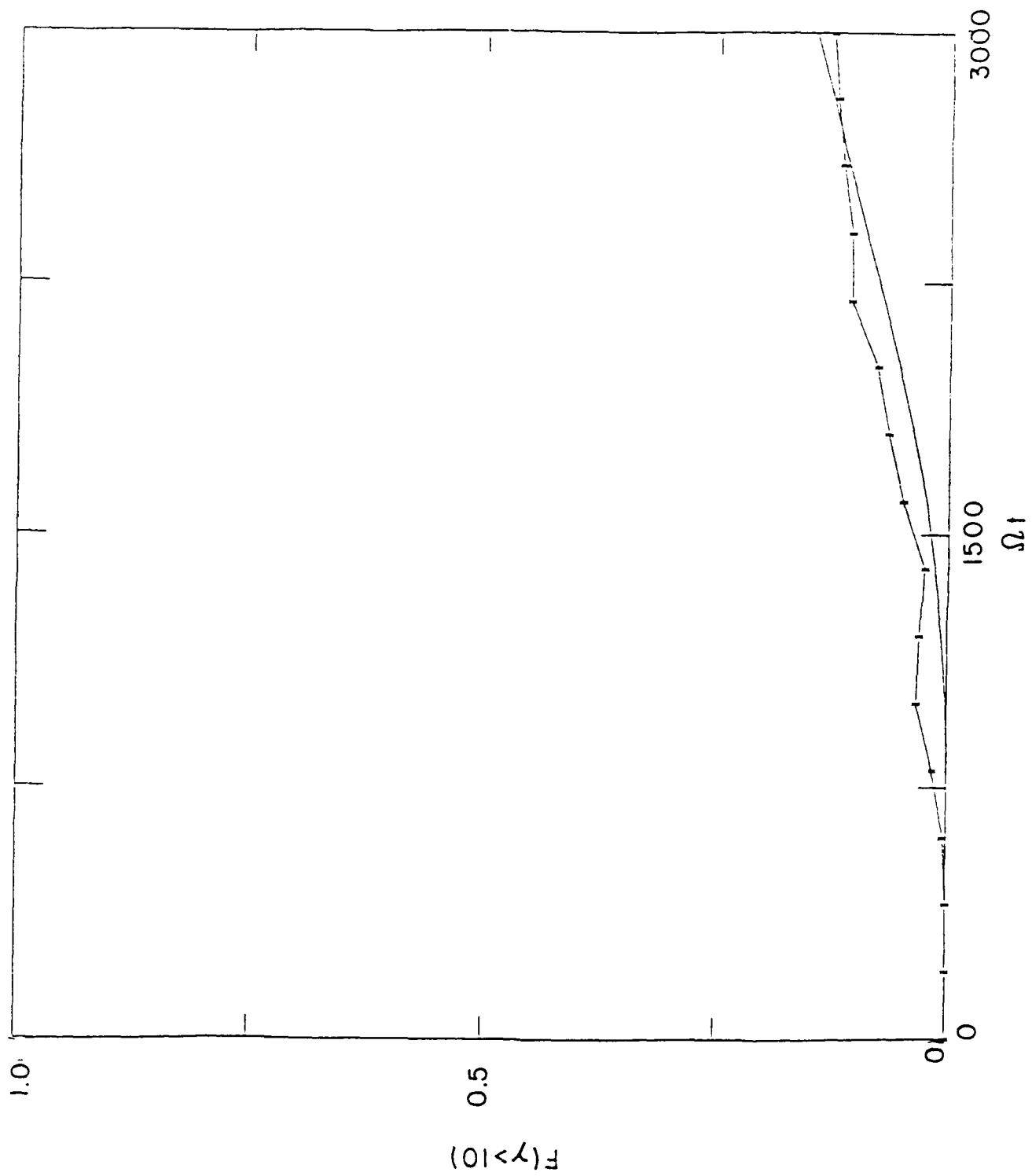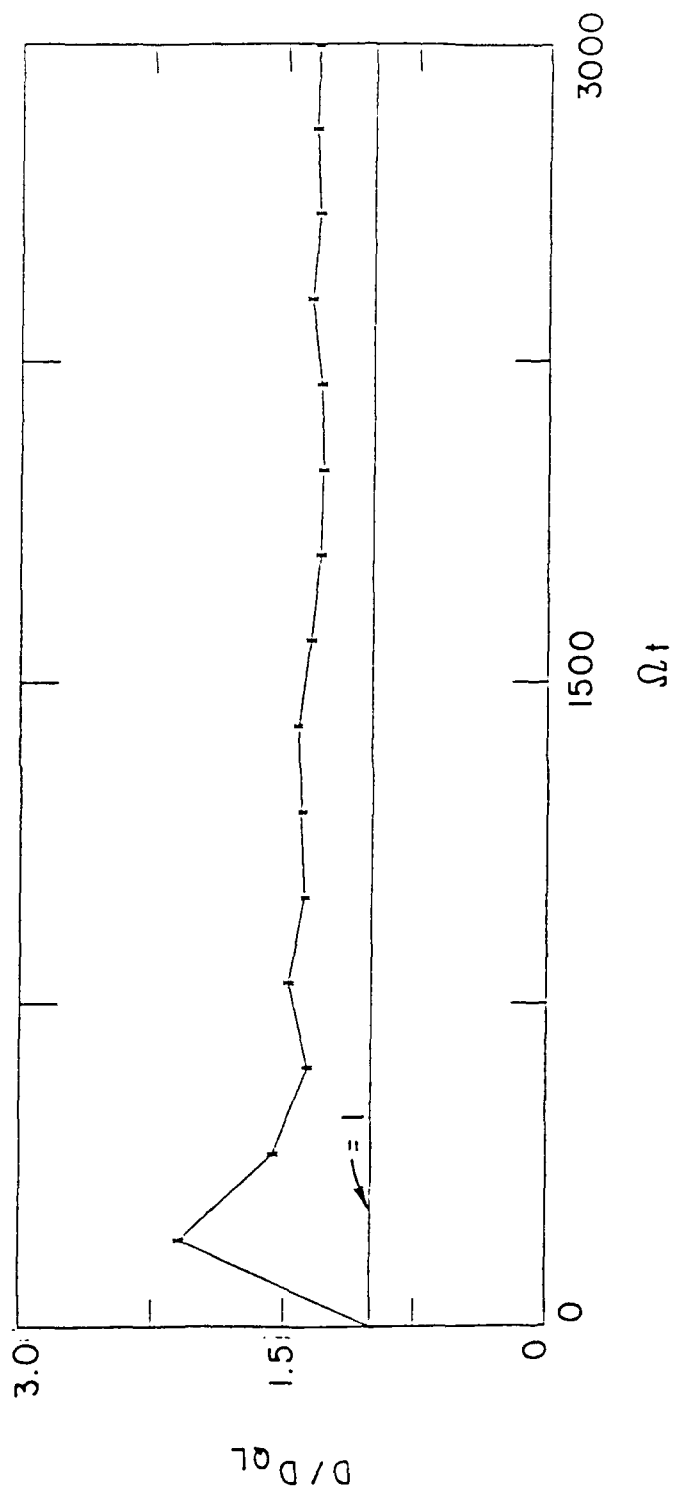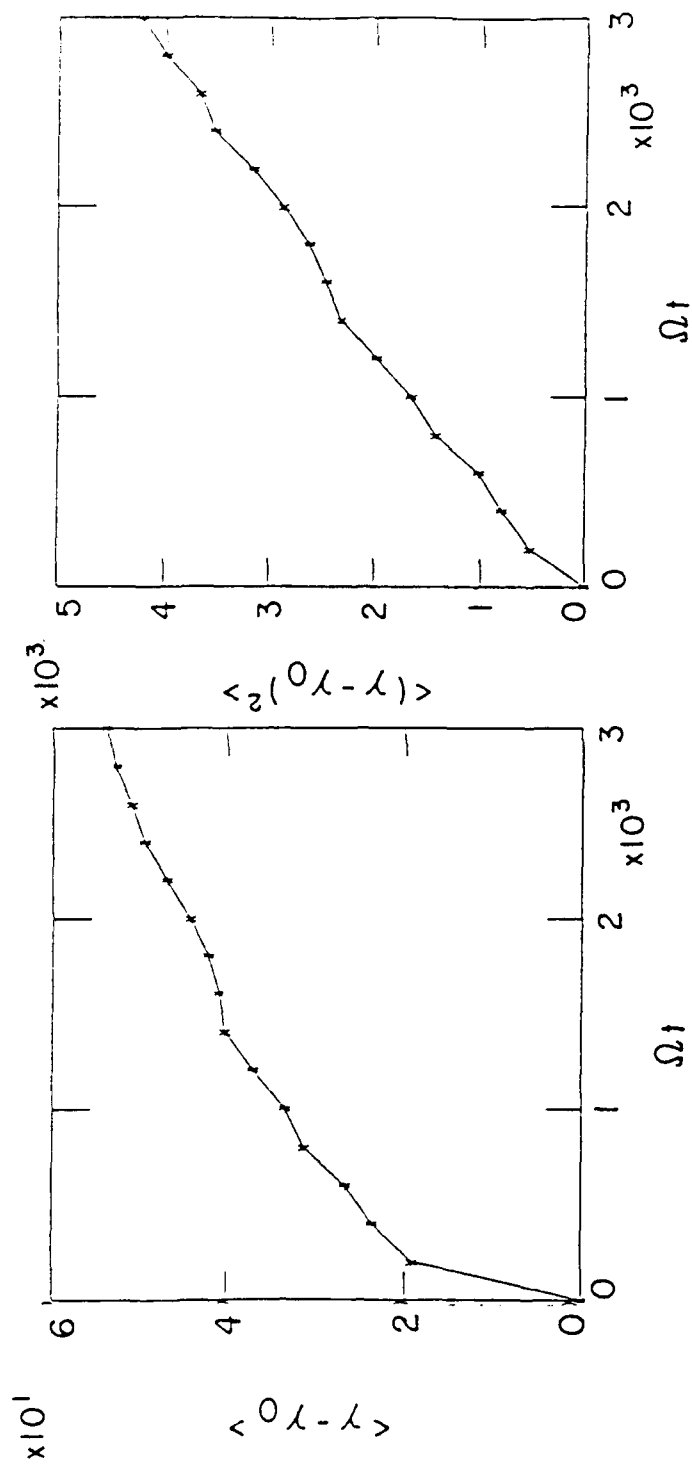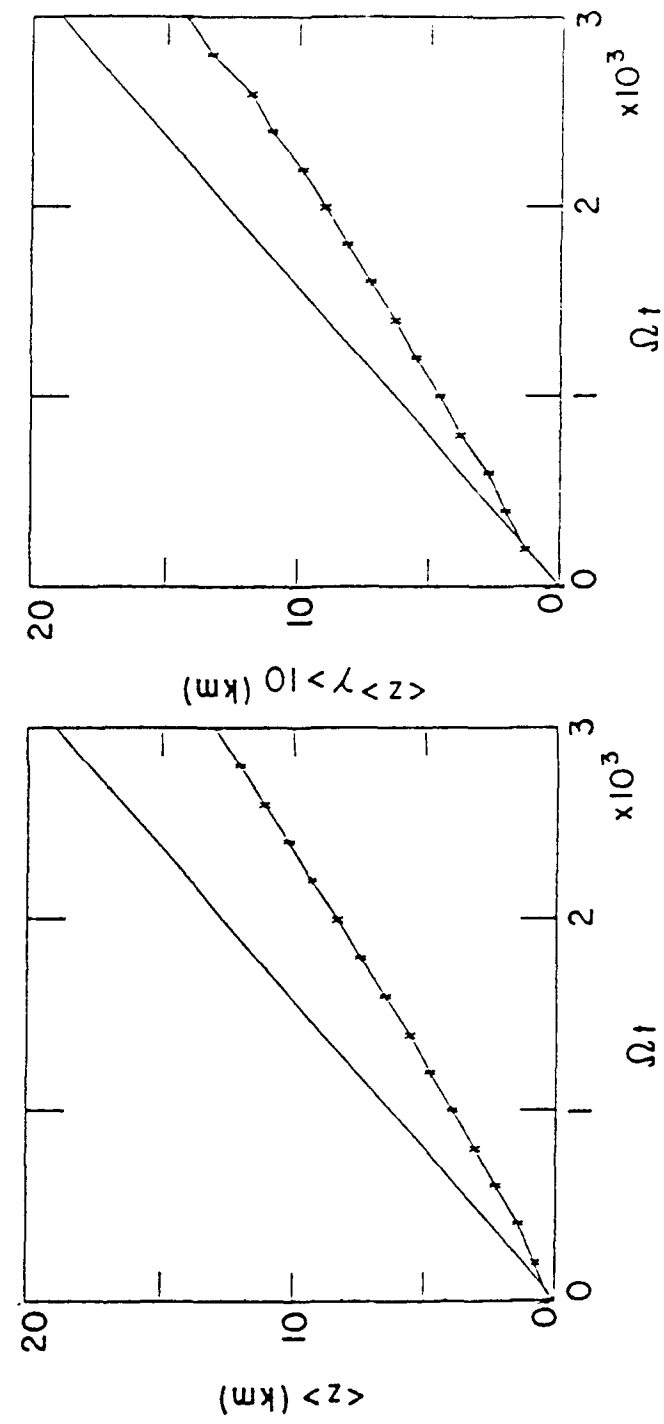
Figure 15d-e

Figure 15f

$F(\gamma > 10)$

Ωt

125

Figure 16a-c

126

Figure 16d-e

Figure 16f

Ωt

$F(y > 10)$

Figure 17a

$$\frac{\langle \gamma - \gamma_0 \rangle}{\langle \gamma - \gamma_0 \rangle_{QL}}$$

129

Figure 17b

130